Master's thesis

NTNU
Norwegian University of Science and Technology
Faculty of Natural Sciences
Department of Materials Science and Engineering

Baumann, Jesper Ludvig Saxlund

Wetting properties and interactions between SiO_2-CaO-Al_2O_3 slag and SiC

Master's thesis in Chemical Engineering and Biotechnology
Supervisor: Tangstad, Merete
June 2022

NTNU
Norwegian University of Science and Technology

Baumann, Jesper Ludvig Saxlund

Wetting properties and interactions between SiO_2-CaO-Al_2O_3 slag and SiC

Master's thesis in Chemical Engineering and Biotechnology
Supervisor: Tangstad, Merete
June 2022

Norwegian University of Science and Technology
Faculty of Natural Sciences
Department of Materials Science and Engineering

NTNU
Norwegian University of
Science and Technology

Summary

Wetting properties of $SiO_2.CaO - Al_2O_3$ slags on SiC have been investigated in a wetting furnace. Six compositons of slag were tested on three different SiC materials. All the slags were found to react with the SiC, and it was suggested that the most likely reactions were between SiC and SiO_2 or between SiC and Al_2O_3. This was further backed up by SEM EDS, but no clear answer were found. The reactions made it hard to determine proper contact angles, but the slags appered to wet the SiC neutral-good. Two of the substrates were porous which caused the slag to penetrate and run through them, making it even harder to get proper contact angles.

Fuktingsegenskapene til $SiO_2.CaO - Al_2O_3$ slagg på SiC har blitt undersøkt i en fuktingsovn. Seks sammensetninger av slag ble testen på tre forskjellige SiC materialle. Alle slaggene ble funnet til å reagere med SiC, og det var foreslått at de mest sannsynlige reaksjonene var mellom SiO_2 og SiC eller mellom Al_2O_3 og SiC. Dette var videre støttet opp under av SEM EDS analysen, men ingen klare svar var funnet. Reaksjonene gjorde det vanskelig og fastslå ordentlige kontakt vinkler, men slaggene virket å fukte SiC nøytralt godt. To av substratene var porøse som førte til at slaggene penetrerte og fløt gjennom de, som gjorde det enda vanskligere å finne ordentlige kontakt vinkler.

Abbreviations

SEM: Scanning Electron Microscope

SE: Secondary Electron

BSE: Back Scatter Electron

EDS: Energy-dispersive X-ray Spectroscopy

XRD: X Ray Diffraction

EPMA: Electron Probe Microanalyzer

WDS: Wavelength Dispersive X-ray Spectroscopy

Contents

1 Introduction

Silicon and ferrosilicon production have long been seen as slag free processes, but in later years there have been excavations that show that significant amounts of slag accumulates inside the furnaces. Little research have been done into silicon slags and their interactions in the furnace, so it is unclear to what extent the slag causes problems. The accumulation of slag can lower the usable volume inside the furnace, it can lower the electrical efficiency, it can lower the yield, and it can make work more difficult for the furnace operators and tappers. The slag in the silicon and ferrosilicon processes are mainly composed of SiO_2, Al_2O_3 which are found as impurities in the quartz, and CaO which is often added to the furnace to lower the viscosity of the melt. Iron oxides can also be found in the slag in ferrosilicon furnaces. The goal of this master thesis is to help develop a method to observe and investigate the interactions between the slag and the furnace materials. The wetting behaviour and reactions between different compositions of $SiO_2 - CaO - Al_2O_3$ slags and different SiC materials will be investigated in a wetting furnace to reach this goal.

1.1 Silicon production

Silicon is industrially produced from quartz in submerged arc furnaces. Here quartz is reduced by carbon into its elemental form at high temperatures. This process is called a carbothermic reduction. The overall mass balance can be simplified to equation (1.1), but the process is more complex and is a combination of several different reactions[1].

$$SiO_{2(s)} + 2C(s) = Si_{(l)} + 2CO_{(g)} \qquad \Delta H^0_{298} = 689.8kJ \tag{1.1}$$

The most common submerged arc furnaces uses three phase alternating current through three graphite electrodes that are submerged into the charge. The use of three electrodes makes it possible to have symmetrical heating in the furnace without a bottom electrode, as the currents through the electrodes are synced to cancel out the voltage in the furnace[2]. The electrodes come in three different types. Prebaked, Søderberg, and selfbaking composite electrodes. The prebaked electrodes can be used in smaller silicon furnaces. They are made of segments of prebaked electrode material that can be screwed on top of the electrode as it is being consumed. Søderberg electrodes

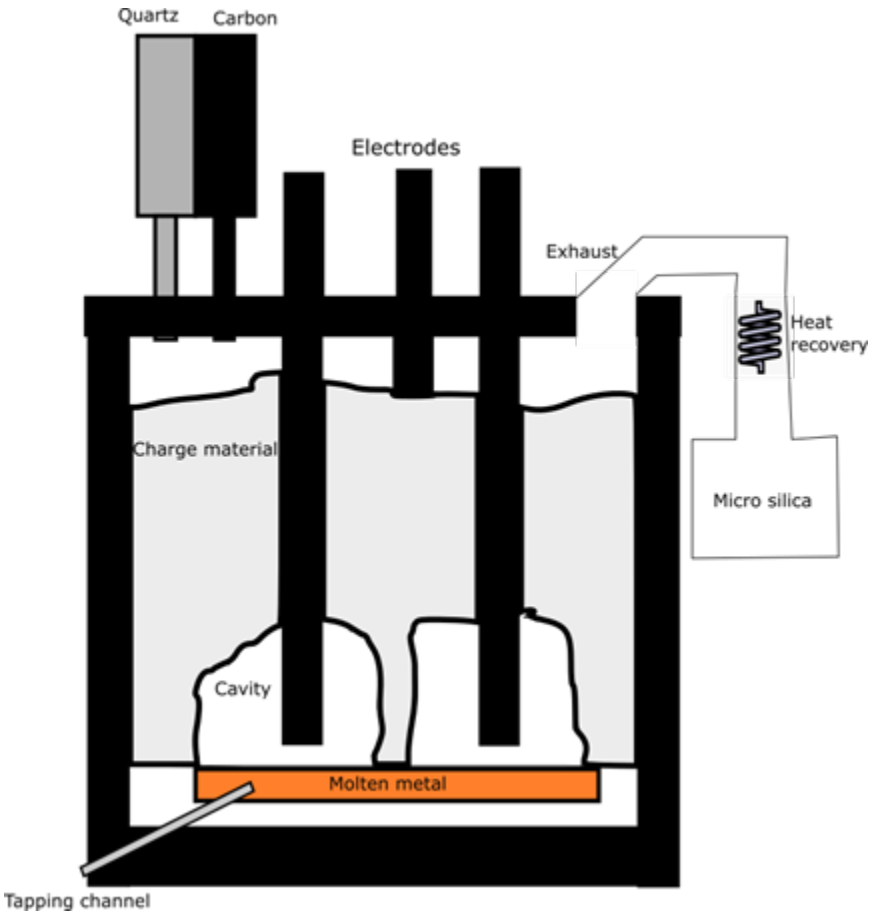

Figure 1: Simple illustration of a submerged arc furnace with gas treatment

can not be used in furnaces for metal silicon production as they can add iron to the metal, but they can be used in ferrosilicon furnaces. They are composed of a solid metal casing filled with electrode mass. This mass is melted and baked in the furnace from the furnace heat and the Ohmic heating. Selfbaking composite electrodes are a combination of the prebaked electrode and the Søderberg electrode. They have a prebaked core, surrounded by electrode mass. The electrode mass is held in place by a metal ferrule that ends before the active zone of the furnace. Selfbaking composite electrodes can be used in larger silicon furnaces and ferrosilicon furnaces.[2]

In the furnace operation, electrical energy is fed through the electrode and arcs into the liquid metal bath. A cavity forms around the electrode tips as the reactions here happens faster than the materials flow.[3]. Figure 1 shows a simple illustration of a submerged arc furnace for silicon production.

The furnace can qualitatively be described as split into two parts. The inner, hot part at and

around the cavity, where SiO_2 reacts with SiC to form Si, SiO, and CO, and the upper cooler part where condensation of SiO gas and reactions between SiO and C to form SiC happens. The charge is added at the top of the furnace. It is quickly heated to between 700 and 1300°C by the temperature of the rising gases, and by their exothermic reaction with air in the headspace of the furnace (1.2) (1.3). The rising gasses will be in large parts be SiO gas that can react with the carbon in the charge according to equation (1.4). This reaction is very important as it captures SiO gas that would otherwise have a large probability to escape the furnace, and it is therefore one of the main reactions to ensure a high yield. [4] [3]

$$CO_{(g)} + \frac{1}{2}O_{2(g)} = CO_{2(g)} \qquad \Delta H^0_{298} = -283.0kJ \tag{1.2}$$

$$SiO_{(g)} + \frac{1}{2}O_{2(g)} = SiO_2(s) \qquad \Delta H^0_{298} = -807.9kJ \tag{1.3}$$

$$SiO_{(g)} + 2C_{(s)} = SiC_{(s)} + CO_{(g)} \qquad \Delta H^0_{298} = -79.5kJ \tag{1.4}$$

The charge will move down further into the furnace where it heats up. At temperatures above 1500°C, the SiO_2 and the carbon can react together to form SiC according to equation (1.5). However this will be a very slow reaction as it is a solid-solid reaction until the quartz melts at between 1700-1900°C so it can be ignored. [4]

$$SiO_2(s) + 3C_(s)) = SiC_(s)) + 2CO_(g)) \qquad \Delta H^0_{298} = -617.9kJ \tag{1.5}$$

The material, composed of SiO_2, SiC, C, and Si, arrives at the inner part in the furnace. Here the temperature is above 1800-2000°C. The total unbalanced reaction in this area is given by equation (1.6) [1].

$$SiO_2 + SiC + C = Si + SiO + CO \qquad \Delta H^0_{298} = 769.3kJ \tag{1.6}$$

Schei et al. states that the reactions that happens would be reaction (1.7)-(1.9) , where the SiO producing reactions (1.7) (1.8) would be much slower than reaction (1.9) [4]. Kinetic investigation by Filsinger and Bourrie supports both that the reactions (1.7), (1.8), and (1.9) happen in the

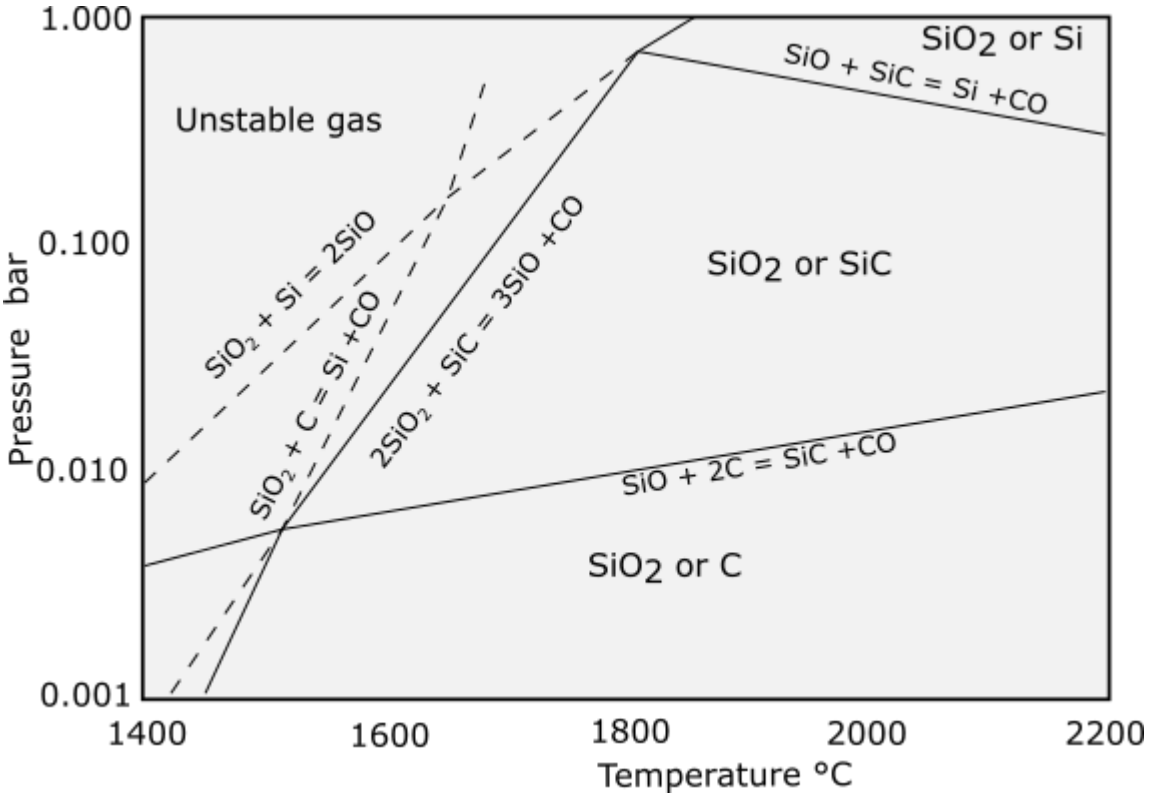

Figure 2: Equilibrium SiO pressure above the condensed phases SiO_2−C, C-SiC, SiO_2−SiC, SiO_2−Si, and SiC-Si. From Production of high silicon alloys[4].

inner area and that reaction (1.9) is faster than the SiO producing reactions[5].

$$2SiO_{2(l)} + SiC_{(s)} = 3SiO_{(g)} + CO_{(g)} \qquad \Delta H^0_{298} = 1474.3kJ \tag{1.7}$$

$$SiO_{2(s/l)} + Si_{(l)} = 2SiO_{(g)} \qquad \Delta H^0_{298} = 705.0kJ \tag{1.8}$$

$$SiO_{(g)} + SiC_{(s)} = 2Si_{(l)} + CO_{(g)} \qquad \Delta H^0_{298} = 64.3kJ \tag{1.9}$$

Figure 2 shows the equilibrium SiO pressure over the condensed phases[4], from this it shows that for silicon to be produced by reaction (1.9) a high SiO partial pressure is required.

Unreacted SiO gas flow up through the furnace where it condensates to Si, SiC and SiO_2 in the cooler parts of the furnace (1.10)(1.11)[1]. A low temperature at the top of the furnace is wanted as the condensation is exothermic and is faster at lower temperature.

$$2SiO_{(g)} = Si_{(s)} + SiO_{2(s)} \qquad \Delta H^0_{298} = -705.0kJ \tag{1.10}$$

$$3SiO_{(g)} + CO_{(g)} = 2SiO_{2(s)} + SiC_{(s)} \tag{1.11}$$

The rest of the gas, consisting of CO/CO_2 and SiO oxidizes the charge top and leaves the furnace through the exhaust. The SiO in the gases can be condensated to microsilica according to reaction (1.3) and the remaining gases can go through an energy recovery system [3].
The yield in the for the silicon process is defined by equation (1.12).

$$Si_{yield} = \frac{Si_{tapped}}{SiO_{2added}} \tag{1.12}$$

The loss comes mainly from SiO gas escaping the furnace, but Folstad and Tangstad has shown that some Si goes into a slag that accumulates in the furnace [6]. The main way of increasing the yield is to increase the rate SiO reacts with carbon (1.4)(1.10) to prevent the SiO to exit through the exhaust. This can be done by having a high SiO reactivity of the carbon material [1]. Another way is to try to ensure a low temperature in the outer areas of the furnace. Le Chatelier's principle states that lowering the temperature would drive an endotherm reaction forward, and the SiO condensation (1.3) is endotherm. Stoking can also be done to increase the yield. Stoking is done by inserting a long rod to shift the material toward the high temperature zone. It also compacts the cavity, prevents formation of gas channels, and ensures that condensates do not glue up the charge [3] [2]

2 Theory

2.1 Silicon Carbide

Silicon carbide (SiC) is a non oxide-ceramic used in several industries. SiC has several properties that makes it great in high temperature electronic devices as well as an abrasive and for cutting. These qualities include high hardness, high melting point, good thermal and chemical stability, and high oxidation and erosion resistance. SiC is traditionally produced in the Acheson process, where silica sand is reacted with carbon at temperatures between 2200-2500°C. It is important in the silicon and ferrosilicon production as an intermediate product as mentioned in 1.1.[7] [8] [9] SiC has several different polytypes which falls into two main categories, cubic SiC (beta-SiC) and non-cubic SiC (alpha-SiC). Experiments by Baumann has shown that alpha-SiC is produced at temperature higher than 2100°C with higher temperatures creating higher percentage of alpha-SiC[10]. Jayakumari and Tangstad found that beta-SiC would transform into alpha-SiC at 2100°C, aided by higher amount of elemental silicon, and they found that gaseous SiC would condensate as alpha-SiC at 2000°C[11].

2.1.1 SiC oxidation

Experiments on SiC, in oxygen containing atmosphere and at elevated temperatures, have shown that SiC oxidizes. The oxidation of SiC is generally described as two different regimes. Active oxidation, which happens at low partial pressures of oxygen, and passive oxidation. In passive oxidation a protective layer of SiO_2 is created on the surface, while in active oxidation the SiO_2 is usually volatized.[12] [13] [14]

Experiments by Park et al.[15] at 1200°C in air, shows that dense layers of oxidized silicon form the surface of the SiC. They found SiO, Si_2O_3, and SiO_2 as the oxidation species in this layer with Si_2O_3 as the dominant species.

Investigations by Amy et al.[16] has shown that oxidation of SiC will happen at room temperature, and that the reactiveness is determined by the SiC polytype.

2.2 Slag properties

Electrical tests have shown that the conductivity in liquid slags is largely ionic which shows that liquid slags have ionic structures[17]. Herasymenko[18] [19] was the first to theorize that the oxides

in liquid slag form complexes with the oxygen. He proposed that the common elements in steel manufacture had a varying likelihood of forming complexes. Elements like Ca, Mg, and Mn have a very small inclination to form complexes and would exist almost exclusively as free cations in the slag. Elements like Si and Ti have a strong tendency to form complexes and would largely be found as anion complexes in the liquid slag. Elements like Fe, Cr, and Al have an amphoteric character and would therefore mainly form anions in basic slags, and form cations in acidic slags. The slag structure is decided by how the complex forming slags create structures and by how other elements break up that structure or join the structure. Silicate slags form tetrahedrons as SiO_4^{4-}, where the silicon cation is surrounded by 4 oxygen anions. These tetrahedra joins together by bridging oxygen to form larger structure. Cations like Na^+, Ca^2+, Mg^2+, and Fe^2+ have a tendency to breaks the bridging oxygen bonds to create structures with non binding oxygen and free oxygen, O2-. Cations like Ti^4+, P^5+, Al^3+, and Fe^3+ forms tetrahedra and can therefore join the silica slag to extend the slag structure.[17] Viscosity in slag is dependent on the degree of polymerisation, where high degree of polymerisation gives high viscosity, and the temperature will also affect the viscosity through the Arrhenius relations.[20]

Surface tension in a fluid occurs because the cohesive forces within the bulk fluid are stronger compared to the attractive forces between the fluid molecules and the surrounding gas. This causes there to be an asymmetric force field at the surface which puts it under tension. The largest parameters determining the surface tension are the temperature and the composition of the different phases. The compositions determine the cohesive forces inside the fluid and the attractive forces between the gas and the fluid molecules. Temperature tends to lower the surface tension. It does so by increasing the energy and velocity of the molecules, which works against the intermolecular cohesive forces. Exceptions to this can be liquids with high SiO_2 content. In these liquids, the SiO_2 forms complex molecular structures as mentioned earlier. Rising temperature will cause the structure to start to break up, which causes there to be an increasing amount of dangling bonds at the surface. This causes the surface free energy to increase which gives a greater surface tension.[21]

2.3 Wetting behaviour

The wetting behaviour of a liquid slag on a solid is characterized by its contact angle (θ) and is governed by the interactions between the interfacial tensions $\gamma_{LG}; \gamma_{LS}; \gamma_{SG}$, and the gravitational forces. The relationship between the interfacial tensions and the contact is given by Young's equation (2.1)[22].

$$\gamma_{SG} = \gamma_{LS} + \gamma_{LG} \cdot cos\,(\theta) \tag{2.1}$$

The wettability of the system is primarily affected by the temperature, chemical reactions, and surface topography. The temperature generally increases the wettability and the wettability increases further if chemical reactions are involved[23]. An increase in roughness of the surface topography causes the contact angle to decrease for non wetting systems and increase for wetting systems. The relationship between the roughness and the contact angle was given by Wenzle[24] as equation (2.2), where R is the ratio between the true surface area and the theoretical smooth surface area .

$$cos\,(\theta_{rough}) = R \cdot \cos\,(\theta_{smooth}) \tag{2.2}$$

An increasing porosity of the solid has been found to decrease the contact angle of wetting systems, but has little effect on non wetting systems[25]. Liquid viscosity will affect the dynamic wetting by slowing down the wetting rate, but it has little effect on the final contact angle[26].
Investigations into dynamic wetting and the effects of surface roughness have been done by Cazabat and Stuart[27]. They found that for wetting liquids on rough surfaces are initially being driven by capillary forces much like how it spreads on smooth surfaces, but is rapidly followed by a regime where the liquid rapidly spreads into the pores and crevices. Here the capillary driving force is much larger and the wetting speed is much higher than when compared to wetting on a smooth surface. The crevices and pores eventually consumed the liquid and the spreading slowed down. They also found that while the spreading force was given by the apparent contact angle at high angles, at low angles the local angles given by the crevices and pores dominates and the average force will only depend on the surface structure.[27]

2.3.1 Reactive wetting

Reactive wetting occurs when there are chemical reactions between the fluid and the substrate. The reaction causes a mass transfer across the interface which lowers the interfacial free energy, which in turn increases wettability. Aksay et al.[28] proposed to change γ_{LS} in Young's equation (2.1) with

$$\gamma_{LS} = \gamma^0_{LS} + \Delta G_{LS} \tag{2.3}$$

,where $\Delta \mathrm{G}^{LS}$ is the change in Gibbs free energy due to the reaction, to calculate the contact angle in reactive systems. Investigation by Landry and Eustathopoulos[29] showed that the contact angle in a reactive system decreases as the reaction progresses while at the same time a new product layer is produced on the substrate surface, and that the finale angle ends up being very close to the angle that would be found if the liquid were directly wetting the product.

2.3.2 Oxide layer

Wetting on materials covered by an oxide layer changes the wetting properties. Investigations into the influence of oxidation of silicon species shows that the formation of surface silicon oxides causes the wettability to go down in wetting systems. Variations in surface oxygen concentrations leads to different interfacial tensions which can lead to uneven wetting. The oxide layer got less stable with rising temperatures which made a higher oxygen pressure required to keep a stable oxide layer. The wettability were found to be largely dependent on the oxidized layer and the temperature, with increasing superheating leading to increased wetting in all cases.[30]

Investigations into the wetting of silicon on oxidized SiC showed that at initial conditions, the silicon wetted the oxidized SiC with a contact angle of around 75°. This was quite close to the contact angle between silicon and SiO_2 (83°). The contact angle rapidly dropped to around 40°as the silicon consumed the oxide layer. They concluded with that the wetting behaviour was largely governed by the oxide layer at the start, but this rapidly changed as the silicon infiltrated the oxide layer and got in direct contact with the SiC.[31]

2.3.3 Wetting of silicon slags

Investigation of wetting between SiO_2-CaO slag and SiC by Safarian and Tangstad[32] checked four different slag composition with SiO_2% between 47-60%. The wetting test were done on compressed SiC powder and on a solid SiC substrate. The tests showed that the slags had a relatively high wettability with wetting angles from $20^\circ - 73^\circ$ with the solid SiC, and the slags had very low contact angles on the SiC powder before they penetrated into the substrate. They found that the slag composition mainly determined the degree of wetting, with higher SiO_2 content led to higher contact angle, while the heating rate had no significant effect.

Mailliart, Chaumat and Hodaj[33] studied the wetting of slag composed of $62wt\%\, SiO_2$; $23\%\, CaO$; $15\%\ Al_2O_3$ on polycrystalline silicon carbide at temperatures ranging from 1100 to 1590°C. They found that the slag a contact angle of around 20°for temperatures 1300-1500°C and around 50°at 1590°C, and that the spreading kinetics increases with temperature. They observed bubble formation which they theorized could be reactions between SiO_2 and SiC and between Al_2O_3 and SiC (2.4) (2.5), but they believed it as more likely to be oxygen dissolved into the liquid slag given the oxygen pressure of the atmosphere.

$$SiC_{(S)} + SiO_{2(l)} = SiO_g + CO_g \tag{2.4}$$

$$SiC_{(s)} + Al_2O_{3(l)} = Al_2O_g + SiO_g + CO_g \tag{2.5}$$

Wetting experiments of 55wt% SiO_2 - 30wt% CaO - 15wt% Al_2O_3 slag on solid SiO_2 have been done by Seo et al.[34] The contact angle was found to be 82°at 1350°C, 76°at 1400°C, and 31°at 1470°C. They noted that the angles were notably low at 1470°C, which they suggested might be caused by the wetting mechanism changing at higher temperatures to a case were layers of diffused products contributes greatly to the wetting.
Wetting experiment of CaO-SiO_2 slags on solid SiO_2 at 1600°C by Yoo et al.[35] found an apparent contact angle of around 55°for slags with composition 67.5wt% SiO_2 - 32.5wt% CaO, and an apparent contact angle of around 20°for slags with composition 46wt% SiO_2 - 54wt% CaO.

2.4 Slag in the silicon and ferrosilicon processes

Silicon production has long been seen as a slag free process, but investigations and excavations of furnaces shows that a significant amount of slag exists in the furnaces. The slag in the silicon and ferrosilicon processes are mainly composed of SiO_2, CaO, and Al_2O_3. The ternary phase diagram for the $SiO_2-CaO-Al_2O_3$ system is shown in figure 3.

Investigations by Folstad and Tangstad[6] shows that $SiO_2-CaO-Al_2O_3$ slag accumulates in furnaces, which can cause clogging during tapping and lower the reaction areas in the furnaces. The investigation shows further that the accumulated slag is mainly up against the side walls of the furnaces, but can also accumulate underneath the Si metal. Illustrations of the insides of the excavated furnaces are shown in figure 4. The slags were usually found together with SiC with varying particle sizes. EPMA analysis showed that the slag had a higher SiO_2 content in areas above the tapping hole than from below. The analysis also showed that the slag compositions varied more above the tapping channel than below.

Previous investigation of slag in tapping areas from Si furnaces, by Folstad et al.[37], supports what was found by Folstad and Tangstad. They found that the slag found were mainly composed by $SiO_2-CaO-Al_2O_3$, that the slag were higher in SiO_2 above the tapping hole than below, and in addition they found that the slag had an almost constant CaO/Al_2O_3 fraction.

Investigations of slag compositions in the ferro silicon process have been done by Jusnes et al.[38] with slag collected from a FeSi75% submerged arc furnace. The average composition of the slag tapped from one of the furnaces investigated were 37 $wt\%\ SiO_2$, 36 $wt\%\ Al_2O_3$, *and* 28 $wt\%\ CaO$. The Al_2O_3 content of the slag comes from impurities in the quartz while the CaO is added to the furnace to decrease the viscosity of the slag. The viscosity was found to range between 1.9 and 6.6 poise at 1800°C under normal tapping conditions. Slag sample collected when the slag had visually very high viscosity were found to have a SiO_2 content of 72 wt%.

Samples taken from the top of the furnace contained mainly unreacted SiO_2, carbon, and slag containing mainly SiO_2 and FeO. There was also some Si metal that could have come from materials moving up through the furnace or it could have been an indication that the surface temperature was sufficiently high to drive the metal producing reaction.

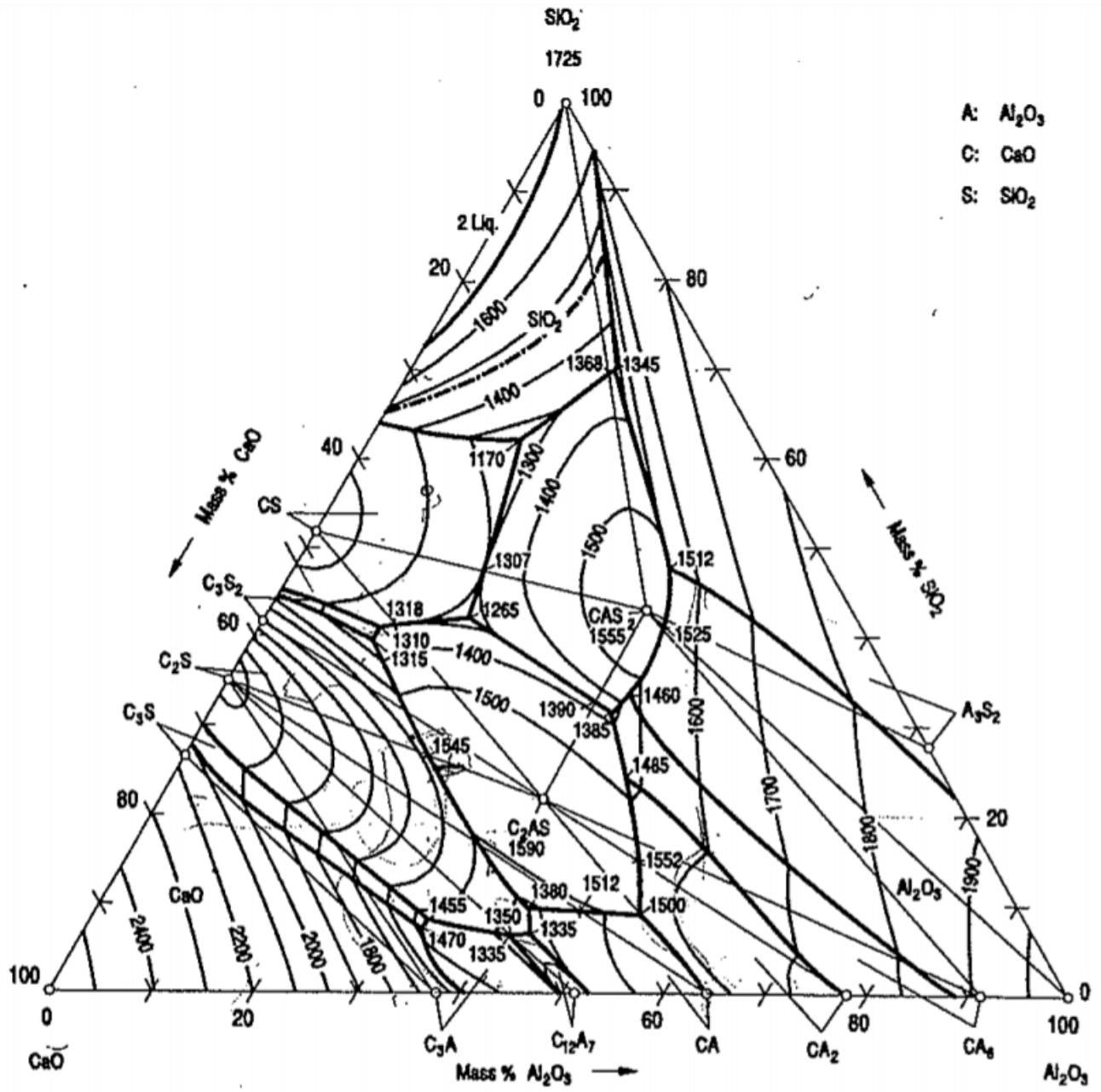

Figure 3: Ternary phase diagram of the $SiO_2-CaO-Al_2O_3$ system.[36]

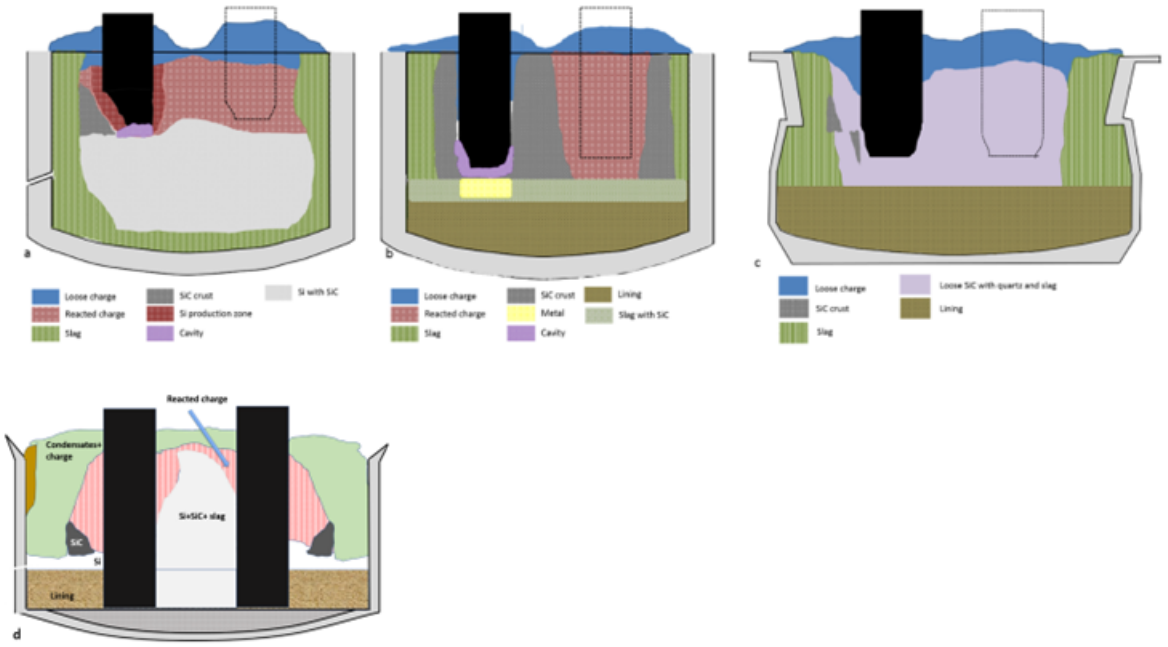

Figure 4: The zones found in four different furnaces during excavation [6]

Slag samples taken from the electrode leg consisted of SiO_2 and a slag phase of SiO_2 and FeO. FeO in the slag were expected as iron oxide pellets were added to the furnace. The reason that FeO was not found in the tapped slag were probably caused by that FeO reduce at a higher area in the furnace than SiO_2.

Nell and Joubert [39] investigated the phase chemistry of digout samples from high grade ferrosilicon furnaces that were experiencing problems. They found that the samples contained slag and SiC, where the slag had an unexpectedly high percentage of alumina. The oxide phase assemblages found were:

- $Ca_2Al_2SiO_7$; $CaAl_2Si_2O_8$; $CaAl_{12}O_{19}$
- $Ca_2Al_2SiO_7$; $CaAl_4O_7$
- $Ca_2Al_2SiO_7$; $CaAl_2Si_2O_8$; Al_2O_3
- $CaAl_2Si_2O_8$; $Al_6Si_2O_{13}$; $slag$

The samples were found to have a heterogeneous composition with the alumina content varying

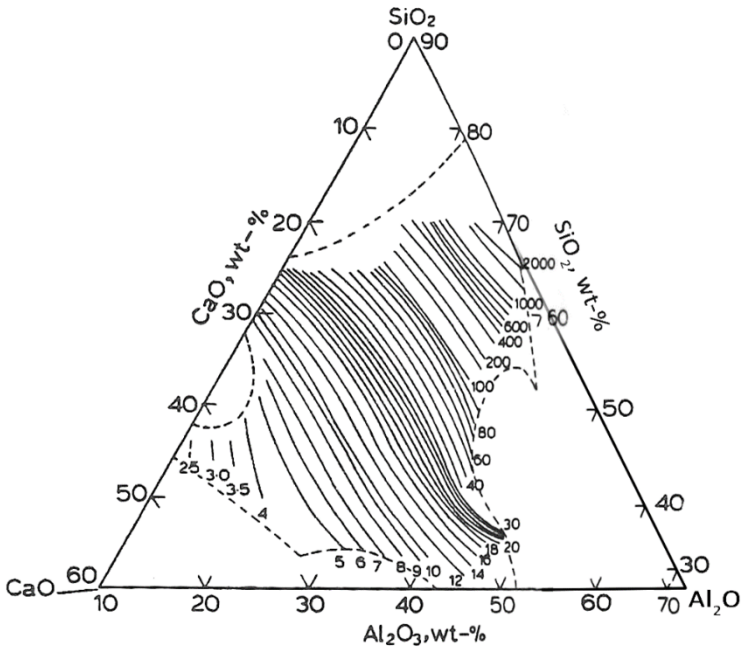

Figure 5: Iso viscosity of $SiO_2-CaO-Al_2O_3$ slags at 1500°C[4]

by up to 30% over hundreds of microns. This suggested that the phases did not crystallize under equilibrium conditions.

2.5 $SiO_2-CaO-Al_2O_3$ slags

2.5.1 Viscosity

The viscosity of $SiO_2-CaO-Al_2O_3$ at 1500°C is shown in figure 5. The viscosity in molten $SiO_2-CaO-Al_2O_3$ slags are largely dependent on the depolymerisation of the slag structure. The Al_2O_3 act as a substitute for the SiO_2 in the slag structure which keeps the viscosity largely constant as long as $SiO_2+Al_2O_3$ is constant. This makes the slags viscosity highly dependent on the CaO fraction as it breaks up the slag structure. This is further supported by several investigations[40] [41]. From figure 5 on can see that the largest effect on the viscosity happens at low percentages of CaO. Between around 5% to 6% there is a decrease of around 1000 poise, while between 18% to 35% the decrease in viscosity are under 100 poise. A viscosity model for $SiO_2-CaO-Al_2O_3$ slag has been created using Raman spectroscopy techniques. In this model the

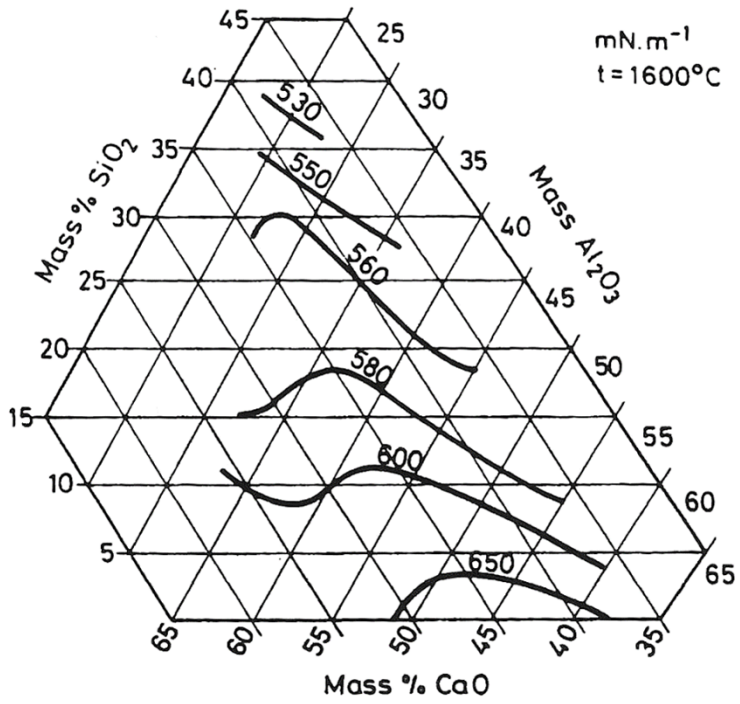

Figure 6: Iso tension of $SiO_2-CaO-Al_2O_3$ slags at 1600°C[21]

viscosity can be found by looking at the ratio between the low and high wavenumber vibrational bands (R), and the Arrhenius equation. R was fitted to the Arrhenius equation using curve fitting. Equation (2.6) shows the model.[42]

$$log(\eta) = -14.80 - 1.87 \cdot R + \frac{33943 \cdot R^{0.27}}{T} \tag{2.6}$$

2.5.2 Surface tension

Isotension lines at 1600°C for the $SiO_2-CaO-Al_2O_3$ system is shown in figure 6. Here it is shown that the tension in the system decreases with increasing SiO_2 content. This is further shown in figure 7. Figure 8 shows the surface tension against Al_2O_3 concentration. From this it is shown that the surface tension increases with increasing Al_2O_3 content.

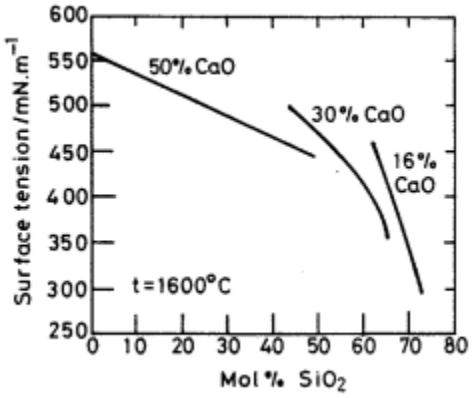

Figure 7: Surface tension of $SiO_2-CaO-Al_2O_3$ slags by SiO_2 content at 1600°C[21]

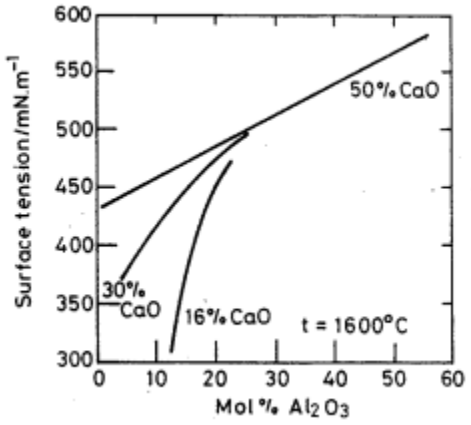

Figure 8: Surface tension of $SiO_2-CaO-Al_2O_3$ slags by Al_2O_3 content at 1600°C[21]

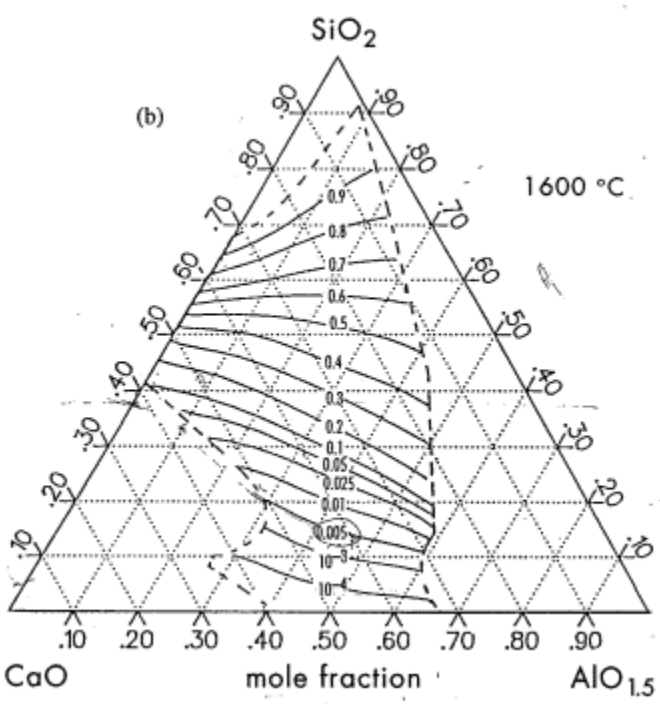

Figure 9: Thermodynamic activities of SiO_2 at 1600°C[43]

2.5.3 Thermodynamic activity

The thermodynamic activity shows how large chemical potential the different species in a real substance have. The thermodynamic activity of a specie is dependent on pressure, temperature, and composition of the substance. Thermodynamic activities of SiO_2, CaO, and $AlO_{1.5}$ at 1600°C are shown in figures 9-11[43].

From figure 9 one can see that at low concentration of constant SiO_2% a higher concentration of CaO decreases the activity of SiO_2, while a higher concentration of Al_2O_3 increases it. This seems to be true for SiO_2 concentrations from 0% to around 60%. At 60% it switches and higher concentration of Al_2O_3 lowers the activity, while higher concentration of CaO increase it.

From figure 10 one can see that the activity of CaO rapidly drops with decreasing amount of CaO with higher concentration of SiO_2 decreasing the activity of CaO more than Al_2O_3.

From figure 11 one can see that CaO lowers the activity of $AlO_{1.5}$ more than SiO_2 does.

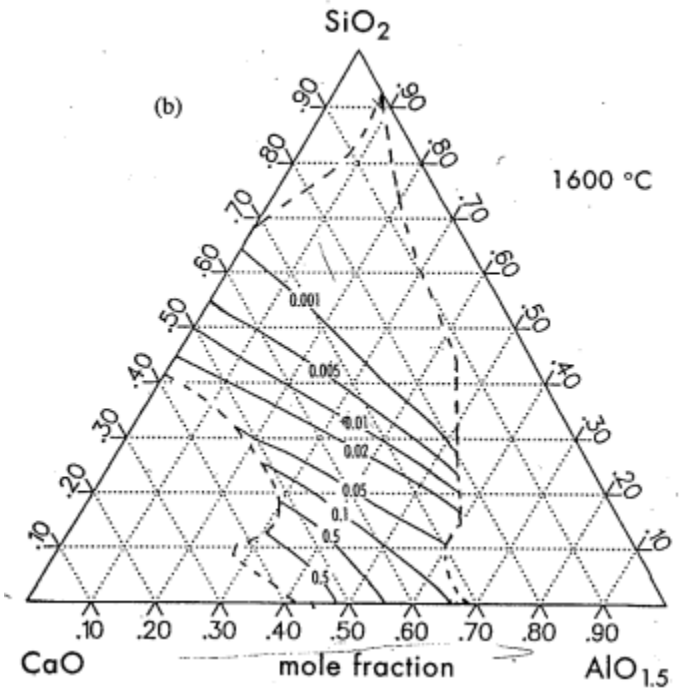

Figure 10: Thermodynamic activities of CaO at 1600°C[43]

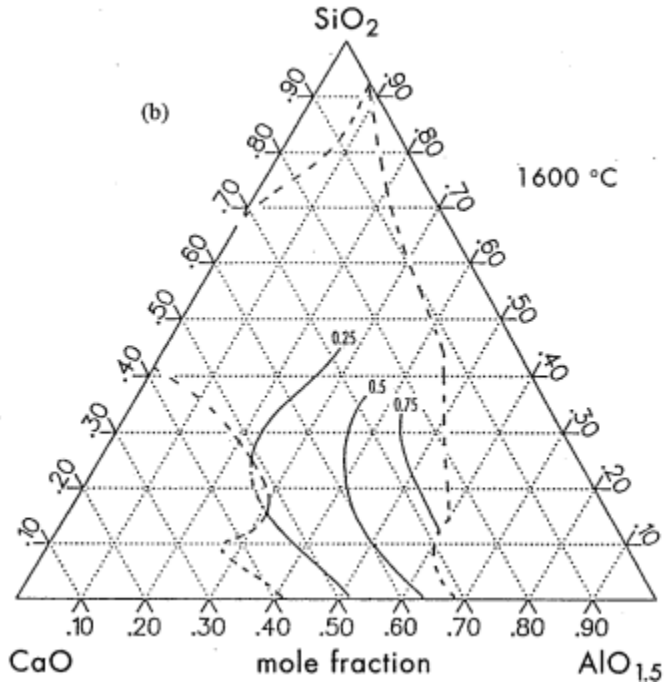

Figure 11: Thermodynamic activities of $AlO_{1.5}$ at 1600°C[43]

2.5.4 Reactions between $SiO_2-CaO-Al_2O_3$ slags and SiC

Hou et al.[44] have investigated the reactions between $SiO_2-CaO-Al_2O_3$ slags and SiC particles. They tested slags with SiO_2 content between 29% and 56%. They found that the basicity had a large effect on the weight loss rate of the SiC particles. The weight loss rate decreased with increasing basicity up to 0.8, but at rising basicity over 0.8 the weight loss rate was found to be increasing up to a basicity of 1.2. They explained this by the fact that rising basicity lowers the activity of SiO_2 which inhibits the reaction, but it also lowers the viscosity which gives better kinetic conditions for mass transfer which promotes the reaction. The thermodynamic activity dominates the reaction at basicity lower than 0.8, and at higher basicity the kinetic factors dominate. The Al_20_3 content was found to decrease the weight loss rate drastically. This was because Al_20_3 lowers the activity of SiO_2 and it raises the viscosity of the slag, which both inhibits the reaction. Increasing temperatures were found to increase the weight loss rate of the SiC. This is because the rising temperature increases the partial pressure of SiO gas and it decreases the viscosity in accordance with the Arrhenius equation.

3 Experimental

3.1 Materials

The slag used were produced by Shokouh Haghdani[45]. The intented composition of the different slags and the composition confirmed by XRF are shown in table 1. The atomic percent, basicity ($\frac{CaO}{SiO_2+Al_2O_3}$), liquidus temperature, and SiO_2 activities for the slags are shown in table2. The slag samples had a weight of $25 \pm 5\ mg$ Three different substrates were used. The substrates were made from sintered SiC from a crucible, SiC produced by Haley Hoover by transformed coal[46], and alpha SiC from Washington Mills. The SiC pieces made from transformed coal were created in a crucible were at the bottom SiO gas was created by reaction 1.8. The SiO gas then travels through carbon material which creates SiC by reaction 1.4.[46] The sintered SiC were checked with XRD to be over 99% SiC, the composition found are shown in figure 3. The composition of the transformed coal are shown in table 4.

The sintered SiC substrate were made by cutting out circular discs with 8 mm diameter from a

Table 1: The intended and XRF confirmed compositions of the slags

Slag no.	Intended composition			XRF composition		
	SiO_2 [wt%]	CaO [wt%]	Al_2O_3 [wt%]	SiO_2 [wt%]	CaO [wt%]	Al_2O_3 [wt%]
1	55	20	25	53.43	20.46	26.11
2	55	30	15	54.76	28.88	16.35
3	55	40	05	53.36	41.40	5.24
4	60	20	20	58.41	20.77	20.84
5	60	30	10	59.84	29.32	10.84
6	70	20	10	68.20	21.16	10.63

Table 2: Composition in atomic percent, basicity ($\frac{CaO}{SiO_2+Al_2O_3}$), liquidus temperature, and SiO_2 activities for the slags. The liquidus temperature is estimated from figure 3 [36]. The SiO_2 activities are estimated from figure 9 [43]

Slag no.	SiO_2 [at%]	CaO [at%]	Al_2O_3 [at%]	$\frac{CaO}{SiO_2+Al_2O_3}$	Liquidus [°C]	SiO_2 activity
1	58.89	24.16	16.96	0.32	1460	0.55
2	57.44	32.46	10.11	0.48	1300	0.56
3	52.93	44.00	3.06	0.79	1340	0.58
4	62.85	23.94	13.21	0.31	1390	0.65
5	61.29	32.17	6.54	0.47	1340	0.65
6	70.21	23.34	6.45	0.30	1450	0.79

crucible. The substrates made from transformed coal and alpha SiC were made by grinding them flat and into a shape that would fit in a 1 cm^2 square. The grinding were done with a MD-Piano 220 diamond grinding disc.

Table 3: Composition of the sintered SiC substrate. Carbon were not measured and the results were normalized to 100%

Si [at%]	Fe [at%]	Ti [at%]	Co [at%]	Ga [at%]
99.9	0.021	0.020	0.010	0.009

Table 4: Composition of the transformed coal substrate. Some unreacted coal exists in the pieces.

SiC [wt%]	Si [wt%]
72	7

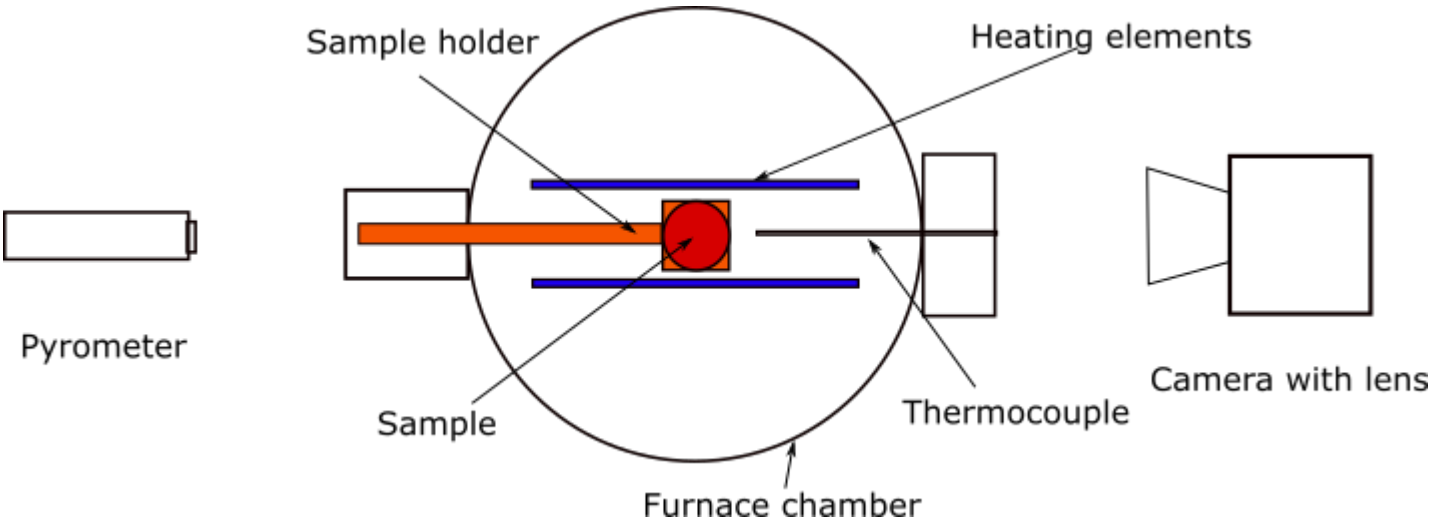

Figure 12: Illustration of the wetting furnace setup

3.2 Equipment

The wetting test is done in a cylindrical furnace, using the sessile drop method. On two of the sides of the furnace there are windows. One of the windows allow a pyrometer to measure the temperature inside the furnace. The other window allows pictures to be taken of the sample with a camera. The sample holder is made of graphite and can slide in and out of the furnace. When in its inner most position, it is located in the middle of the graphite heating elements, and the position is such that a thermocouple can properly measure the temperature of the sample. Inside the furnace there are also graphite radiation shields. The thermocouple is a B type thermocouple which can measure temperature to around 1800°C. The thermocouple is calibrated using the known melting points of copper and iron. The temperature measured by the thermocouple guides the operation of the furnace to be at the correct temperature at the correct time. The pyrometer is a Keller PZ40 pyrometer with working temperatures between 900-2400°C. It uses a two color measuring technique. It is pointed toward the middle of the sample holder. The camera is an Allied Vision Prosilica GT 2000C with a Navitar 12X zoom lens. A simplified illustration of the wetting setup is shown in figure 12. The characterization was done on a Zeiss ultra 55 SEM, with a Bruker EDS. The EDS results were processed by the program Esprit 1.9.

Magnification	70x	100x	1000x
Pixel size [$\mu m^2/px$]	23.81	11.09	0.12

Table 5: Pixel size at the different magnifications

3.3 Method

3.3.1 Substrate preparation

The sintered SiC substrate were made by cutting out circular discs with 8 mm diameter from a crucible. The substrates made from transformed coal and alpha SiC were made by grinding them flat and into a shape that would fit into the 1 cm^2 square sample holder. The grinding were done with a MD-Piano 220 diamond grinding disc.

3.3.2 Substrate porosity analysis

SEM SE pictures were taken of the substrates. They were taken with 70x, 100x, and 1000x magnification. The pixel sizes in the porosity analysis are shown in table 5. The porosity analysis were done using ImageJ. The threshold were set to were the pores appeared black and the bulk material were mostly white. Analyse particles were done with sizes 1-Infinity. The resulting data were then plotted.

3.3.3 Wetting calibration

Calibration of the thermocouple were done at the start of each furnace session or after ten runs. It is done by heating iron and copper past their melting point and observing when they were completely melted. The measured temperature at the time of melting were compared to the known melting points of the metals. Linear regression between the measured melting points were done to get the calibrated temperature over the whole temperature span.

3.3.4 Wetting test

The temperature profile for the wetting test were created. The general temperature profile is shown in13. The hold temperature were adjusted to ensure the calibrated temperature were 1600°C. The substrate was placed in the sample holder. The slag sample was weighed and placed on top of

the substrate. The sample holder was carefully slid into the furnace chamber and the chamber was closed up. The air was evacuated from the furnace chamber using a vacuum pump until the pressure reached under 2 mbar. The vacuum pump was closed off and the furnace chamber was flushed with argon at a rate of 1 l/min. When the pressure reached atmospheric pressure the argon rate was lowered to 0.1 l/min. The temperature profile was then loaded into the furnace program and the program was turned on. Pictures were automatically taken at a rate of 1 per second. The pictures were analysed using a post processing program that measured the contact angles.

Test with six slags of different composition were done on the sintered SiC. Test with two slags of different composition were done on the transformed coal. Test with two slags of different composition were done on the alpha SiC. The different slag-substrate pairs are shown in table 6. 3 samples were done for each pair.

Table 6: The slag-substrate pairings numbered

Pair				Substrate
#1	55	20	25	Sintered SiC
#2	55	30	15	Sintered SiC
#3	55	40	5	Sintered SiC
#4	60	20	20	Sintered SiC
#5	60	30	10	Sintered SiC
#6	70	20	10	Sintered SiC
#7	55	20	25	Transformed Coal
#8	70	20	10	Transformed Coal
#9	55	20	25	Alpha SiC
#10	70	20	10	Alpha SiC

3.3.5 SEM/EDS analysis

The samples were characterized by using EDS. The EDS were done at two different areas on each sample. At each area at least two sampling points were chosen for each distinct area. Each point was collected over 30 seconds. The spectrums were quantified using a ZAF analysis.

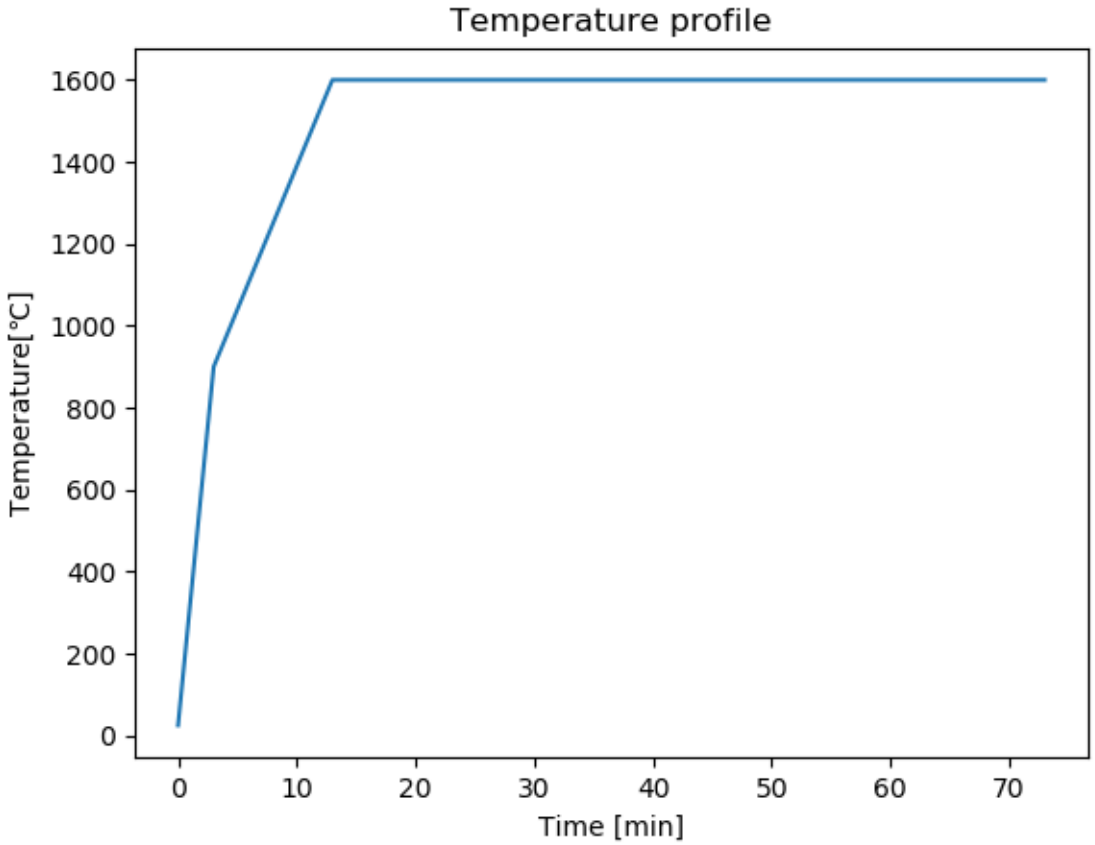

Figure 13: Temperature profile for the wetting experiments. 3 minutes to 900°C, 10 minutes to 1600°C, hold up to 1 hour

4 Results

4.1 Porosity

Porosity of the substrate pieces were analysed from SEM pictures using ImageJ. SEM pictures, average porosity, and pore size distribution for the substrates are shown here.

4.1.1 Sintered SiC

Figure 14 shows the pore percentage for the pieces of sintered SiC. Figure 15 shows the pore size distribution of the pores for the pieces of sintered SiC. Figure 16 shows a SEM SE picture with its corresponding porosity contour at 1000x magnification. SEM pictures of all pieces used in the porosity analysis are shown in appendix A. Pixel size for sintered SiC piece 1-6 is 0.12 [$\mu m^2/px$] From figures 14-16 one can see that he porosity of the sintered SiC were all under 15% with piece number 2 having as low as 4%, the pores found are of small sizes, mainly under 20 pixels large, and that the surface roughness does show up as pores on the contours.

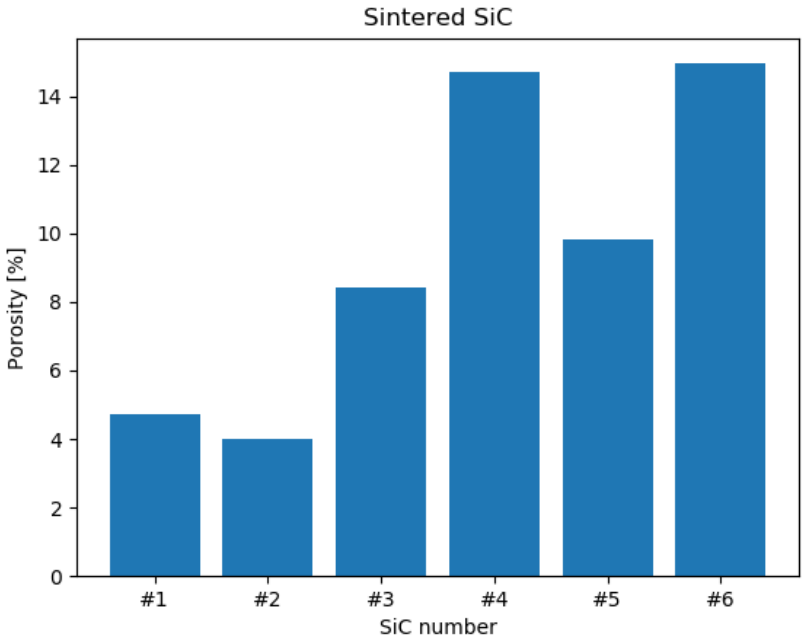

Figure 14: Average porosity of 6 pieces of sintered SiC

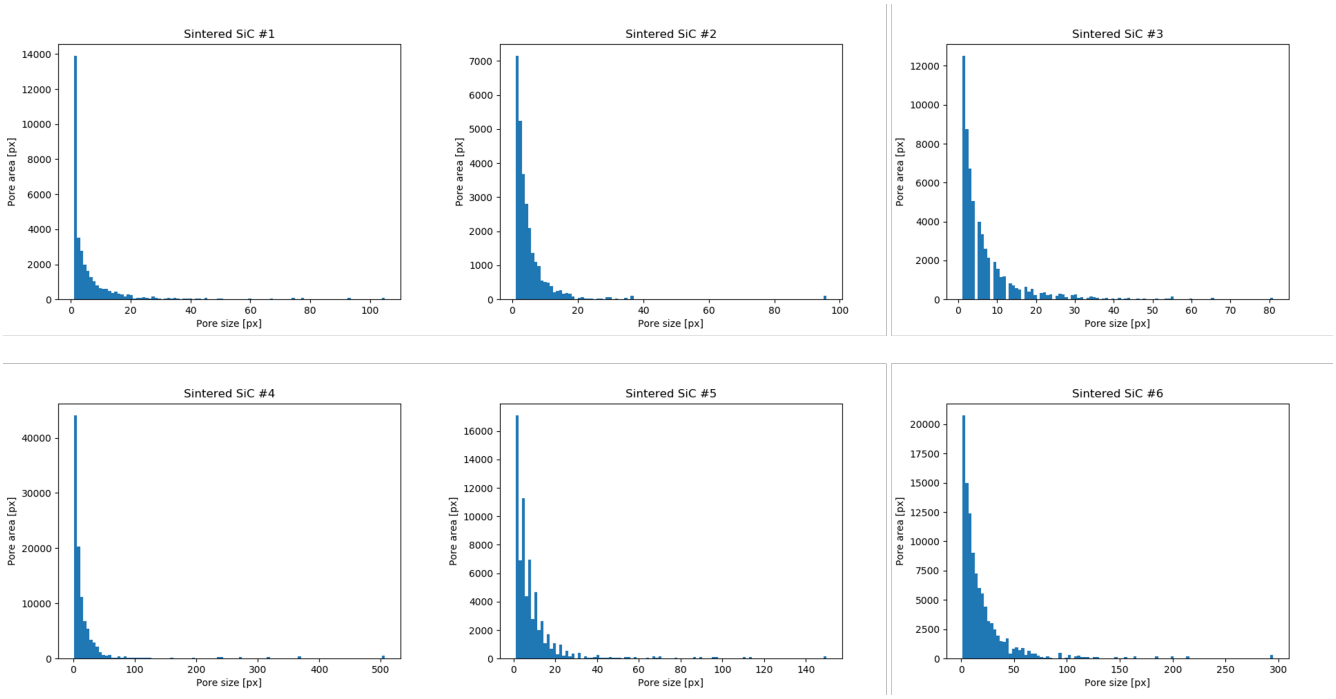

Figure 15: Pore size distribution from 6 pieces of sintered SiC

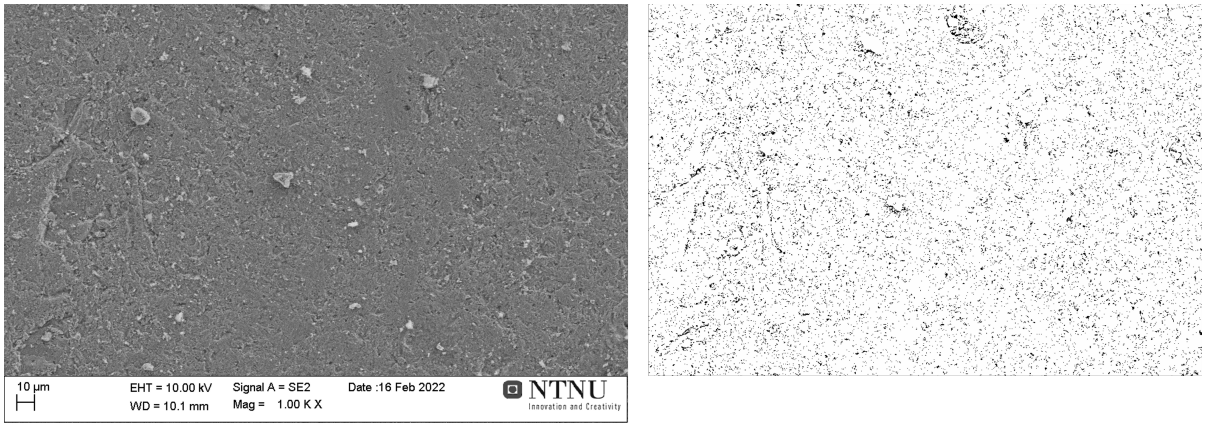

Figure 16: SEM picture (left) and porosity contour(right) of sintered SiC at 1000x magnification

4.1.2 Transformed coal

Figure 17 shows the pore percentage for the pieces of transformed coal. Figure 18 shows the pore size distribution of the pores for the pieces of transformed coal. Figure 19 shows a SEM SE picture with its corresponding porosity contour at 70x magnification. Figure 20 shows a SEM SE picture with its corresponding porosity contour at 1000x magnification. SEM pictures of all pieces used in the porosity analysis are shown in appendix A. Pixel sizes for transformed coal pieces 1-6 are 11.09[µm^2/px]. Pixel sizes for transformed coal pieces 7-9 are 23.81[µm^2/px]

From figures 17-20 one can see that the porosity of the transformed coal were mainly over 20% with number 3, 4, and 5 reaching over 30% and number 6 reaching over 40%, there are several large pores throughout the material, and that the bulk material is also full of pores.

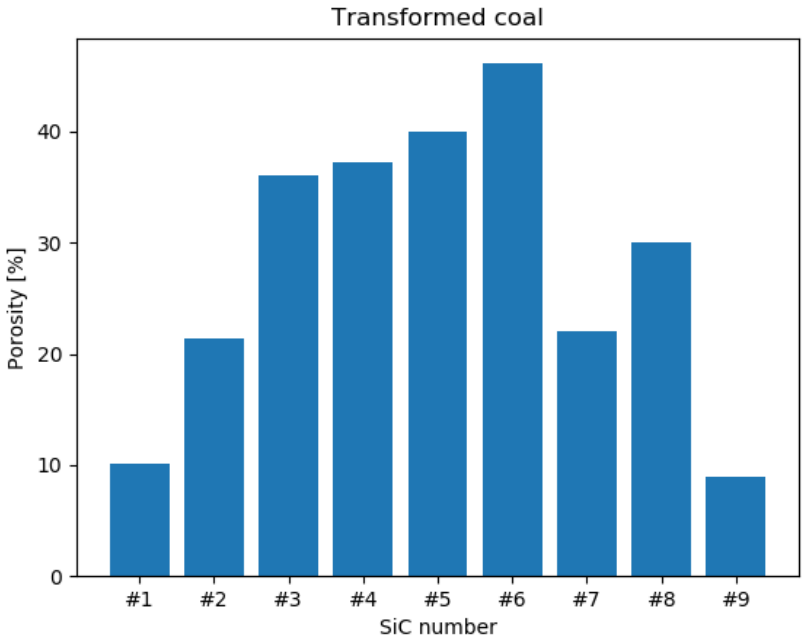

Figure 17: Average porosity of 9 pieces of transformed coal

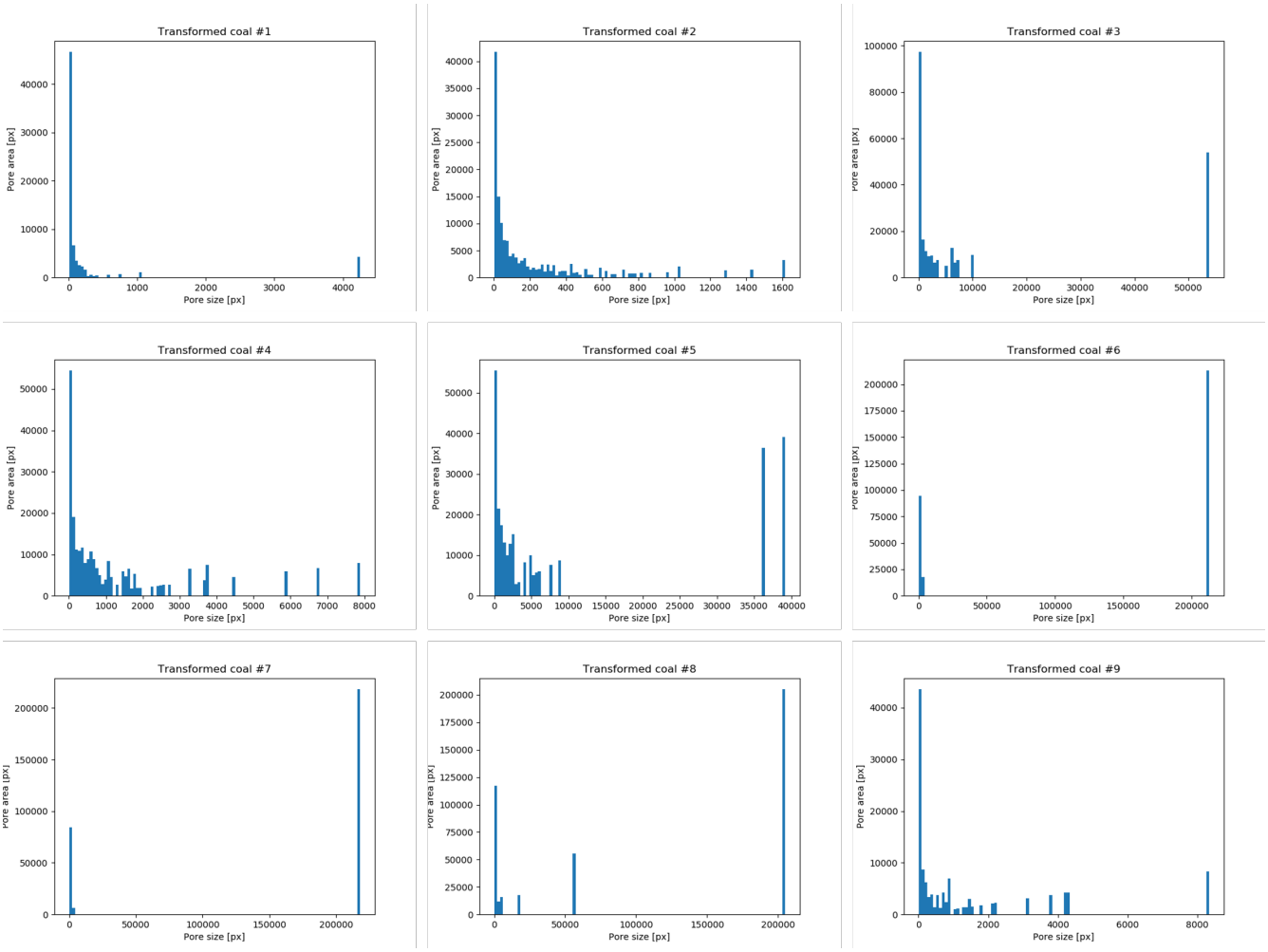

Figure 18: Pore size distribution from 9 pieces of transformed coal

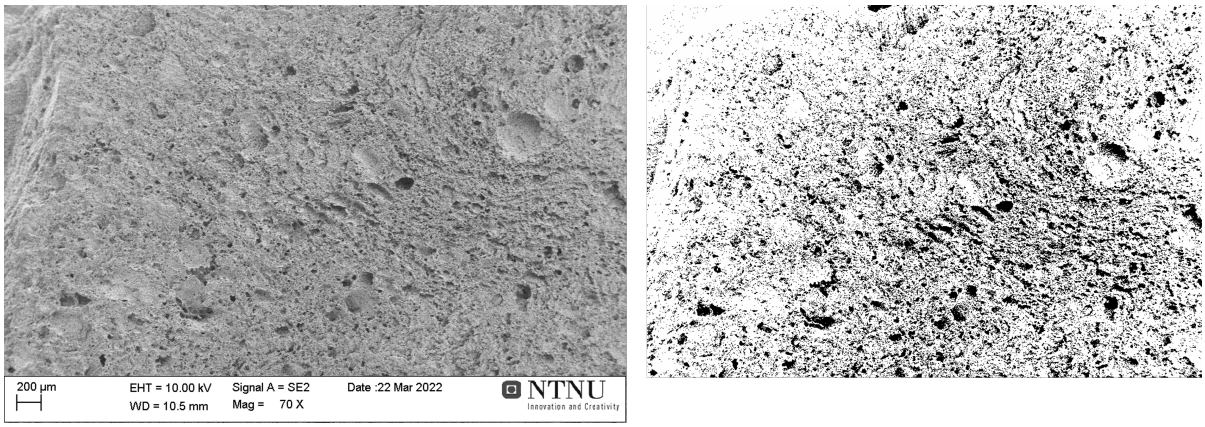

Figure 19: SEM picture (left) and porosity contour(right) of transformed coal at 70x magnification

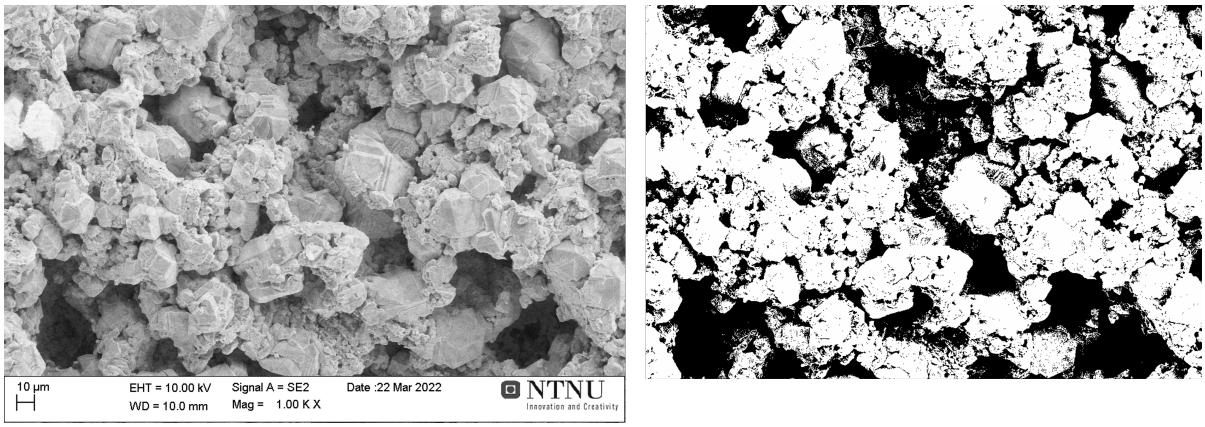

Figure 20: SEM picture (left) and porosity contour(right) of transformed coal at 1000x magnification

4.1.3 Alpha SiC

Figure 21 shows the pore percentage for the pieces of alpha SiC. Figure 22 shows the pore size distribution of the pores for the pieces of alpha SiC. Figure 23 shows a SEM SE picture with its corresponding porosity contour at 70x magnification. Figure 24 shows a SEM SE picture with its corresponding porosity contour at 1000x magnification. SEM pictures of all pieces used in the porosity analysis are shown in appendix A.Pixel sizes for alpha SiC pieces 1-6 are 11.09[µm^2/px]. Pixel sizes for alpha SiC pieces 7-9 are 23.81[µm^2/px]

From figures 21-24 one can see that the porosity of the alpha SiC were mainly over 20% with number 4 and 5 reaching over 40% and number 6 reaching over 60%, there are several large pores and crevices throughout the material, and that the bulk material is relatively pore free.

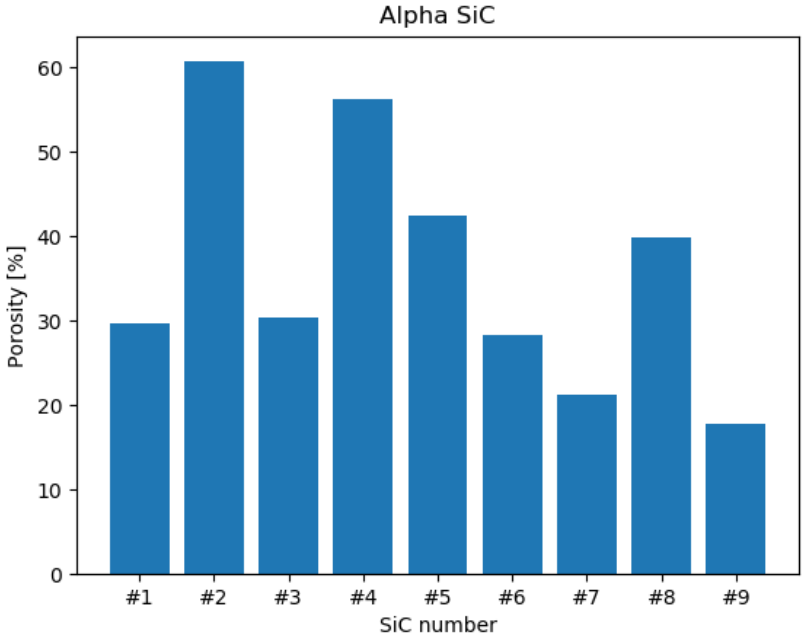

Figure 21: Average porosity of 9 pieces of alpha SiC

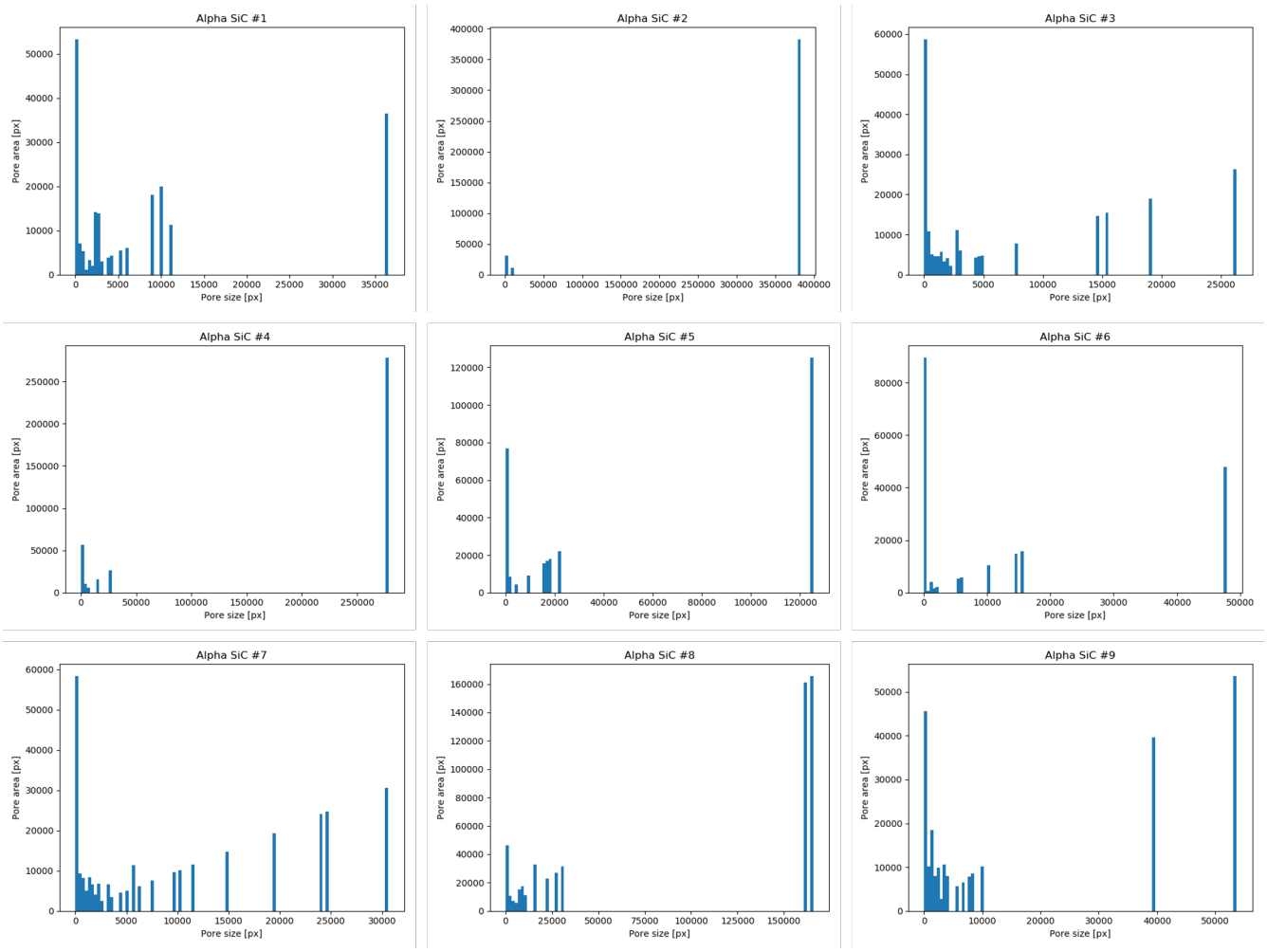

Figure 22: Pore size distribution from 9 pieces of transformed coal

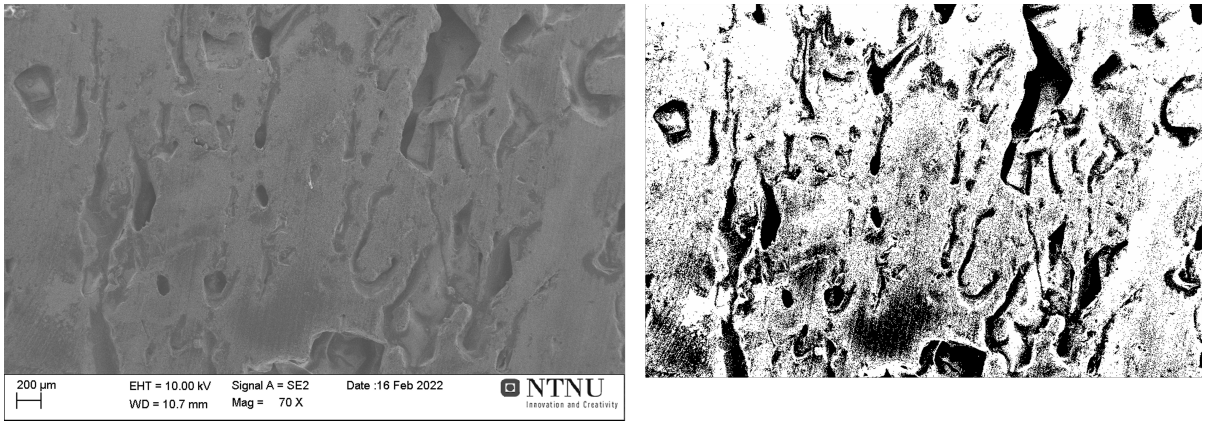

Figure 23: SEM picture (left) and porosity contour(right) of alpha SiC at 70x magnification

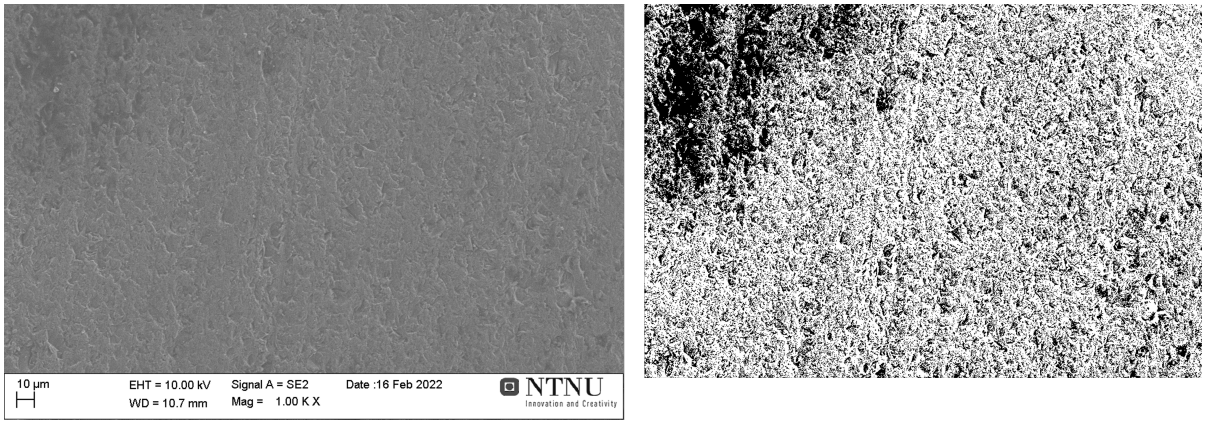

Figure 24: SEM picture (left) and porosity contour(right) of alpha SiC at 1000x magnification

4.1.4 Comparison

Figure 25 show a comparison of the average porosities of the different SiC materials. The sintered SiC shows a low porosity at under 10% and standard deviation of 4.7. The transformed coal have a larger porosity at over 25% and a standard deviation of 13.2. The alpha SiC have the largest porosity with over 35% and a standard deviation of 14.8.

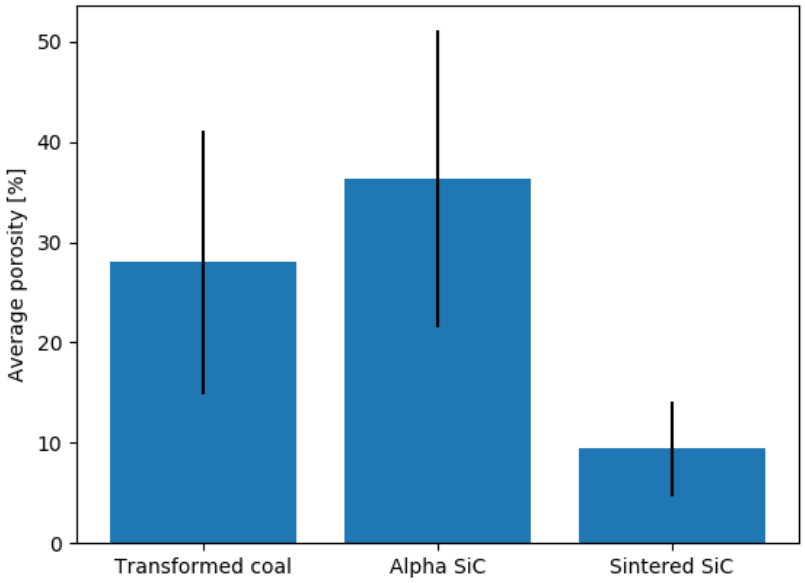

Figure 25: Average porosity of the different substrates, with standard deviation.

4.2 Wetting

Pictures from the wetting test, gathered contact angles, average contact angles, and contact angles in relation to basicity are shown here.

4.2.1 $55SiO_2 - 20CaO - 25Al_2O_3$ on sintered SiC

Plotted contact angles against time for $55SiO_2 - 20CaO - 25Al_2O_3$ on sintered SiC are shown in figure 26. Pictures from the wetting test for sample 3 are shown in figure 27.
Sample 1 showed more signs of reactions than the other samples. Bubble formation could be seen

throughout the experiment. Sample 1 had periods where it spread out over the substrate with a contact angle under 40°before it contracted back to having contact angles around or over 90°. This spreading and contracting moved the slag around on the substrate. When it contracted it left behind smaller droplets of slag on the substrate. Bubbling occurred in these droplets and they appeared to have a contact angle of over 90°.

Sample 2 also showed some signs of reactions, but they were much more subdued. No major movement were observed. The contact angle were quite constant at slightly over 90°.

Sample 3 started by spreading out over the substrate to a contact angles under 40°. It were spread out for 5-6 minutes before it contracted and the contact angle rose to over 90°over a duration of around 10 minutes. This contraction left several smaller droplets on the substrate. The droplets obscured the main slag drop which caused the measured angle to be lower than it actually were. The contact angle stay quite constant with angles close to 80°for the rest of the experiment with small signs of reactions. This was similar to sample 2.

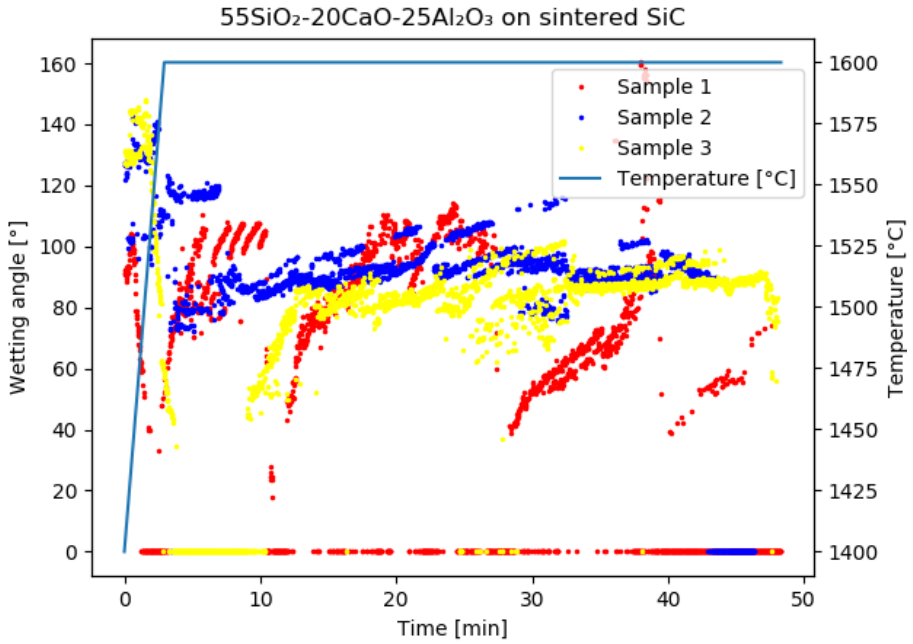

Figure 26: Wetting angle plotted against time, points marked by x are manually added. Time = 0 is set for when the temperature reached 1400°C. The blue line shows the temperature at the given time.

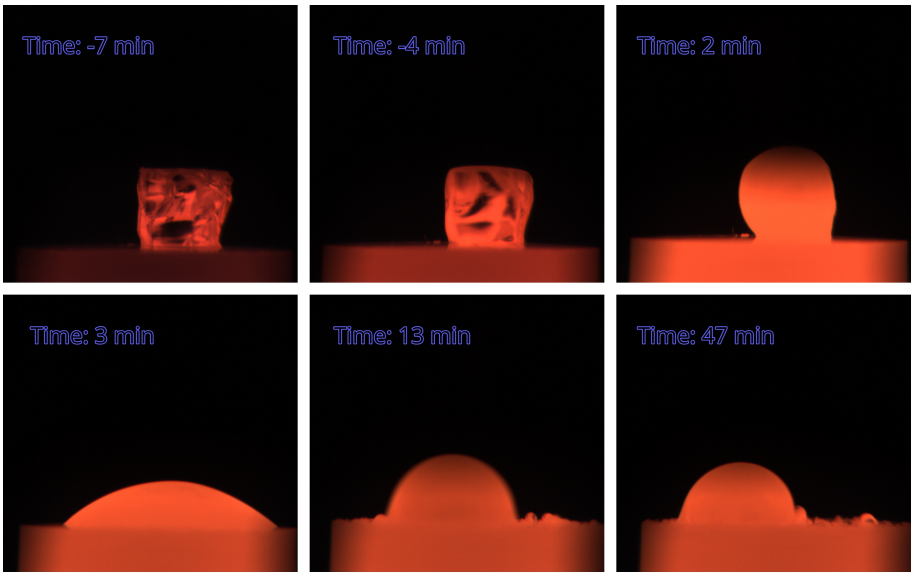

Figure 27: $55SiO_2 - 20CaO - 25Al_2O_3$ on sintered SiC at different points during the sessile drop test.

4.2.2 $55SiO_2 - 30CaO - 15Al_2O_3$ on sintered SiC

Plotted contact angles against time for $55SiO_2 - 30CaO - 15Al_2O_3$ on sintered SiC are shown in figure 28. Pictures from the wetting test for sample 2 are shown in figure 29.

Sample 1 showed signs of reaction throughout the experiment. From minutes 5 to 28 the contact angle fluctuated between 50°and 80°. The cause of the fluctuation were manly inflation and deflation of the slag caused by the reaction. The slag drop moved around the substrate a lot during this period, and left smaller droplets behind. At 28 minutes the slag spread out a bit, dropping the contact angle to 50°. The slag inflated over the next 5 minutes causing the angle to rise to 80°before completely spreading out on the substrate, with a contact angle of 16°. The angle stayed constant for the rest of the test, but some tiny bubbling could be observed.

Sample 2 acted mostly like sample 1 at the start, but it inflated more at 26 and 30 minutes giving angles of 110°. After 30 minutes the slag spread completely over the substrate with an angle of 22°. At 50 minutes the slag contracted a bit, giving it an angle of 45°, which were quite constant to the end. Signs of reaction in form of bubbling were observed throughout.

Sample 3 showed bubbling throughout the test. Initially it spread out over the substrate completely. At 5 minutes the slag contracted and the slag started to move a lot around the substrate

leaving smaller droplets behind. This continued until at 50 minutes the slag settled at 50°, with only minimal signs of reaction.

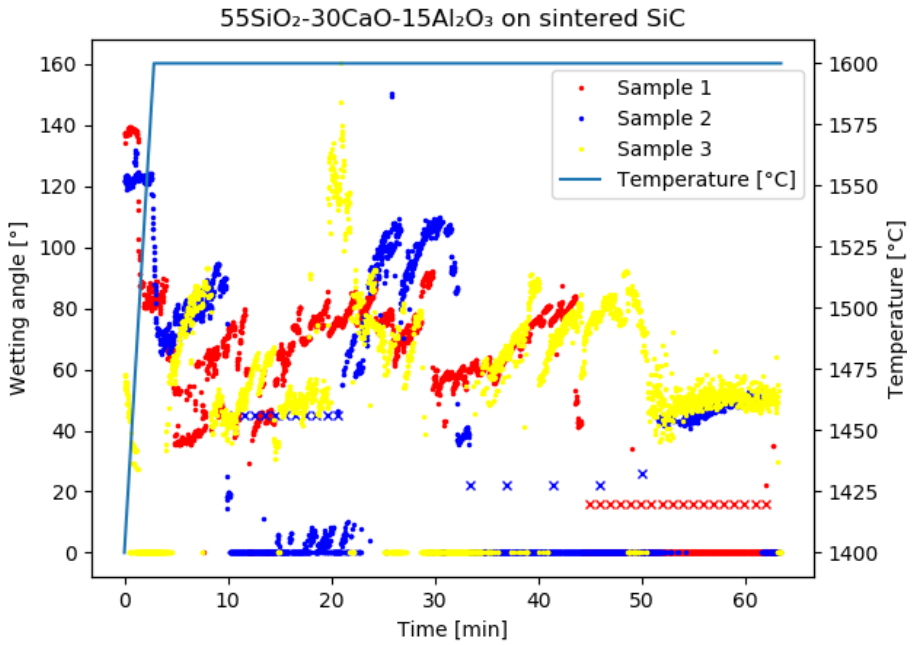

Figure 28: Wetting angle plotted against time, points marked by x are manually added. Time = 0 is set for when the temperature reached 1400°C. The blue line shows the temperature at the given time.

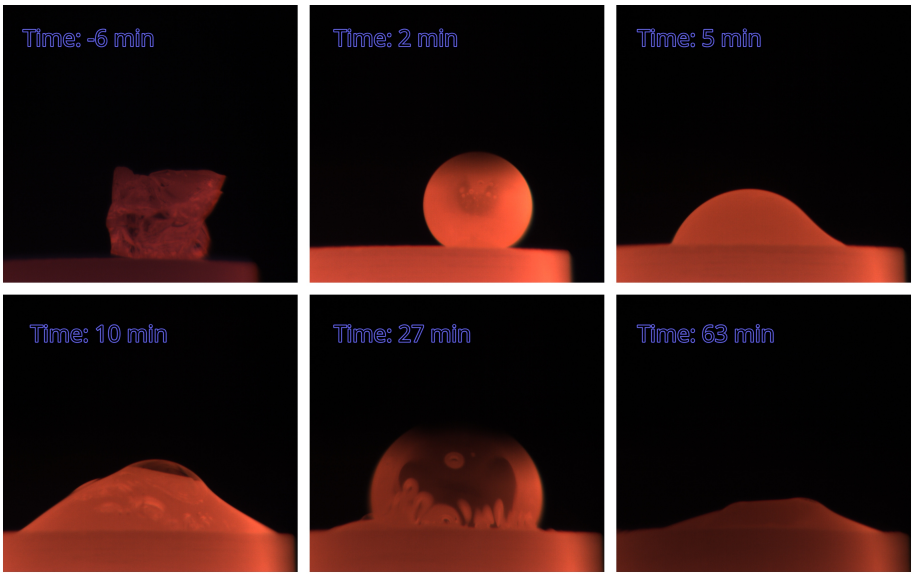

Figure 29: $55SiO_2 - 30CaO - 15Al_2O_3$ on sintered SiC at different points during the sessile drop test.

4.2.3 $55SiO_2 - 40CaO - 05Al_2O_3$ on sintered SiC

Plotted contact angles against time for $55SiO_2 - 40CaO - 05Al_2O_3$ on sintered SiC are shown in figure 30. Pictures from the wetting test for sample 2 are shown in figure 31.

All three samples acted largely the same during the tests. Bubbling occurred throughout the test accompanied by movement across the substrate. Smaller droplets were left behind by the movement. The contact angle fluctuated between 45°and 90°. An exception to this were sample 1 which had contact angles 10°-20°higher than the other samples. Sample 1 had a higher degree of scatter of the measured angles because the slag got partially obscured.

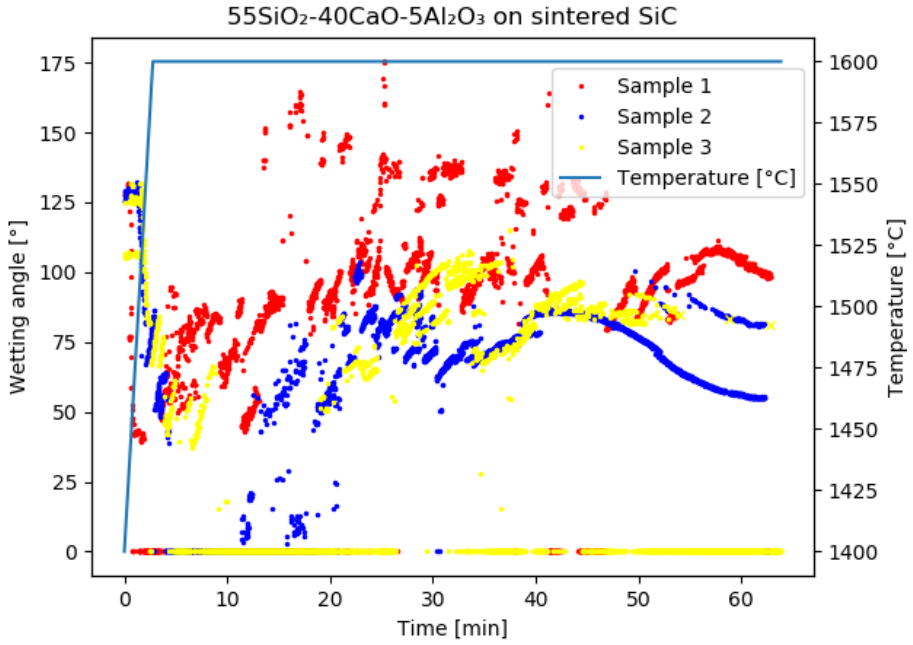

Figure 30: Wetting angle plotted against time, points marked by x are manually added. Time = 0 is set for when the temperature reached 1400°C. The blue line shows the temperature at the given time.

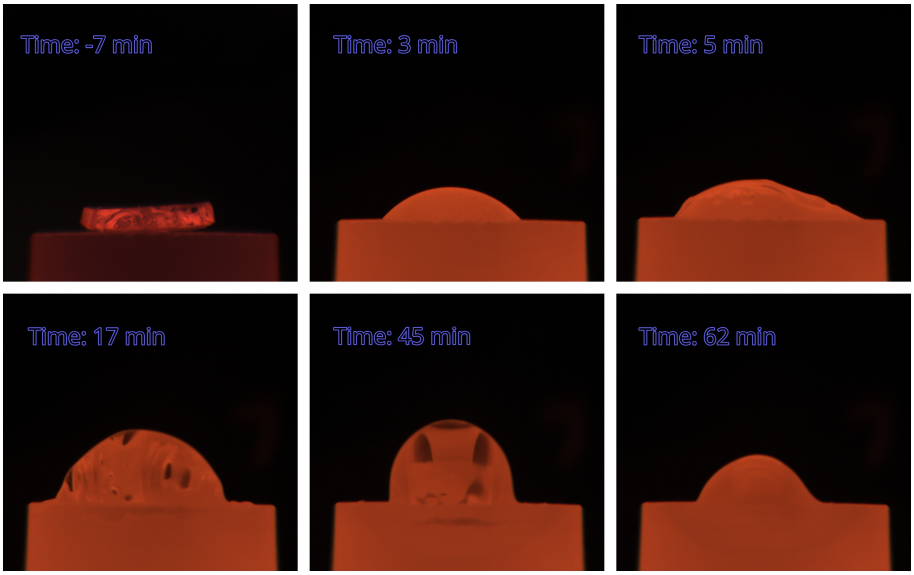

Figure 31: $55SiO_2 - 40CaO - 05Al_2O_3$ on sintered SiC at different points during the sessile drop test.

4.2.4 $60SiO_2 - 20CaO - 20Al_2O_3$ on sintered SiC

Plotted contact angles against time for $60SiO_2 - 20CaO - 20Al_2O_3$ on sintered SiC are shown in figure 32. Pictures from the wetting test for sample 2 are shown in figure 33.

All samples acted the same during the tests. The samples showed lots of movement around the substrate leaving smaller droplets behind. The movements were driven by bubbling and by the slag spreading out followed by it contracting at a different location. Signs of reaction were observed throughout the tests. The contact angles fluctuated between 50°and 120°, with the average angle being at 80°-90°.

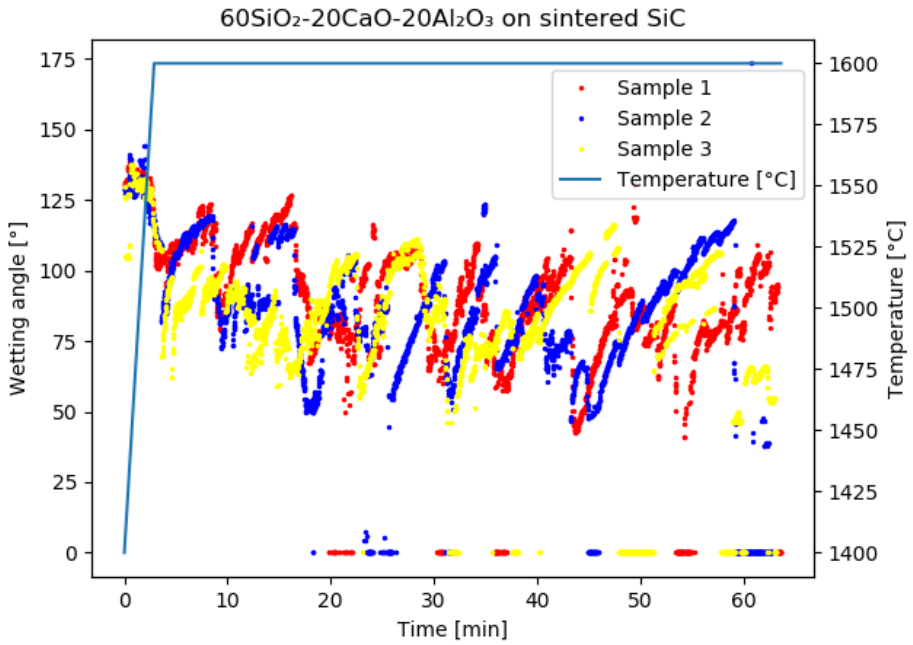

Figure 32: Wetting angle plotted against time, points marked by x are manually added. Time = 0 is set for when the temperature reached 1400°C. The blue line shows the temperature at the given time.

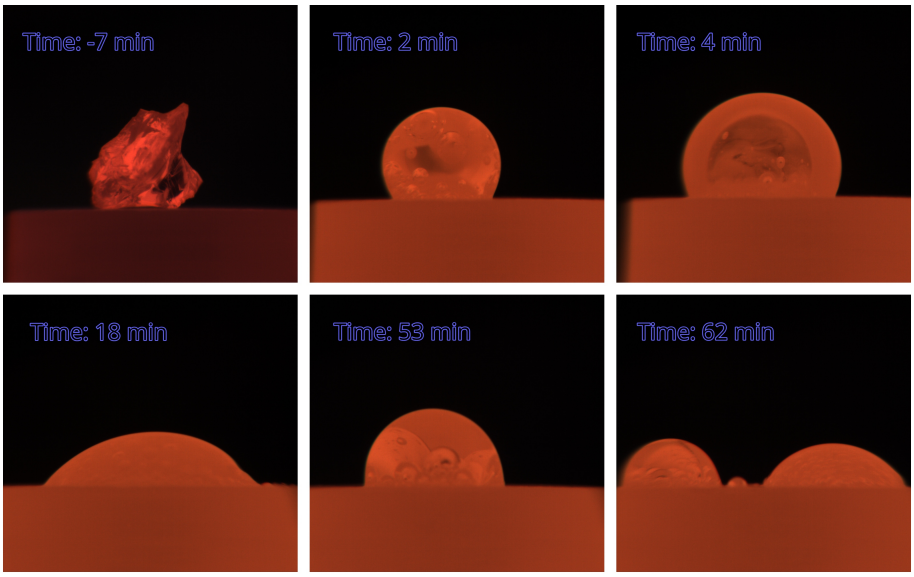

Figure 33: $60SiO_2 - 20CaO - 20Al_2O_3$ on sintered SiC at different points during the sessile drop test.

4.2.5 $60SiO_2 - 30CaO - 10Al_2O_3$ on sintered SiC

Plotted contact angles against time for $60SiO_2 - 30CaO - 10Al_2O_3$ on sintered SiC are shown in figure 34. Pictures from the wetting test for sample 3 are shown in figure 35.

All samples acted the same during the tests. The samples showed lots of movement around the substrate leaving smaller droplets behind. The movements were driven by bubbling and by the slag spreading out followed by it contracting at a different location. Signs of reaction were observed throughout the tests. Initially the contact angle fluctuated between 40°and 125°. At around 40 minutes all samples spread out completely over the substrate, reaching contact angles as low as 25. All samples contracted again towards the end reaching angles of around 80°.

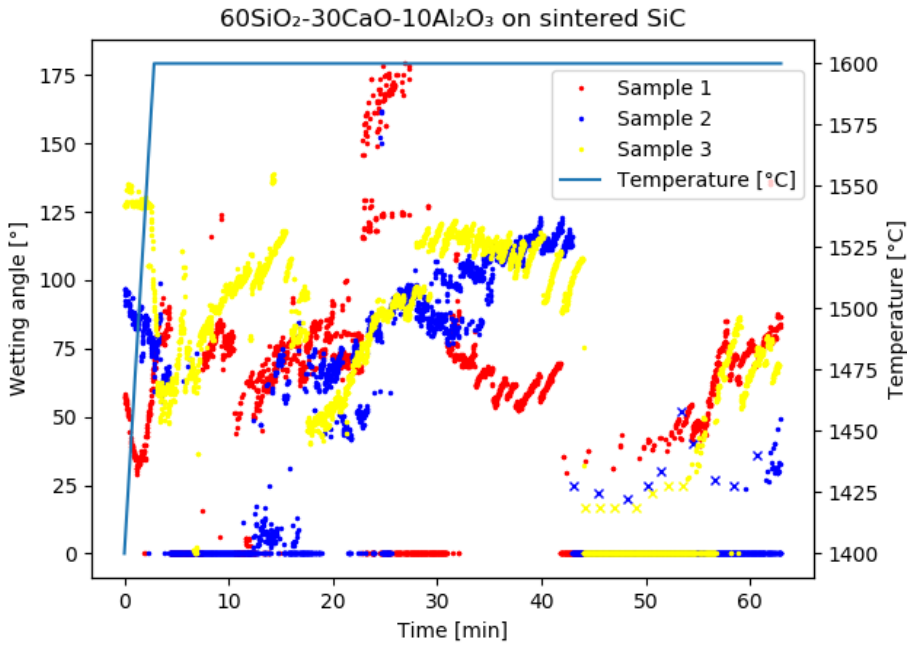

Figure 34: Wetting angle plotted against time, points marked by x are manually added. Time = 0 is set for when the temperature reached 1400°C. The blue line shows the temperature at the given time.

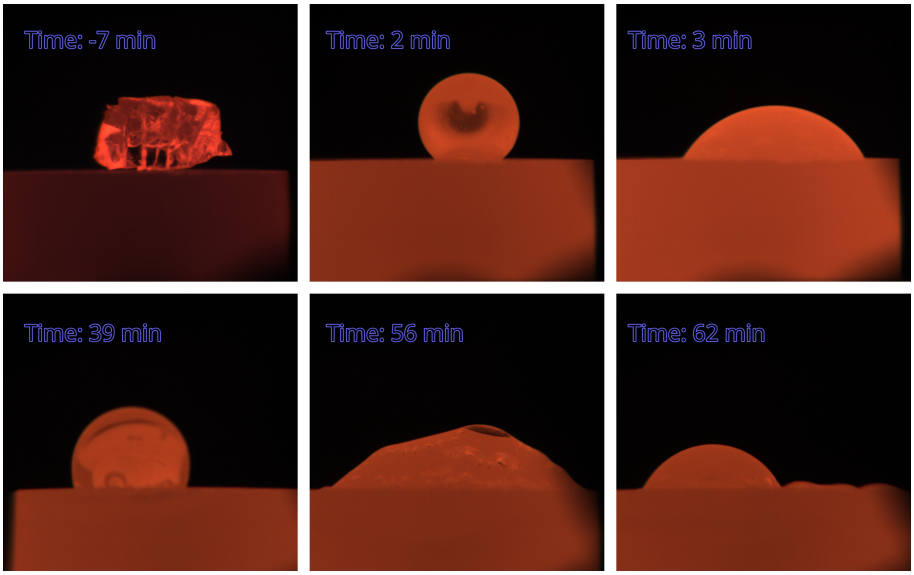

Figure 35: $60SiO_2 - 30CaO - 10Al_2O_3$ on sintered SiC at different points during the sessile drop test.

4.2.6 $70SiO_2 - 20CaO - 10Al_2O_3$ on sintered SiC

Plotted contact angles against time for $70SiO_2 - 20CaO - 10Al_2O_3$ on sintered SiC are shown in figure 36. Pictures from the wetting test for sample 2 are shown in figure 37.

All samples acted the same during the tests. The samples showed lots of movement around the substrate leaving smaller droplets behind. The movements were driven by bubbling and by the slag spreading out followed by it contracting at a different location. Signs of reaction were observed throughout the tests. The contact angles fluctuated between 40°and 100°. The fluctuations were mainly caused by the slag spreading and contracting, but also by the slag inflating and deflating by the reactions.

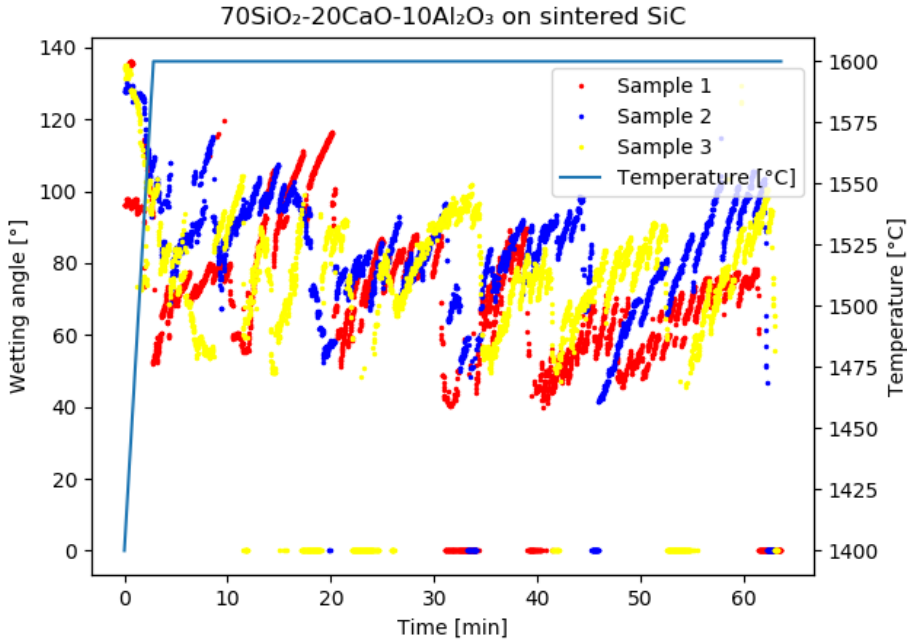

Figure 36: Wetting angle plotted against time, points marked by x are manually added. Time = 0 is set for when the temperature reached 1400°C. The blue line shows the temperature at the given time.

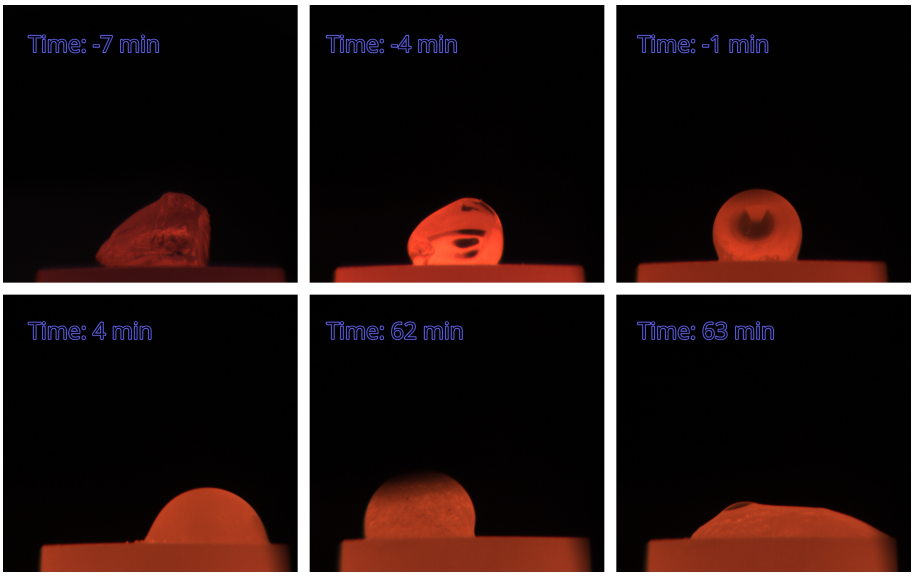

Figure 37: $70SiO_2 - 20CaO - 10Al_2O_3$ on sintered SiC at different points during the sessile drop test.

4.2.7 $55SiO_2 - 20CaO - 25Al_2O_3$ on transformed coal

Plotted contact angles against time for $55SiO_2 - 20CaO - 25Al_2O_3$ on transformed coal are shown in figure 38. Pictures from the wetting test for sample 3 are shown in figure 39.

All samples acted mostly the same during the tests. The samples rapidly spread out over the substrates before they started to penetrate into them. Bubbling were observed while the slag penetrated into the substrate. Sample 1 penetrated the substrate completely more than 10 minutes faster than the other two samples.

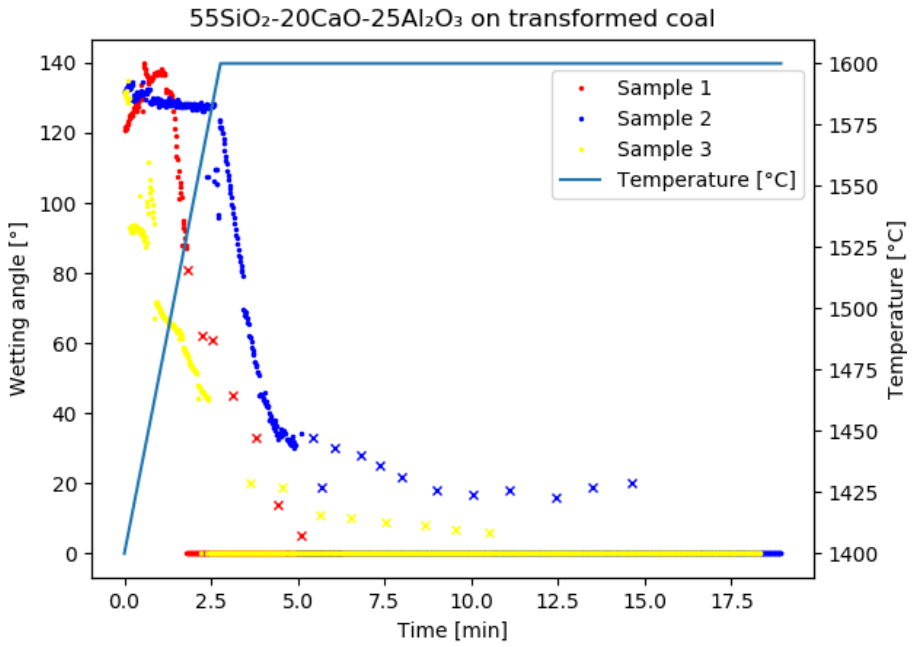

Figure 38: Wetting angle plotted against time, points marked by x are manually added. Time = 0 is set for when the temperature reached 1400°C. The blue line shows the temperature at the given time.

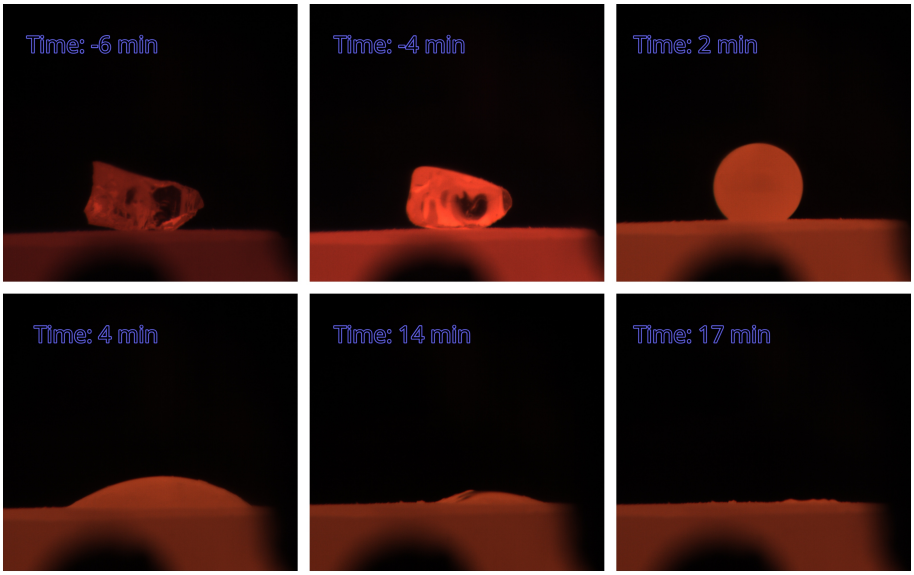

Figure 39: $55SiO_2 - 20CaO - 25Al_2O_3$ on transformed coal at different points during the sessile drop test.

4.2.8 $70SiO_2 - 20CaO - 10Al_2O_3$ on transformed coal

Plotted contact angles against time for $70SiO_2 - 20CaO - 10Al_2O_3$ on transformed coal are shown in figure 40. Pictures from the wetting test for sample 1 are shown in figure 41. Only 1 sample from the $70SiO_2 - 20CaO - 10Al_2O_3$ slag on transformed coal were plotted because the other attempts did not give any usable data.

The slag rapidly spread to around 60°before it started to penetrate into the substrate. The angle dropped further to 15°while the slag penetrated, meanwhile some bubbling were observed.

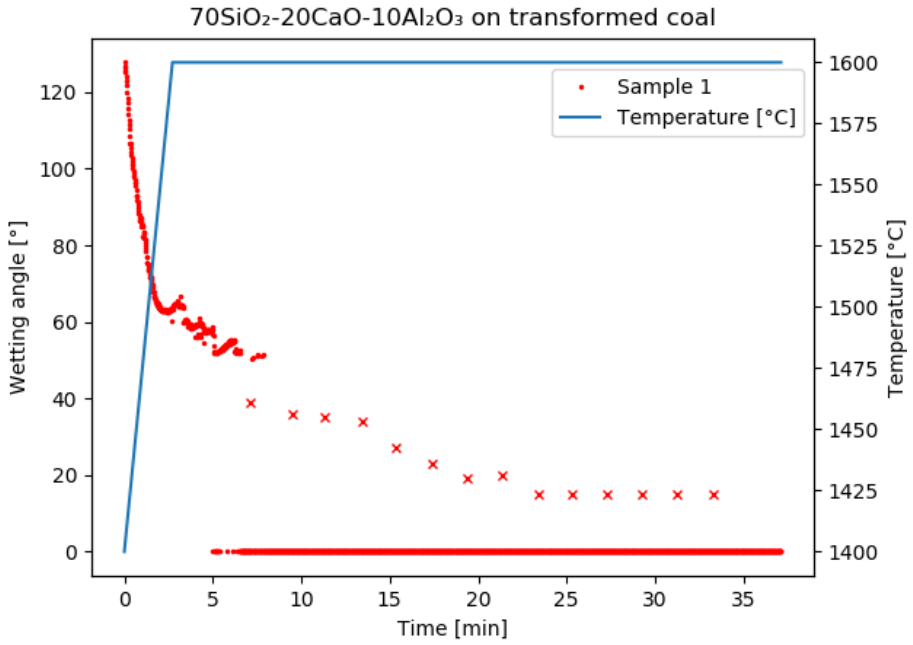

Figure 40: Wetting angle plotted against time, points marked by x are manually added. Time = 0 is set for when the temperature reached 1400°C. The blue line shows the temperature at the given time.

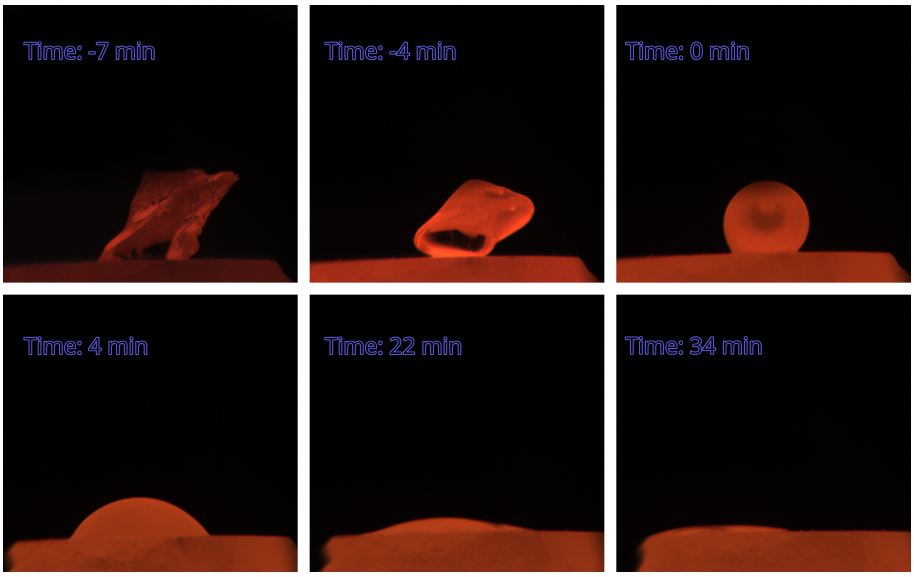

Figure 41: $70SiO_2 - 20CaO - 10Al_2O_3$ on transformed coal at different points during the sessile drop test.

4.2.9 $55SiO_2 - 20CaO - 25Al_2O_3$ on alpha SiC

Plotted contact angles against time for $55SiO_2 - 20CaO - 25Al_2O_3$ on alpha SiC are shown in figure 42. Pictures from the wetting test for sample 1 are shown in figure 43.

All samples acted mostly the same. Reactions in the form of bubbling were observed throughout the tests. The slags spread rapidly out on the substrate to angles around 40°-50°before they started to penetrate into the substrate. They contracted and the angle increased to around 90°at around the 5 minute mark. The contact angle decreased after that as the slag penetrated the substrate fully. It was observed that the slags flowed through the substrate and out the side edge or the other side. Sample 3 used around 10 minutes longer to fully penetrate the substrate than the other samples.

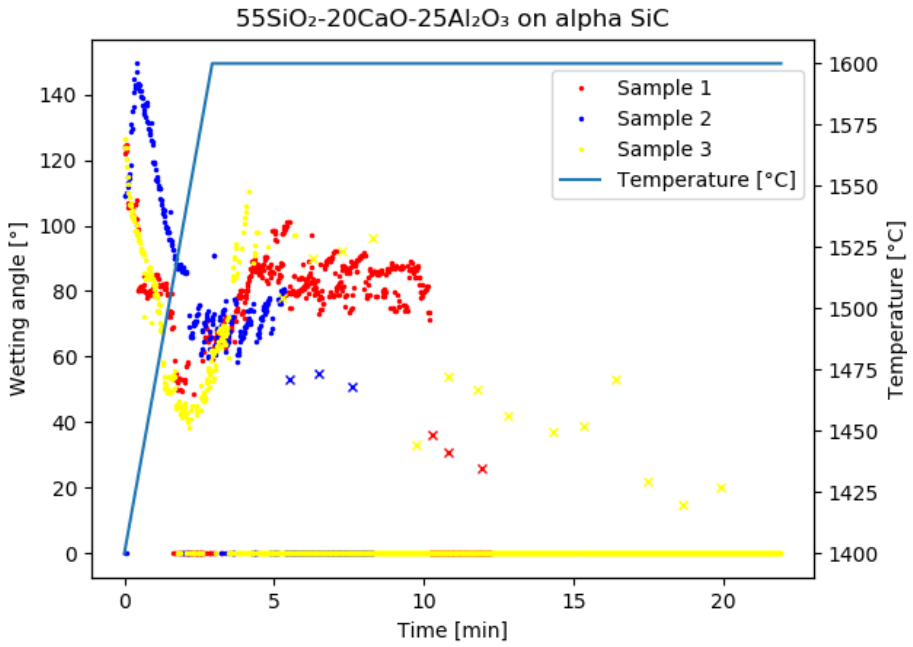

Figure 42: Wetting angle plotted against time, points marked by x are manually added. Time = 0 is set for when the temperature reached 1400°C. The blue line shows the temperature at the given time.

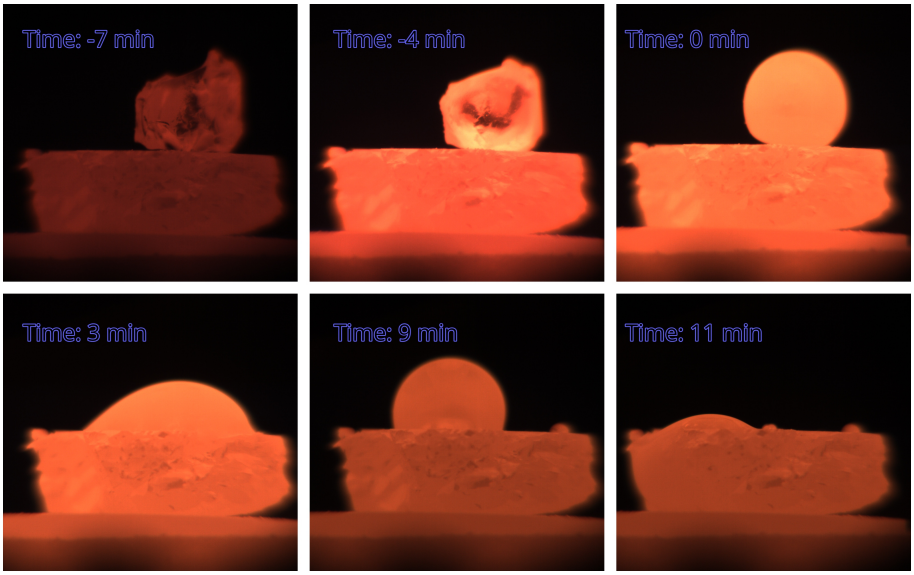

Figure 43: $55SiO_2 - 20CaO - 25Al_2O_3$ on alpha SiC at different points during the sessile drop test.

4.2.10 $70SiO_2 - 20CaO - 10Al_2O_3$ on alpha SiC

Plotted contact angles against time for $70SiO_2 - 20CaO - 10Al_2O_3$ on alpha SiC are shown in figure 44. Pictures from the wetting test for sample 1 are shown in figure 45.

Sample 1 showed signs of reactions throughout the test. It initially spread rapidly out onto the substrate down to a contact angle of 40°. It contracted up to 70°-80°shortly after. It held near constant angle while it penetrated the substrate. It fully penetrated and flowed through the substrate at 38 minutes.

Sample 2 showed signs of reactions throughout the test. It initially spread rapidly out onto the substrate down to a contact angle of 30°. The slag drop rapidly lost volume caused by it penetrating and flowing through the side of the substrate. The contact angle increased to 55°during this. The slag then spread out and moved, causing the volume decrease to drastically slow. The slag held a contact angle between 25°and 40°until it fully penetrated

Sample 3 flowed into and through the substrate during the first 10 minutes.

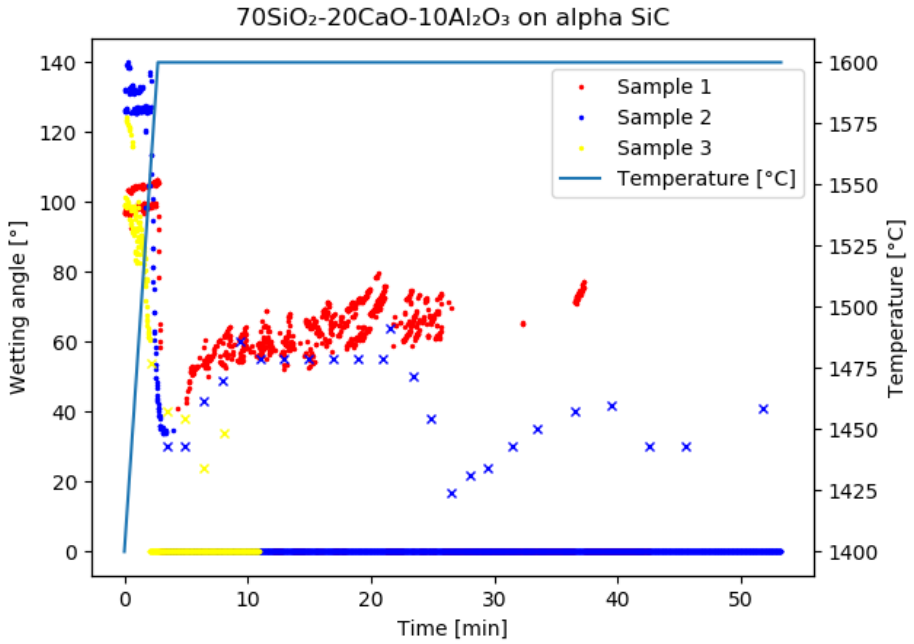

Figure 44: Wetting angle plotted against time, points marked by x are manually added. Time = 0 is set for when the temperature reached 1400°C. The blue line shows the temperature at the given time.

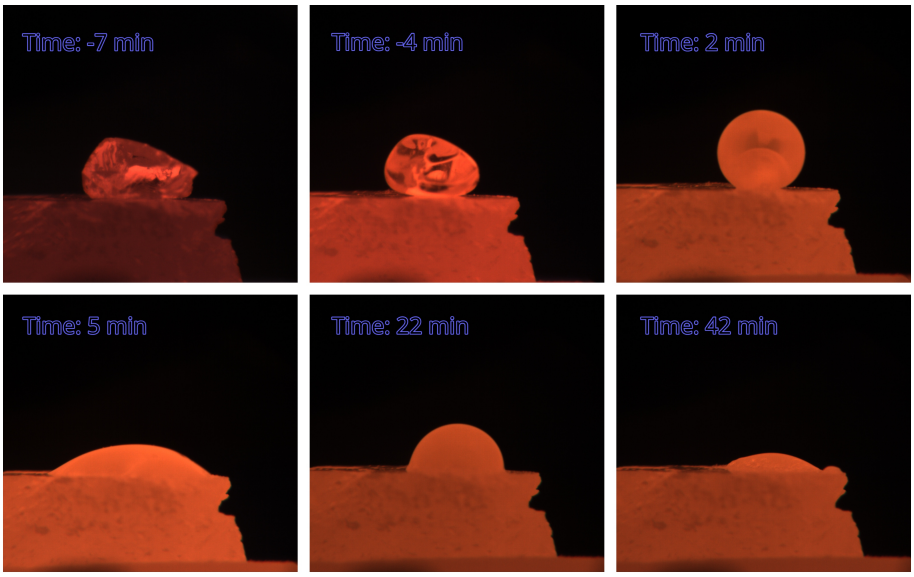

Figure 45: $70SiO_2 - 20CaO - 10Al_2O_3$ on alpha SiC at different points during the sessile drop test.

4.2.11 Comparison

Figure 46 shows the average contact angle of the different test after they have reached the holding temperature of 1600°C. Figures 47-49 shows the average contact angle plotted against the basicity. Figure 47 shows the tests on sintered SiC, figure 48 shows the tests on transformed coal, and figure 49 shows the tests on alpha SiC. Manually added angles have little effect on these averages as there are vanishing few points compared to the detected angels.

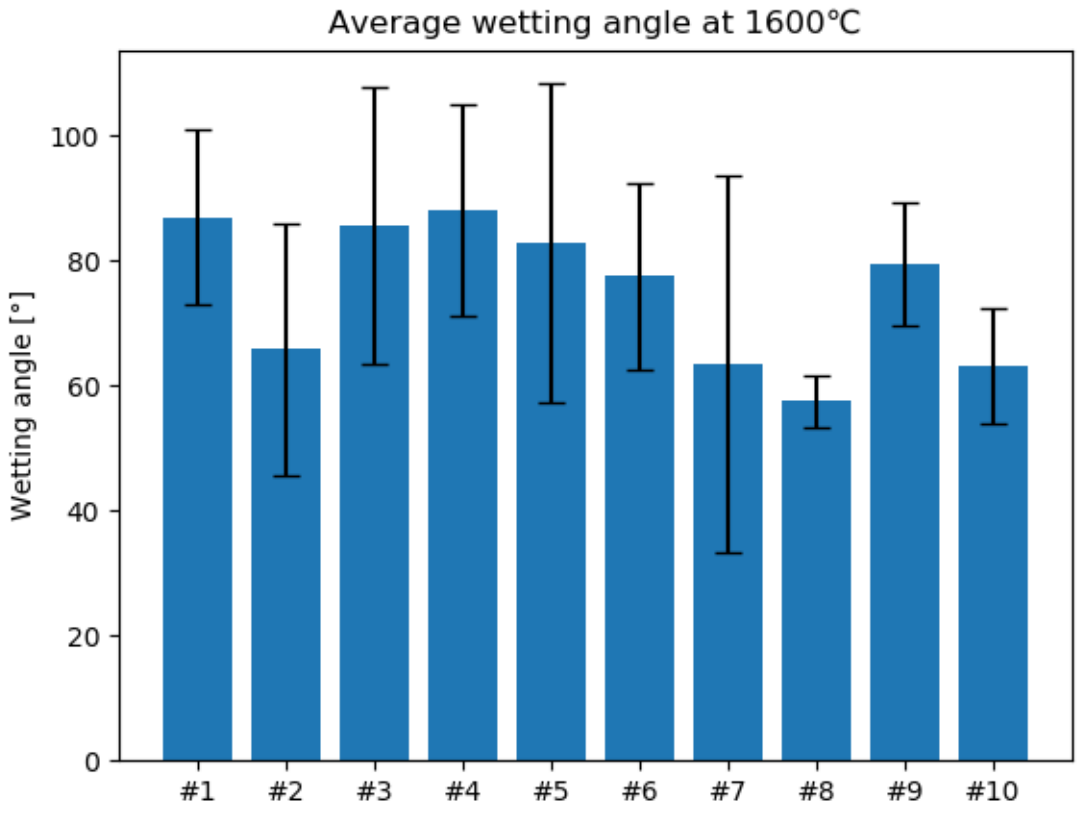

Figure 46: Average wetting angles of the different tests at 1600°C, with standard deviation.

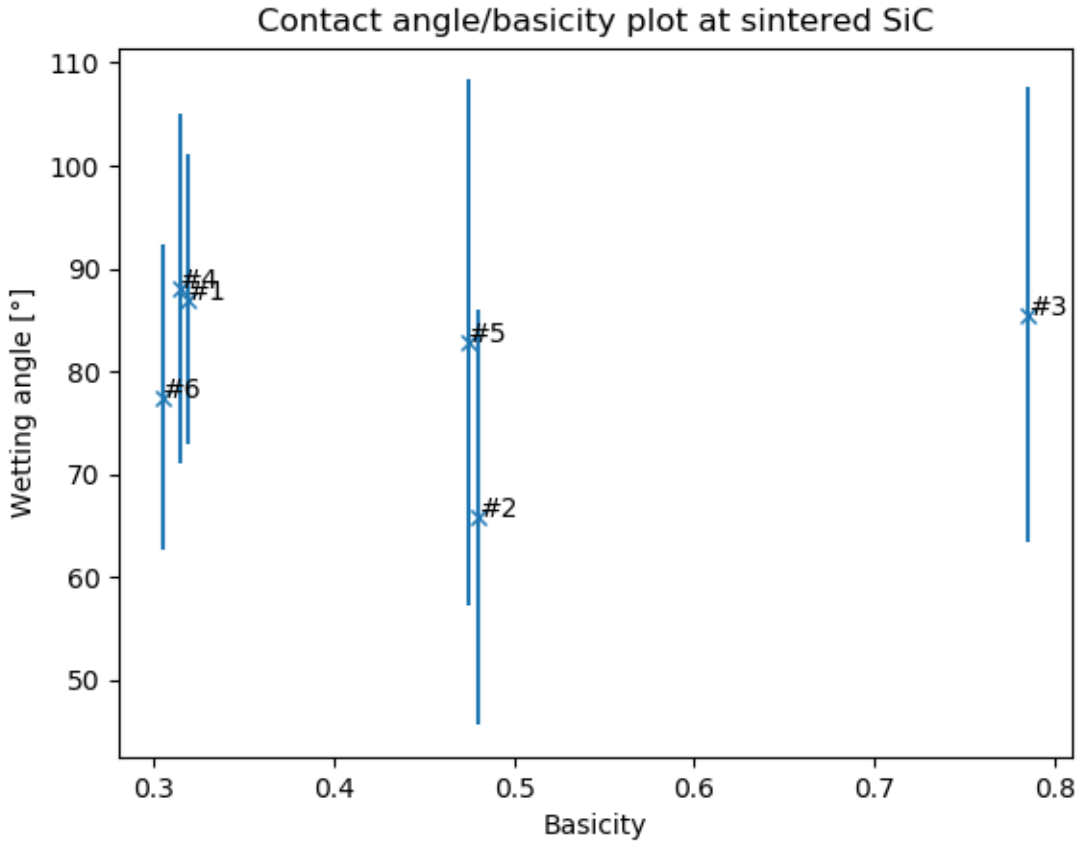

Figure 47: The average contact angle plotted against the basicity (Ca/(Si+Al) of the slags on sintered SiC, with standard deviation.

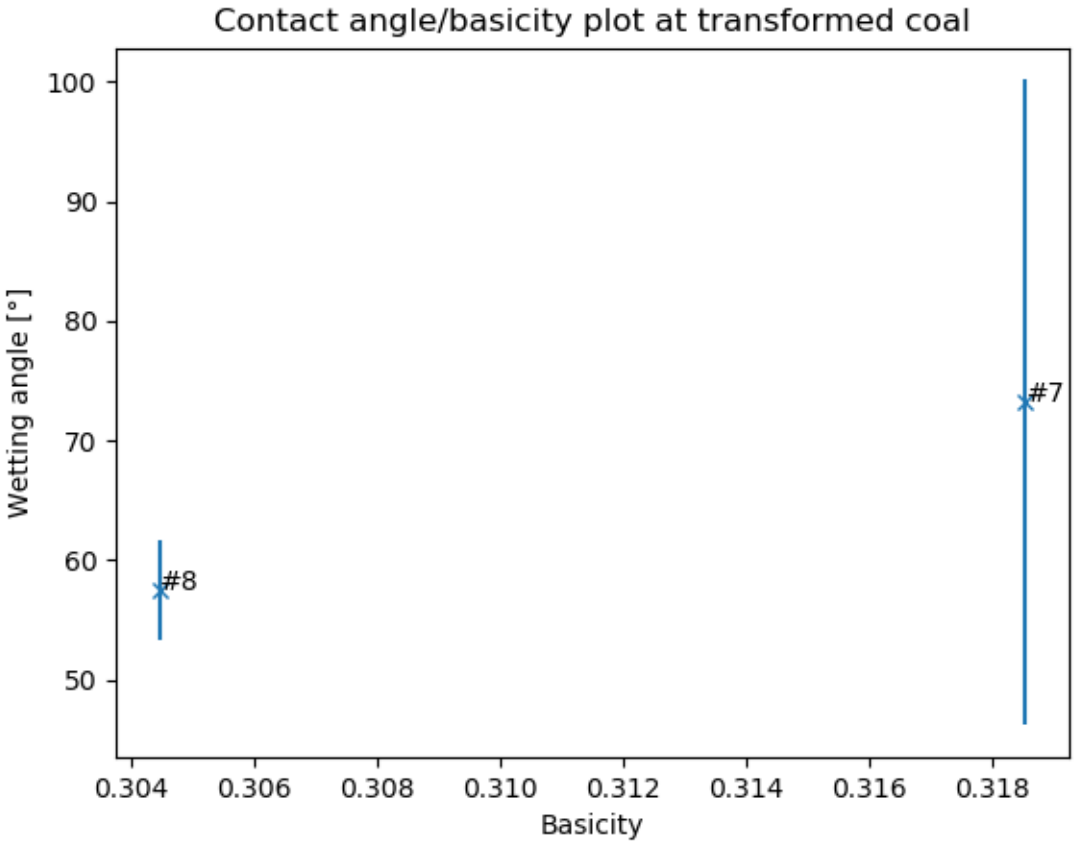

Figure 48: The average contact angle plotted against the basicity (Ca/(Si+Al) of the slags on transformed coal, with standard deviation.

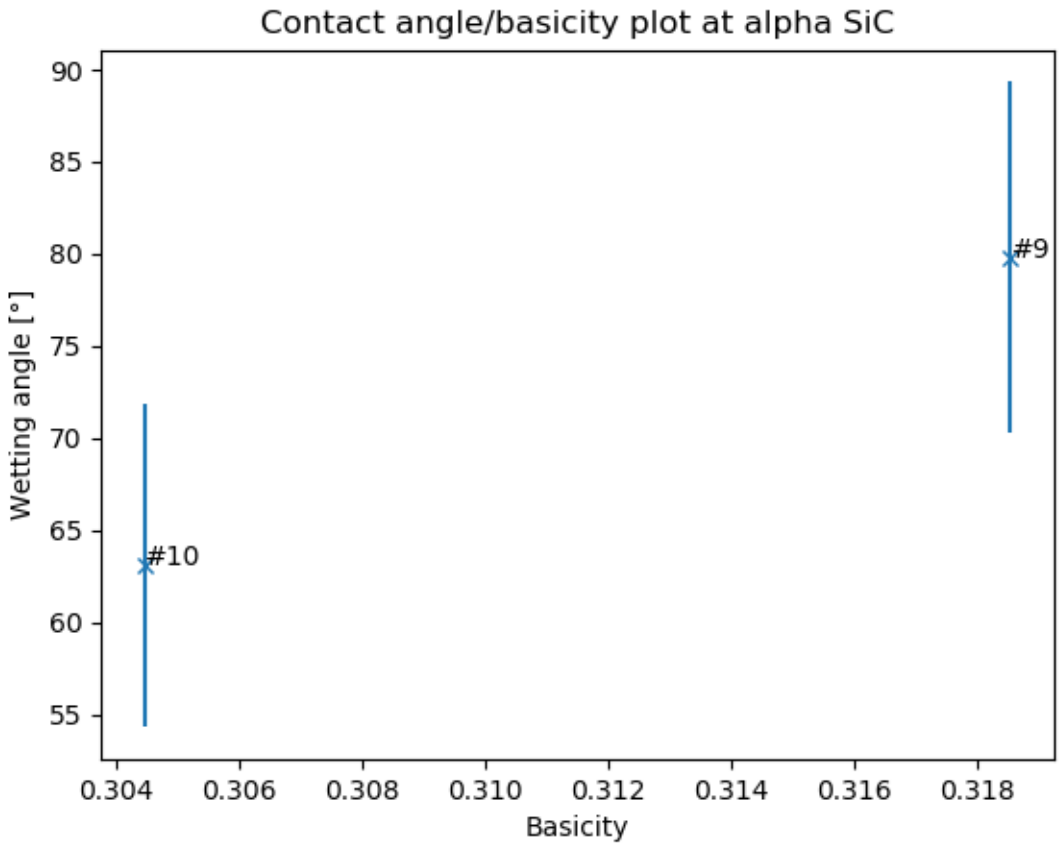

Figure 49: The average contact angle plotted against the basicity (Ca/(Si+Al) of the slags on alpha, with standard deviation.

4.3 EDS

The plotted EDS results for the slags, the fraction of Ca/Al in the slag before and after wetting, and a comparison of composition from before and after wetting are shown here.

4.3.1 $55SiO_2 - 20CaO - 25Al_2O_3$ on sintered SiC

A SEM BSE picture of the $55SiO_2 - 20CaO - 25Al_2O_3$ slag on sintered SiC is shown in figure 50. Normalized atomic percentages of the slag phase, gotten from EDS, of Si, Ca, and Al are shown in figure 51. The Ca and Al content, normalized to 1, are shown in 52. The Ca/Al fraction from before and after the wetting test are shown in table 7. Figure 51 shows that the average composition of the slag were around 38% Si, 23% Ca, and 37% Al. From table 7 it is shown that the fraction of Ca/Al is around the same from before and after the wetting.

Table 7: Normalized Ca/Al fraction from before and after the wetting tests

	Before wetting	After wetting
Ca/Al	0.71	0.72

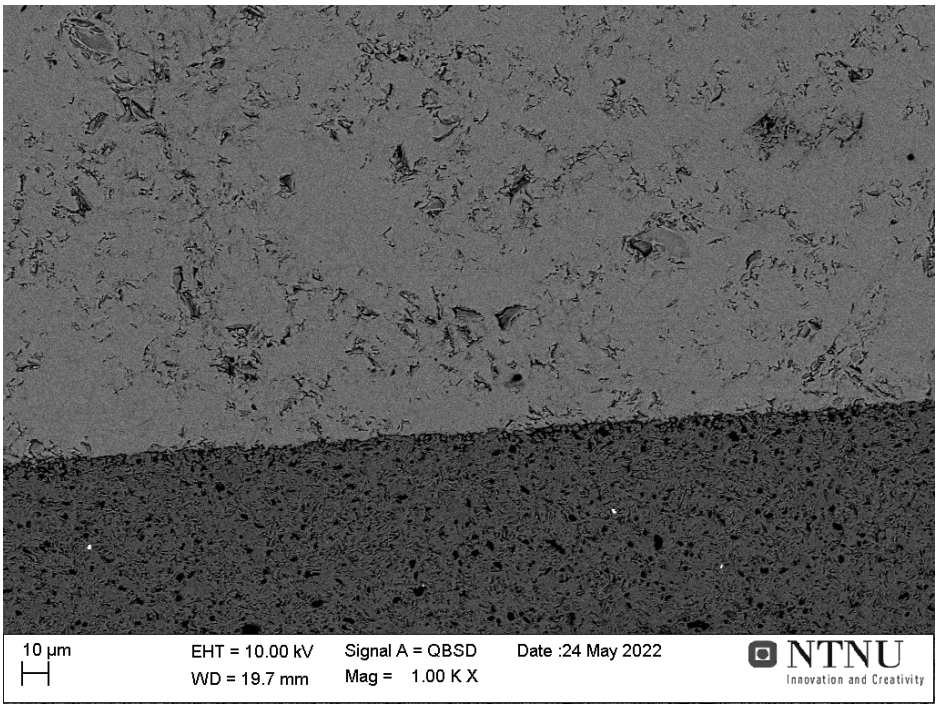

Figure 50: SEM BSE picture of the $55SiO_2 - 20CaO - 25Al_2O_3$ slag on sintered SiC at 1000x magnification

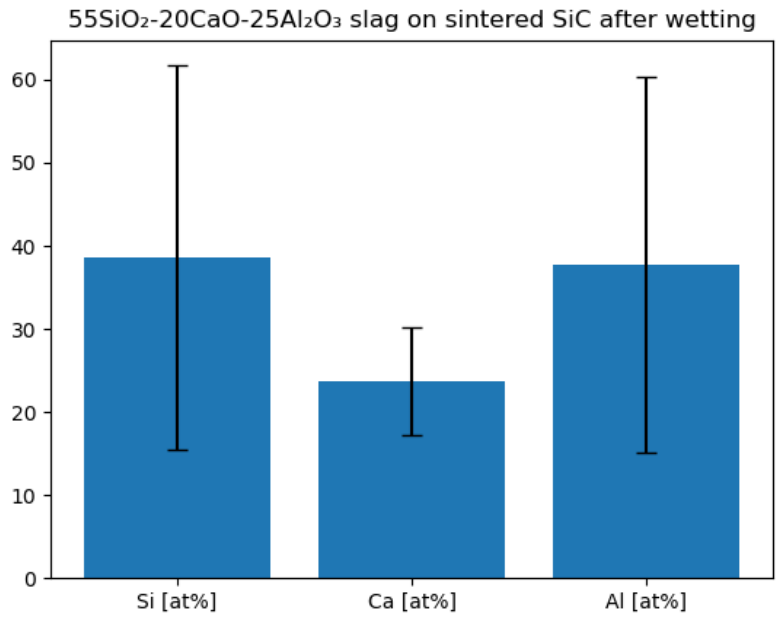

Figure 51: Si, Ca, and Al composition of the slag from EDS, with standard deviation

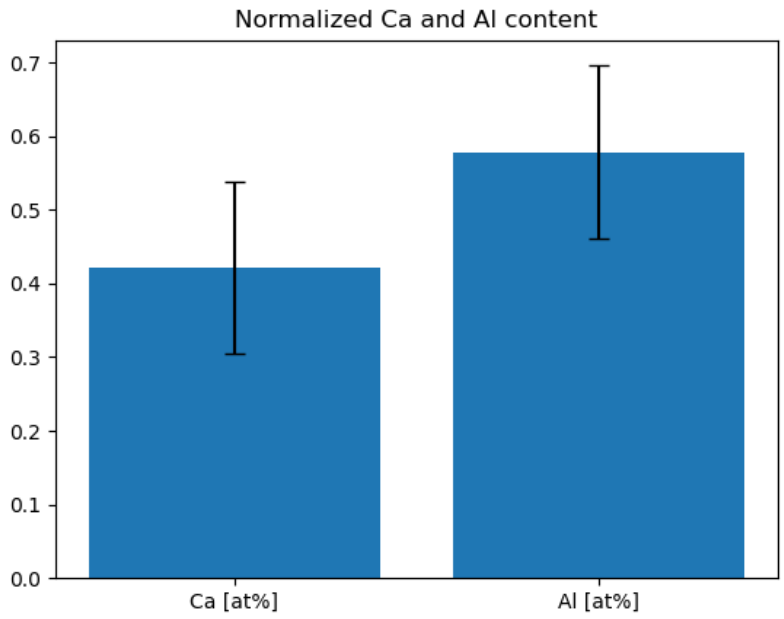

Figure 52: Normalized Ca and Al content in the slag after wetting, with standard deviation.

4.3.2 $55SiO_2 - 30CaO - 15Al_2O_3$ on sintered SiC

A SEM BSE picture of the $55SiO_2 - 30CaO - 15Al_2O_3$ slag on sintered SiC is shown in figure 53. Normalized atomic percentages of the slag phase, gotten from EDS, of Si, Ca, and Al are shown in figure 54. The Ca and Al content, normalized to 1, are shown in 55. The Ca/Al fraction from before and after the wetting test are shown in table 8. Figure 54 shows that the average composition of the slag were around 42% Si, 39% Ca, and 28% Al. An interface area between the slag and the substrate can be seen on the SEM picture. Figure 56 shows the slag composition in the interface area. From table 8 it is shown that the fraction of Ca/Al had increased by 25% from before to after the wetting.

Table 8: Normalized Ca/Al fraction from before and after the wetting tests

	Before wetting	After wetting
Ca/Al	1.61	2.052

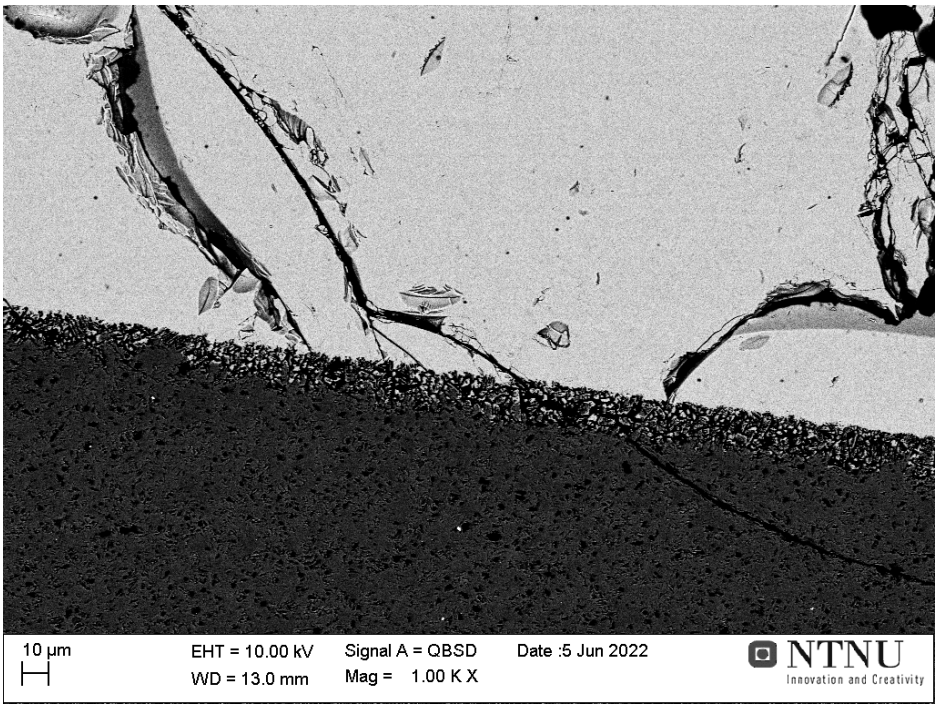

Figure 53: SEM BSE picture of the $55SiO_2 - 30CaO - 15Al_2O_3$ slag on sintered SiC at 1000x magnification

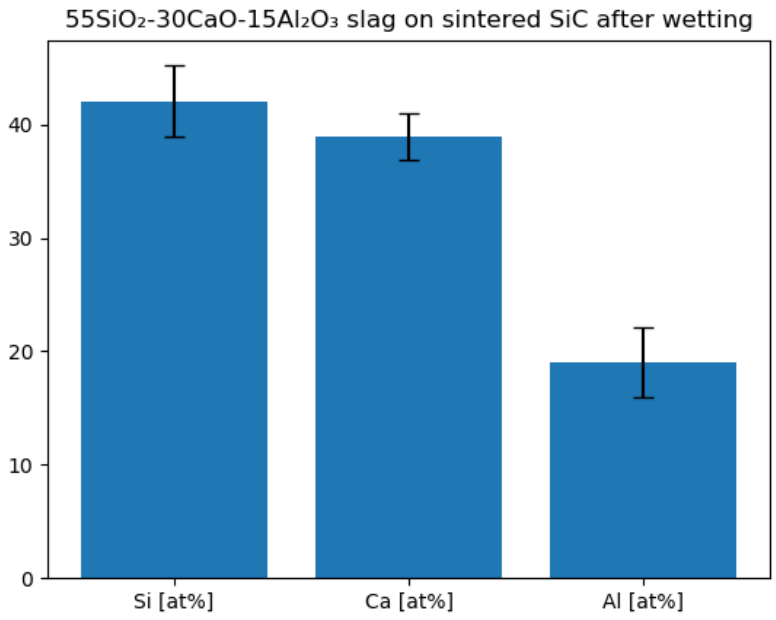

Figure 54: Si, Ca, and Al composition of the slag from EDS, with standard deviation

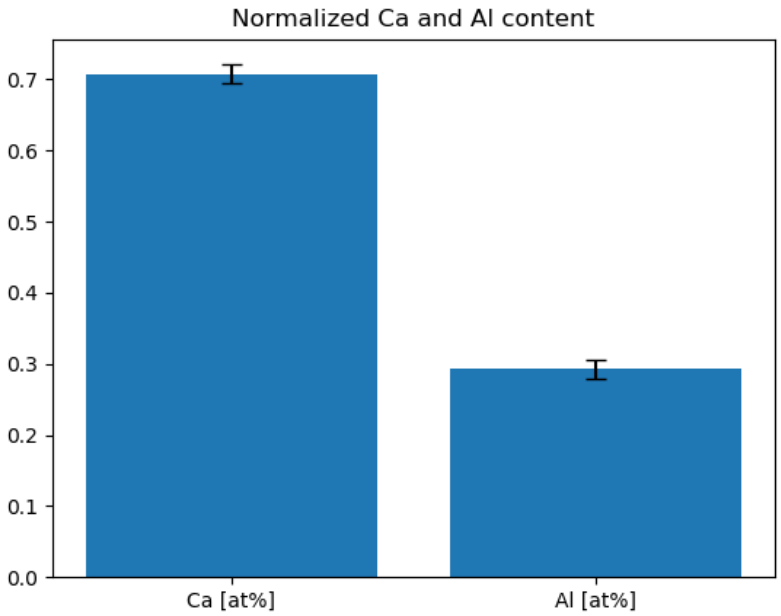

Figure 55: Normalized Ca and Al content in the slag after wetting

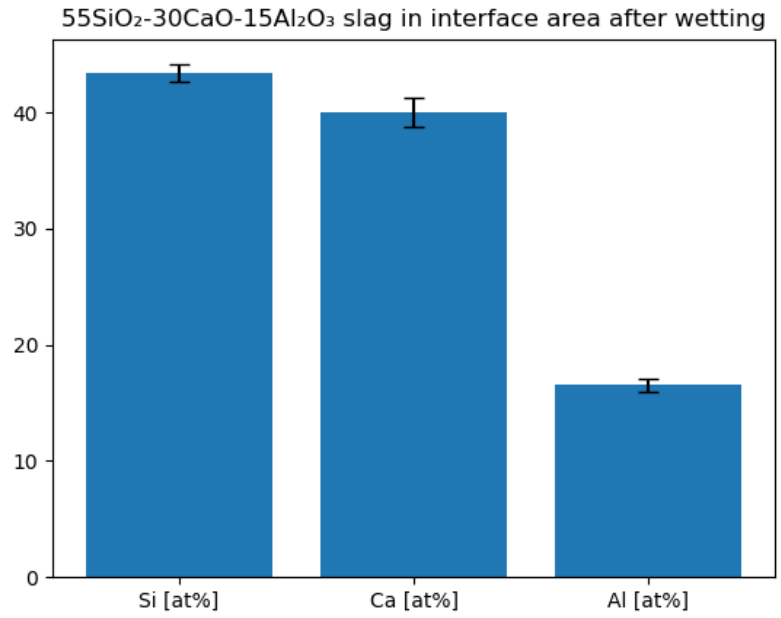

Figure 56: Si, Ca, and Al composition of the slag at the interface area from EDS, with standard deviation

4.3.3 $55SiO_2 - 40CaO - 05Al_2O_3$ on sintered SiC

A SEM BSE picture of the $55SiO_2 - 40CaO - 05Al_2O_3$ slag on sintered SiC is shown in figure 57. Normalized atomic percentages of the slag phase, gotten from EDS, of Si, Ca, and Al are shown in figure 58. The Ca and Al content, normalized to 1, are shown in 59. The Ca/Al fraction from before and after the wetting test are shown in table 9. Figure 58 shows that the average composition of the slag were around 46% Si, 47% Ca, and 7% Al. An interface area between the slag and the substrate can be seen on the SEM picture. Figure 60 shows the slag composition in the interface area. From table 9 it is shown that the fraction of Ca/Al were around the same from before to after the wetting.

Table 9: Normalized Ca/Al fraction from before and after the wetting tests

	Before wetting	After wetting
Ca/Al	7.18	6.89

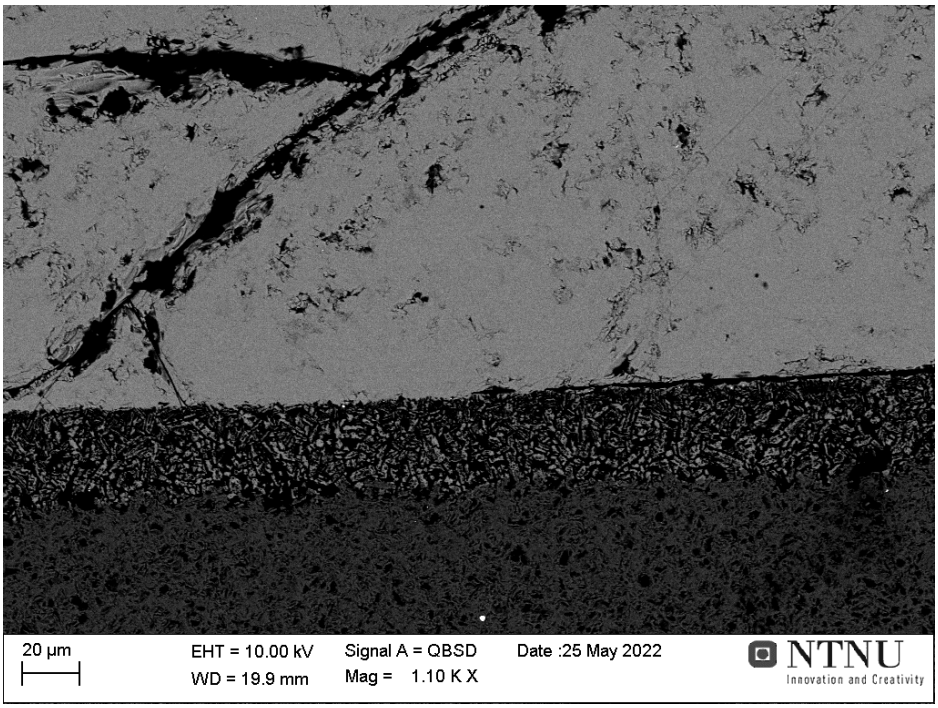

Figure 57: SEM BSE picture of the $55SiO_2 - 40CaO - 05Al_2O_3$ slag on sintered SiC at 1000x magnification

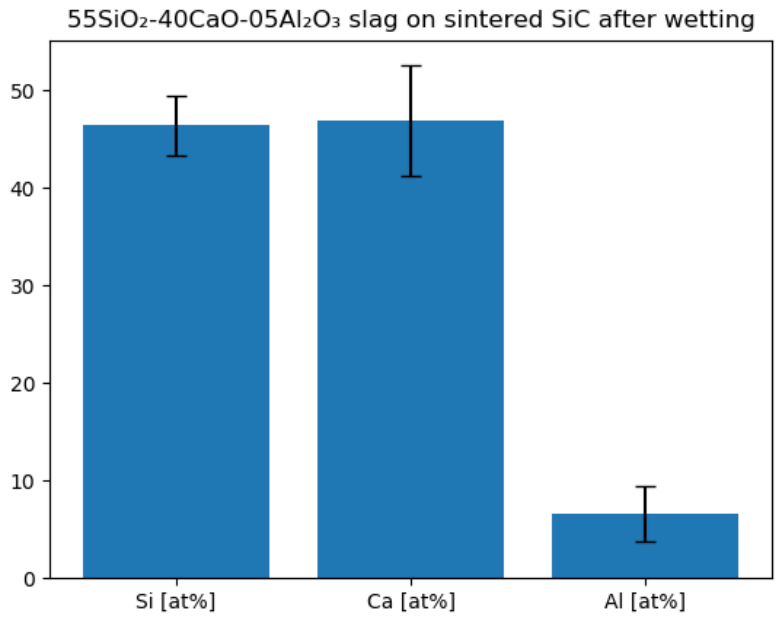

Figure 58: Si, Ca, and Al composition of the slag from EDS, with standard deviation

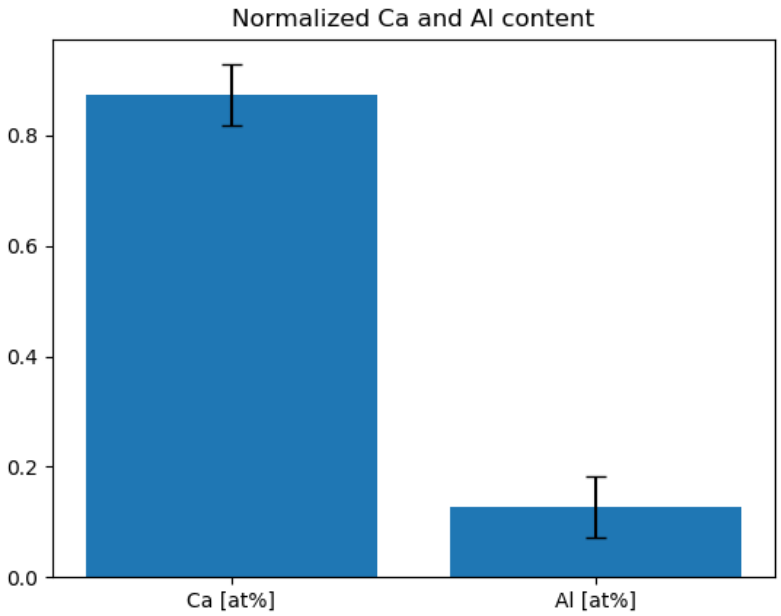

Figure 59: Normalized Ca and Al content in the slag after wetting, with standard deviation.

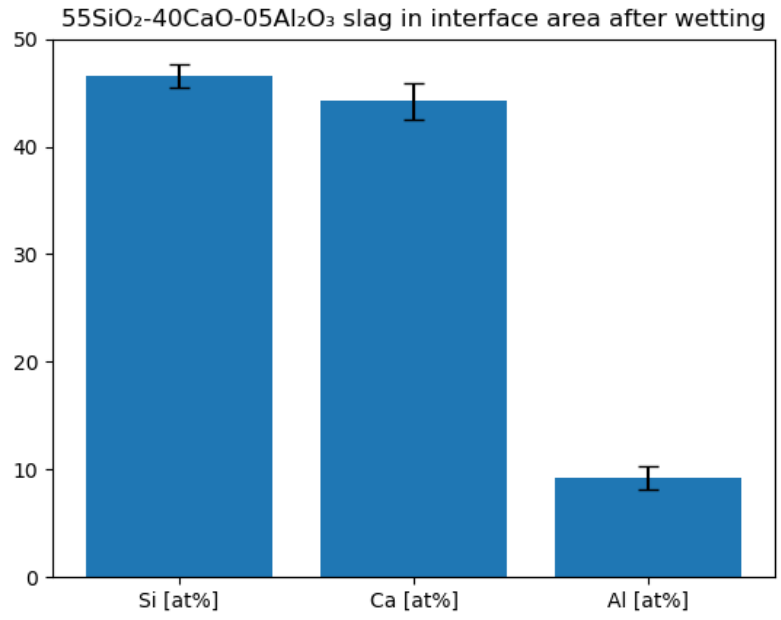

Figure 60: Si, Ca, and Al composition of the slag at the interface area from EDS, with standard deviation

4.3.4 $60SiO_2 - 20CaO - 20Al_2O_3$ on sintered SiC

A SEM BSE picture of the $60SiO_2 - 20CaO - 20Al_2O_3$ slag on sintered SiC is shown in figure 61. Normalized atomic percentages of the slag phase, gotten from EDS, of Si, Ca, and Al are shown in figure 62. The Ca and Al content, normalized to 1, are shown in 63. The Ca/Al fraction from before and after the wetting test are shown in table 10. Figure 62 shows that the average composition of the slag were around 57% Si, 22% Ca, and 21% Al. From table 10 it is shown that the fraction of Ca/Al had increased by around 15% from before to after the wetting.

Table 10: Normalized Ca/Al fraction from before and after the wetting tests

	Before wetting	After wetting
Ca/Al	0.91	1.05

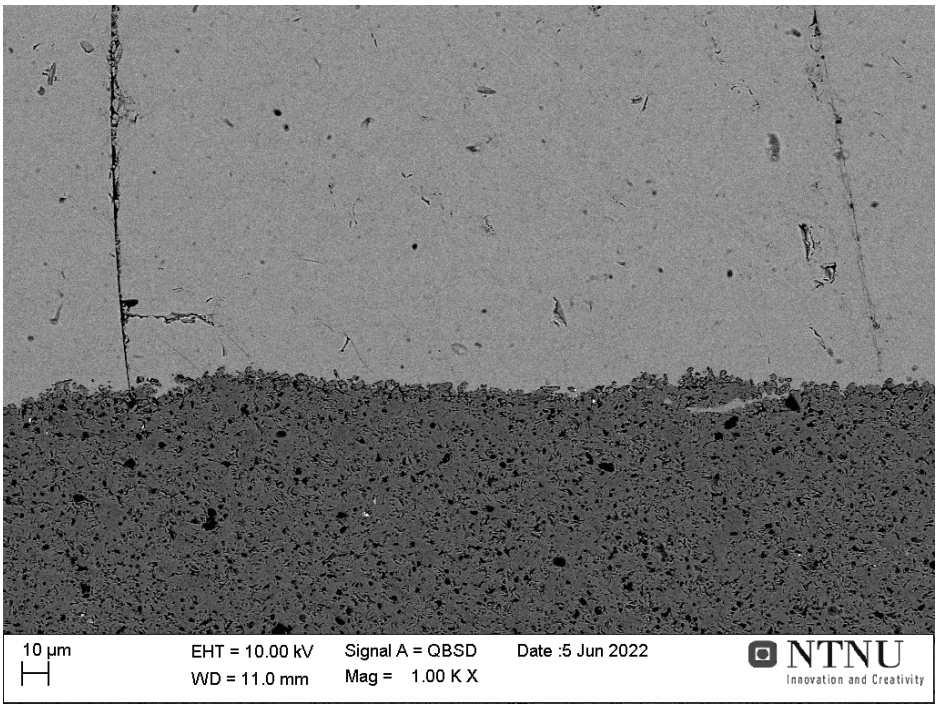

Figure 61: SEM BSE picture of the $60SiO_2 - 20CaO - 20Al_2O_3$ slag on sintered SiC at 1000x magnification

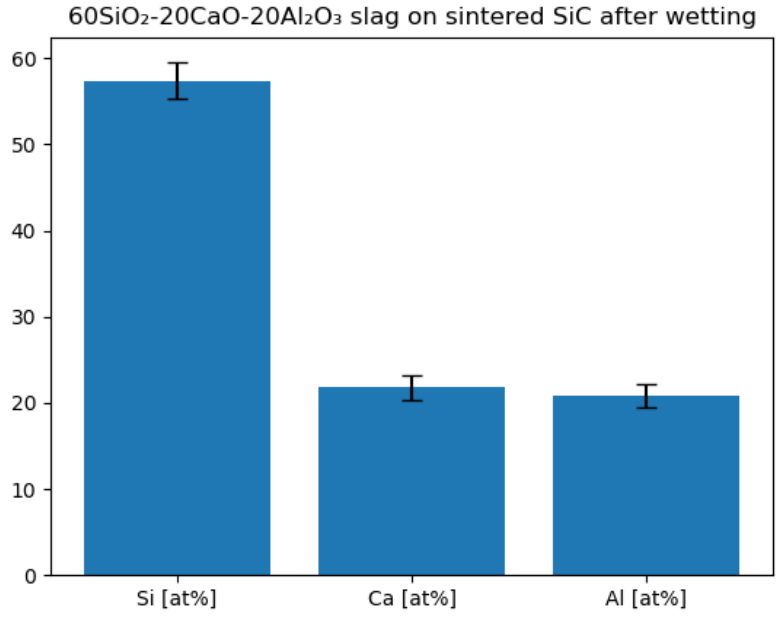

Figure 62: Si, Ca, and Al composition of the slag from EDS, with standard deviation

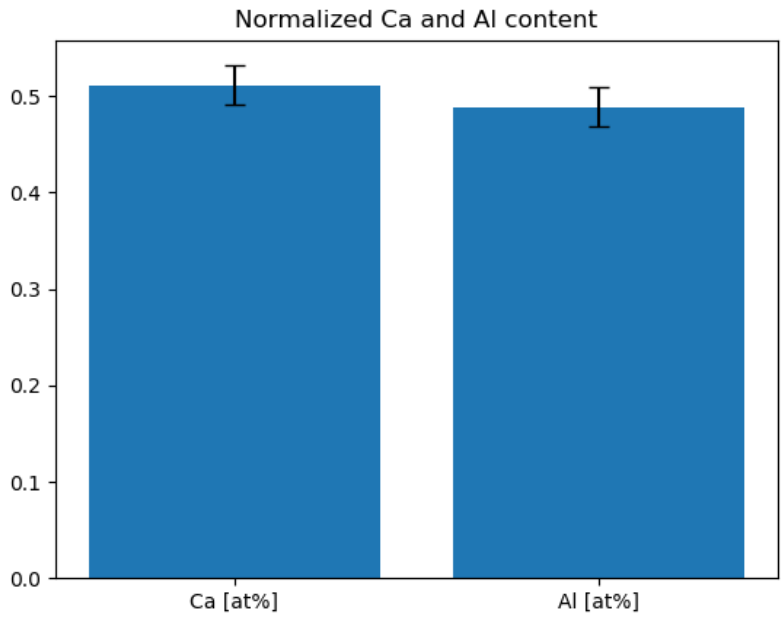

Figure 63: Normalized Ca and Al content in the slag after wetting, with standard deviation.

4.3.5 $60SiO_2 - 30CaO - 10Al_2O_3$ on sintered SiC

A SEM BSE picture of the $60SiO_2 - 30CaO - 10Al_2O_3$ slag on sintered SiC is shown in figure 64. Normalized atomic percentages of the slag phase, gotten from EDS, of Si, Ca, and Al are shown in figure 65. The Ca and Al content, normalized to 1, are shown in 67. The Ca/Al fraction from before and after the wetting test are shown in table 11. Figure 65 shows that the average composition of the slag were around 53% Si, 35% Ca, and 12% Al. An interface area between the slag and the substrate can be seen on the SEM picture. Figure 66 shows the slag composition in the interface area. From table 11 it is shown that the fraction of Ca/Al had increased by around 20% from before to after the wetting.

Table 11: Normalized Ca/Al fraction from before and after the wetting tests

	Before wetting	After wetting
Ca/Al	2.46	2.94

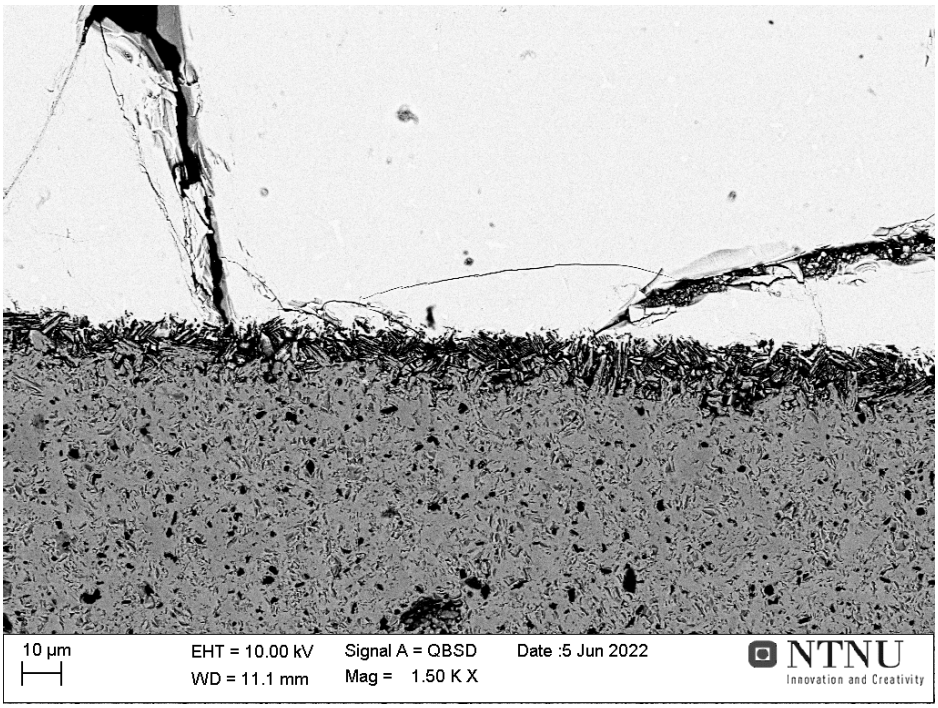

Figure 64: SEM BSE picture of the $60SiO_2 - 30CaO - 10Al_2O_3$ slag on sintered SiC at 1000x magnification

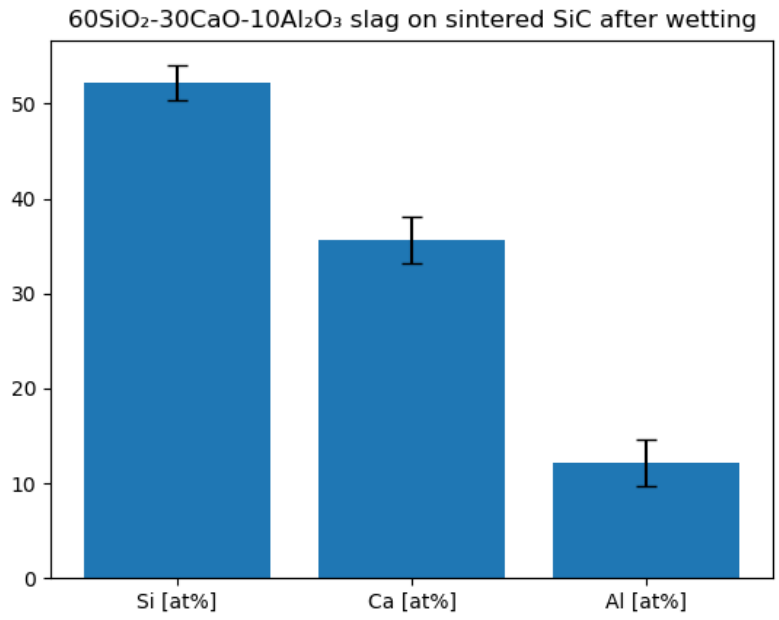

Figure 65: Si, Ca, and Al composition of the slag from EDS, with standard deviation

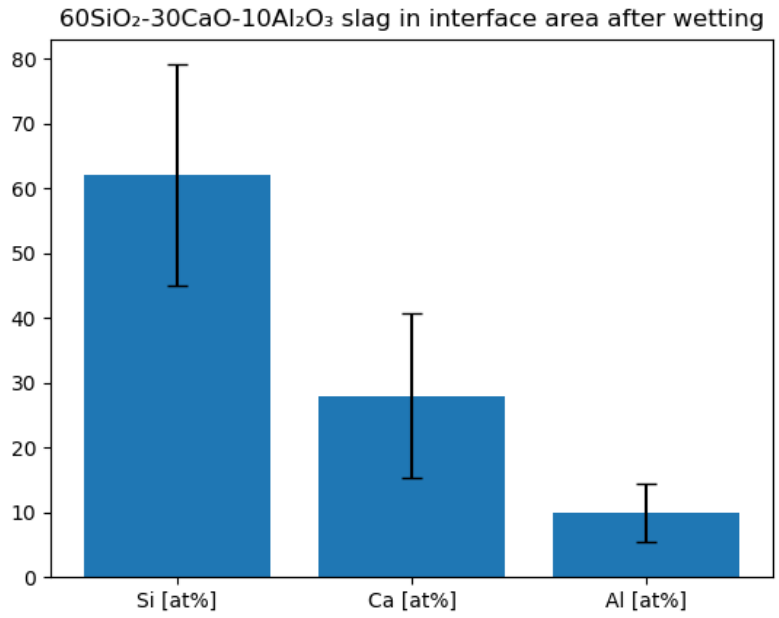

Figure 66: Si, Ca, and Al composition of the slag at the interface area from EDS, with standard deviation

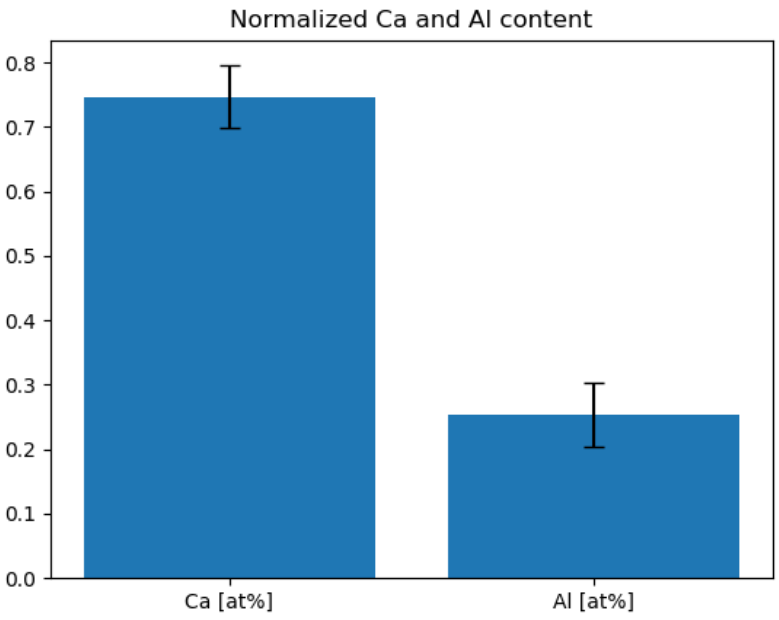

Figure 67: Normalized Ca and Al content in the slag after wetting, with standard deviation.

4.3.6 $70SiO_2 - 20CaO - 10Al_2O_3$ on sintered SiC

A SEM BSE picture of the $70SiO_2 - 20CaO - 10Al_2O_3$ slag on sintered SiC is shown in figure 68. Normalized atomic percentages of the slag phase, gotten from EDS, of Si, Ca, and Al are shown in figure 69. The Ca and Al content, normalized to 1, are shown in 70. The Ca/Al fraction from before and after the wetting test are shown in table 12. Figure 69 shows that the average composition of the slag were around 67% Si, 22% Ca, and 11% Al. From table 12 it is shown that the fraction of Ca/Al had increased by around 7% from before to after the wetting.

Table 12: Normalized Ca/Al fraction from before and after the wetting tests

	Before wetting	After wetting
Ca/Al	1.81	1.94

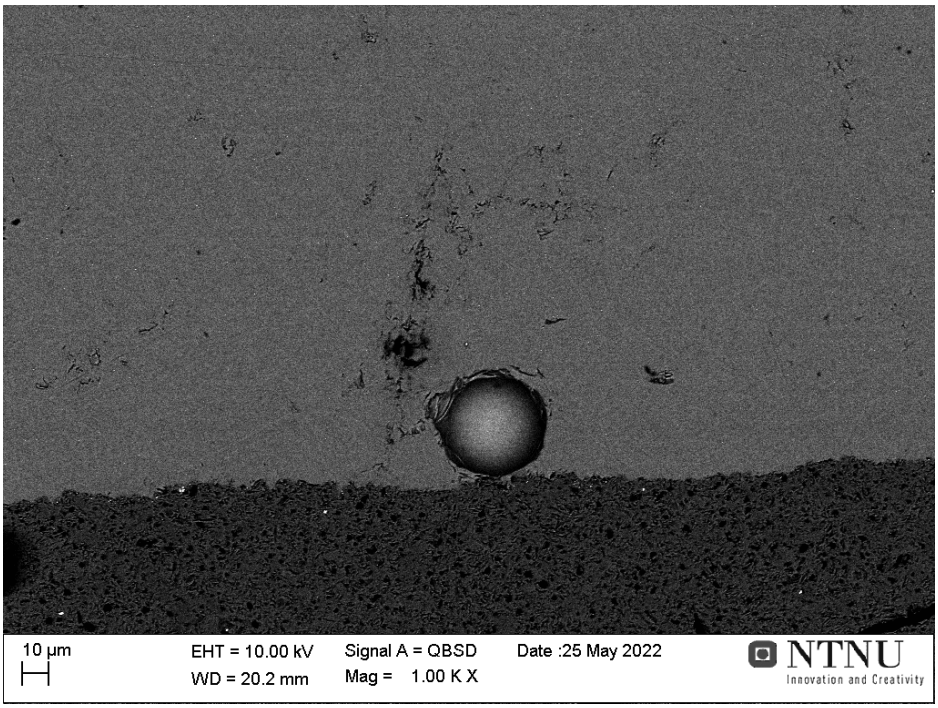

Figure 68: SEM BSE picture of the $70SiO_2 - 20CaO - 10Al_2O_3$ slag on sintered SiC at 1000x magnification

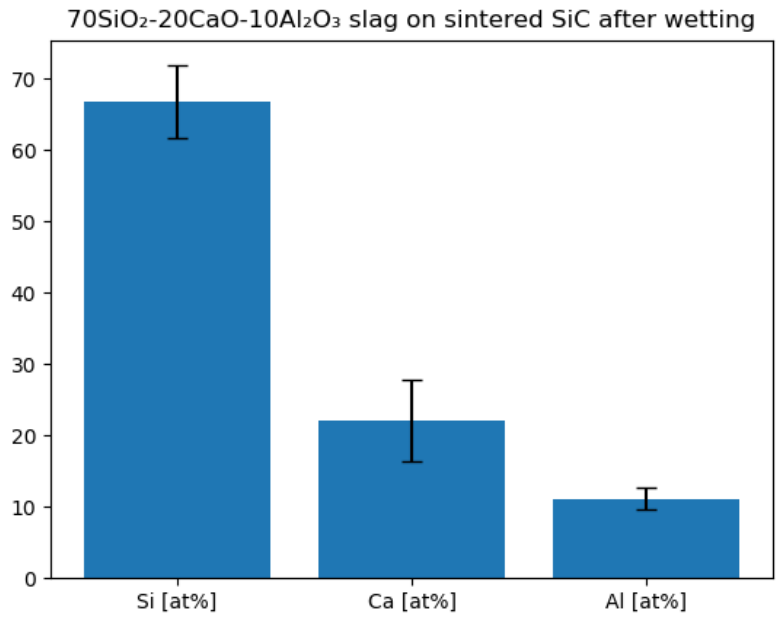

Figure 69: Si, Ca, and Al composition of the slag from EDS, with standard deviation

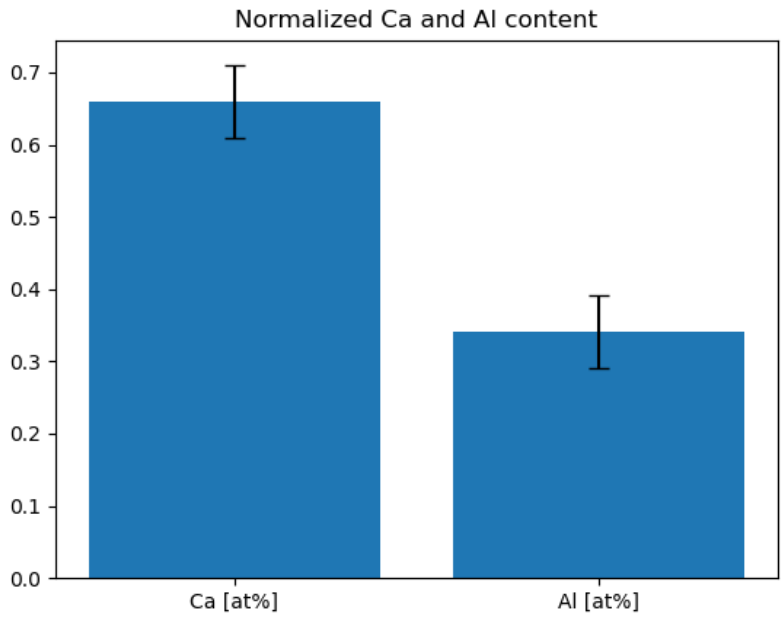

Figure 70: Normalized Ca and Al content in the slag after wetting, with standard deviation.

4.3.7 $55SiO_2 - 20CaO - 25Al_2O_3$ on transformed coal

A SEM BSE picture of the $55SiO_2 - 20CaO - 25Al_2O_3$ slag on transformed coal is shown in figure 71. Normalized atomic percentages of the slag phase, gotten from EDS, of Si, Ca, and Al are shown in figure 72. The Ca and Al content, normalized to 1, are shown in 73. The Ca/Al fraction from before and after the wetting test are shown in table 13. Figure 72 shows that the average composition of the slag were around 71% Si, 11% Ca, and 18% Al. From table 13 it is shown that the fraction of Ca/Al had decreased by around 17% from before to after the wetting. Metallic phases high in iron, silicon, and aluminium were observed.

Table 13: Normalized Ca/Al fraction from before and after the wetting tests

	Before wetting	After wetting
Ca/Al	0.71	0.59

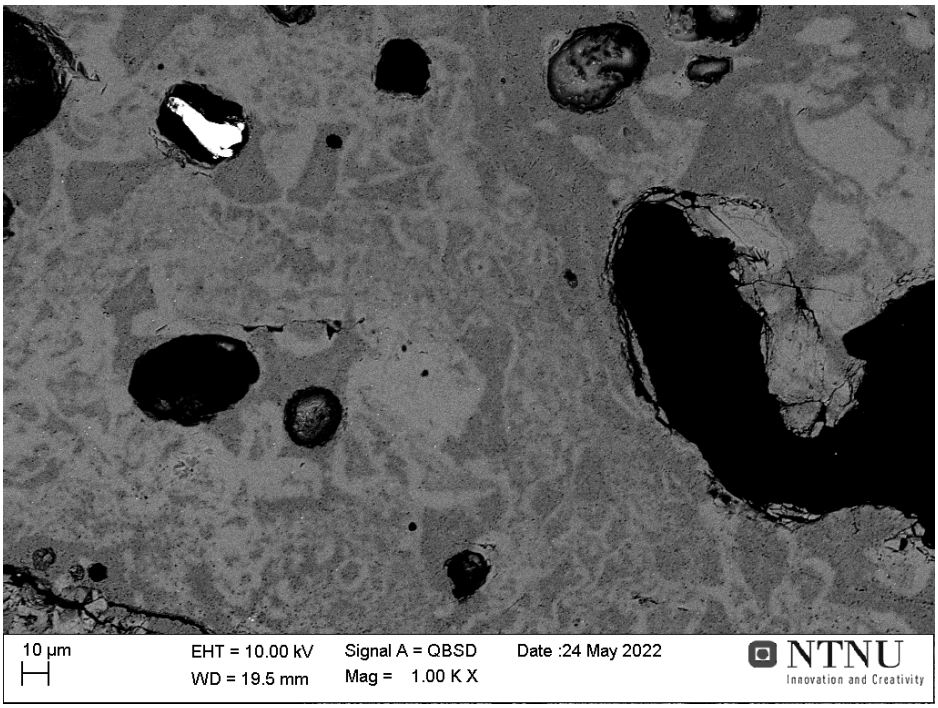

Figure 71: SEM BSE picture of the $55SiO_2 - 20CaO - 25Al_2O_3$ slag on transformed coal at 1000x magnification

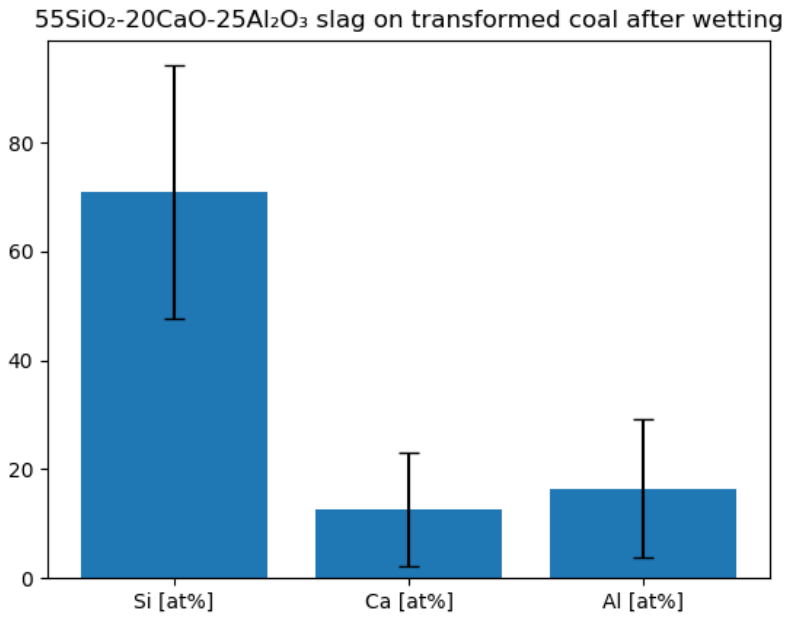

Figure 72: Si, Ca, and Al composition of the slag from EDS, with standard deviation

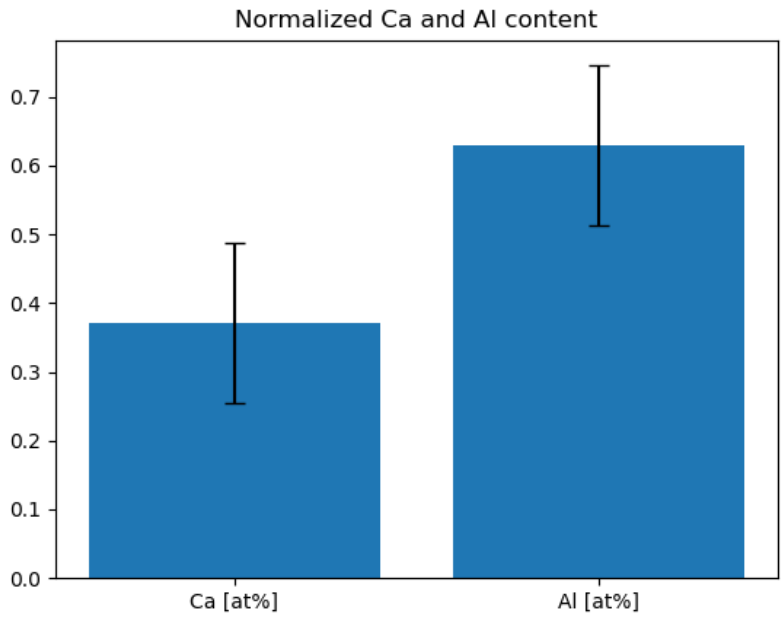

Figure 73: Normalized Ca and Al content in the slag after wetting, with standard deviation.

4.3.8 $70SiO_2 - 20CaO - 10Al_2O_3$ on transformed coal

A SEM BSE picture of the $70SiO_2 - 20CaO - 10Al_2O_3$ slag on transformed coal is shown in figure 74. Normalized atomic percentages of the slag phase, gotten from EDS, of Si, Ca, and Al are shown in figure 75. The Ca and Al content, normalized to 1, are shown in 76. The Ca/Al fraction from before and after the wetting test are shown in table 14. Figure 75 shows that the average composition of the slag were around 78% Si, 4% Ca, and 18% Al. From table 14 it is shown that the fraction of Ca/Al had decreased by around 90% from before to after the wetting. Metallic phases high in iron, silicon, and aluminium were observed.

Table 14: Normalized Ca/Al fraction from before and after the wetting tests

	Before wetting	After wetting
Ca/Al	1.81	0.19

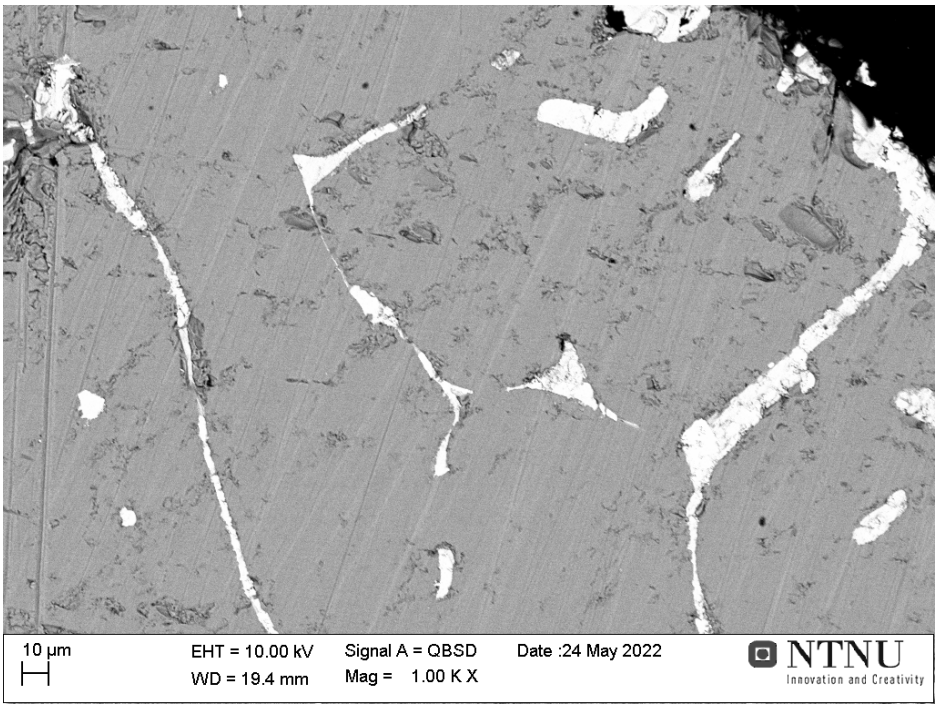

Figure 74: SEM BSE picture of the $70SiO_2 - 20CaO - 10Al_2O_3$ slag on transformed coal at 1000x magnification

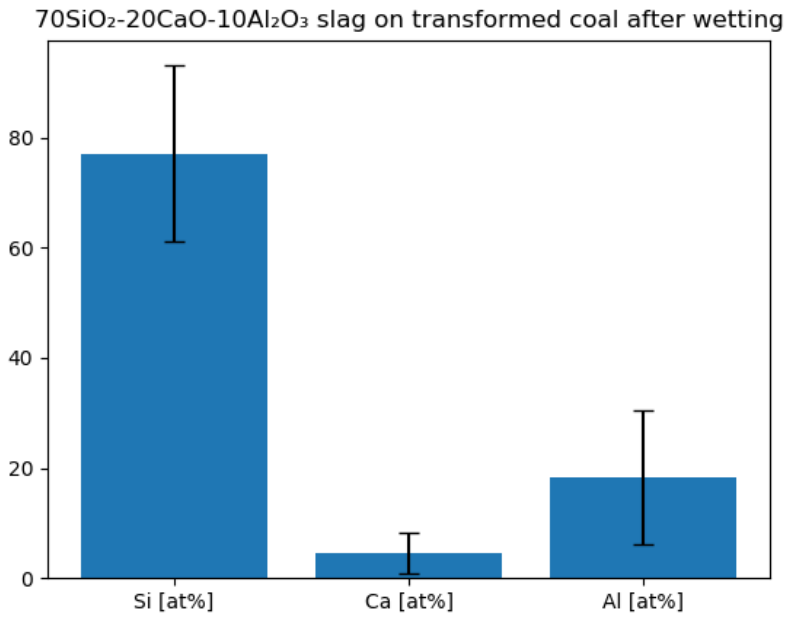

Figure 75: Si, Ca, and Al composition of the slag from EDS, with standard deviation

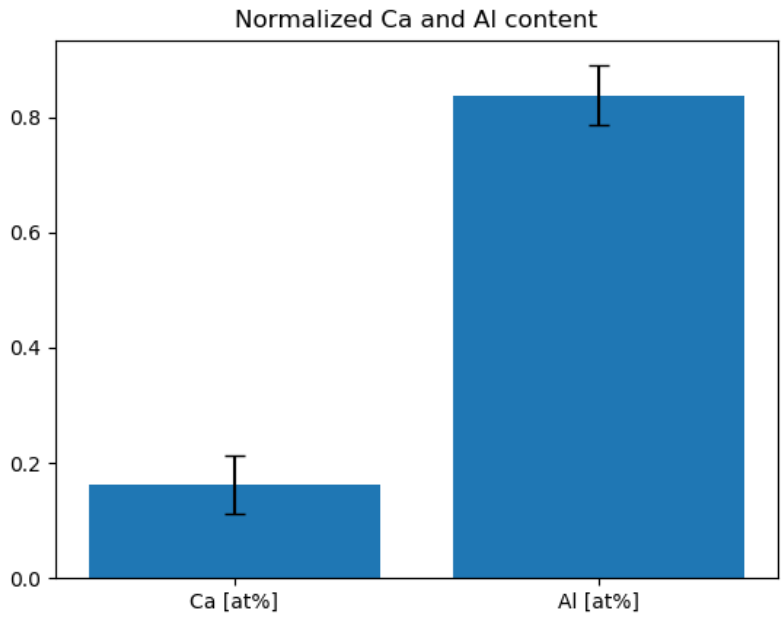

Figure 76: Normalized Ca and Al content in the slag after wetting, with standard deviation.

4.3.9 $55SiO_2 - 20CaO - 25Al_2O_3$ on alpha SiC

A SEM BSE picture of the $55SiO_2 - 20CaO - 25Al_2O_3$ slag on alpha SiC is shown in figure 77. Normalized atomic percentages of the slag phase, gotten from EDS, of Si, Ca, and Al are shown in figure 78. The Ca and Al content, normalized to 1, are shown in 78. The Ca/Al fraction from before and after the wetting test are shown in table 15. Figure 78 shows that the average composition of the slag were around 56% Si, 20% Ca, and 24% Al. From table 15 it is shown that the fraction of Ca/Al had increase by around 23% from before to after the wetting.

Table 15: Normalized Ca/Al fraction from before and after the wetting tests

	Before wetting	After wetting
Ca/Al	0.71	0.87

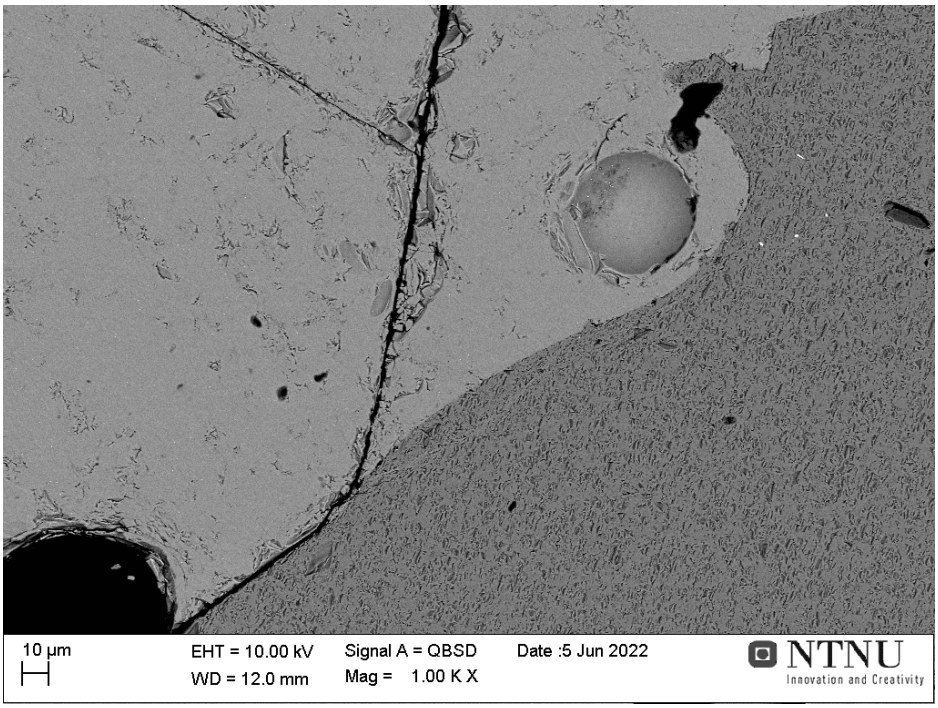

Figure 77: SEM BSE picture of the $55SiO_2 - 20CaO - 25Al_2O_3$ slag on alpha SiC at 1000x magnification

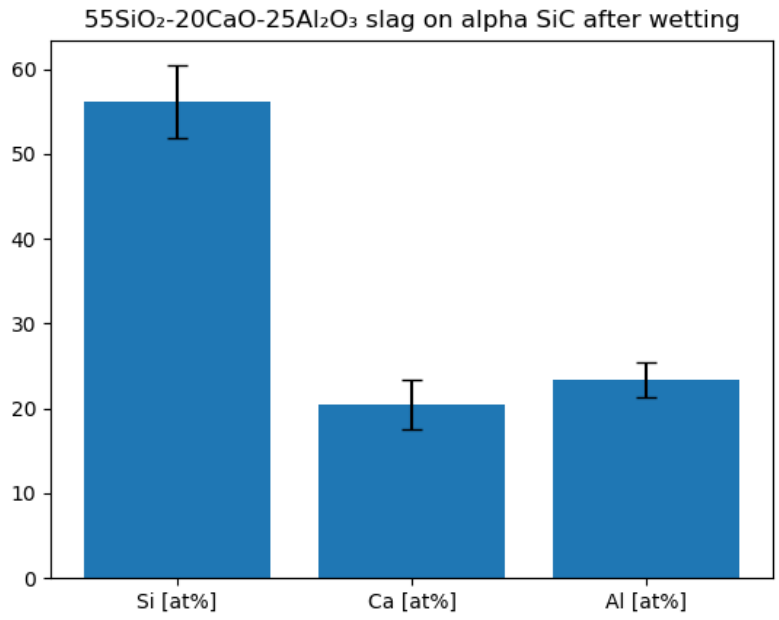

Figure 78: Si, Ca, and Al composition of the slag from EDS, with standard deviation

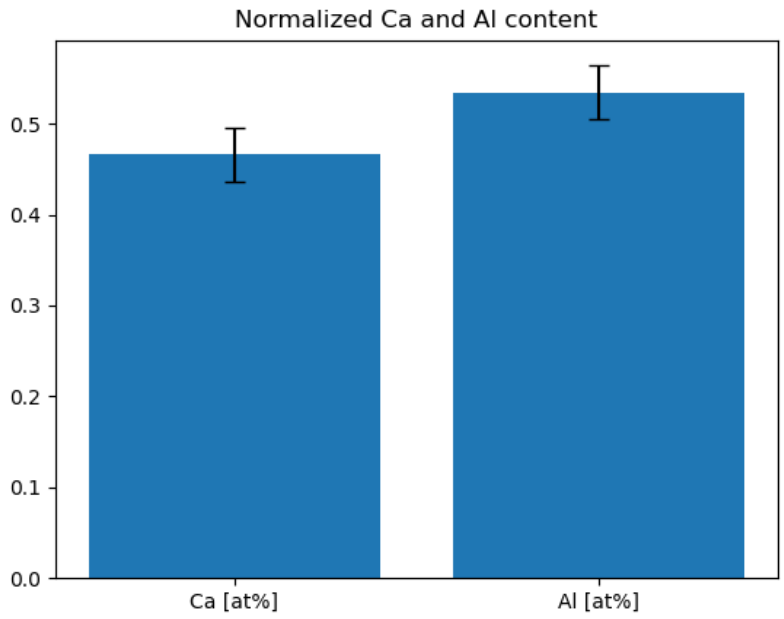

Figure 79: Normalized Ca and Al content in the slag after wetting, with standard deviation.

4.3.10 $70SiO_2 - 20CaO - 10Al_2O_3$ on alpha SiC

A SEM BSE picture of the $70SiO_2 - 20CaO - 10Al_2O_3$ slag on alpha SiC is shown in figure 80. Normalized atomic percentages of the slag phase, gotten from EDS, of Si, Ca, and Al are shown in figure 81. The Ca and Al content, normalized to 1, are shown in 81. The Ca/Al fraction from before and after the wetting test are shown in table 16. Figure 81 shows that the average composition of the slag were around 69% Si, 20% Ca, and 11% Al. From table 16 it is shown that the fraction of Ca/Al were around the same from before to after the wetting.

Table 16: Normalized Ca/Al fraction from before and after the wetting tests

	Before wetting	After wetting
Ca/Al	1.81	1.87

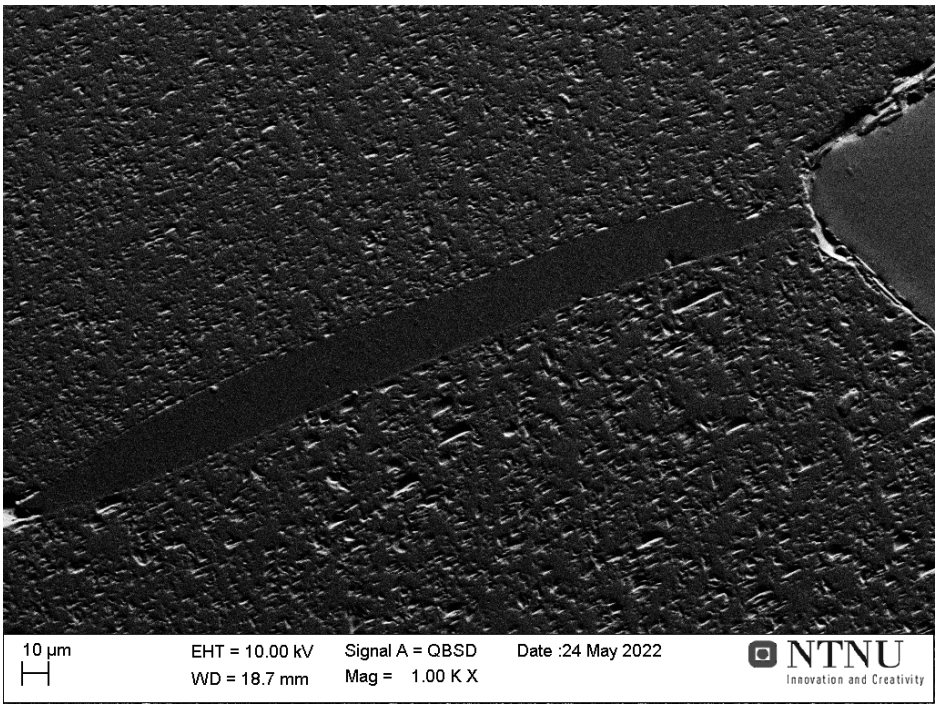

Figure 80: SEM BSE picture of the $70SiO_2 - 20CaO - 10Al_2O_3$ slag on alpha SiC at 1000x magnification

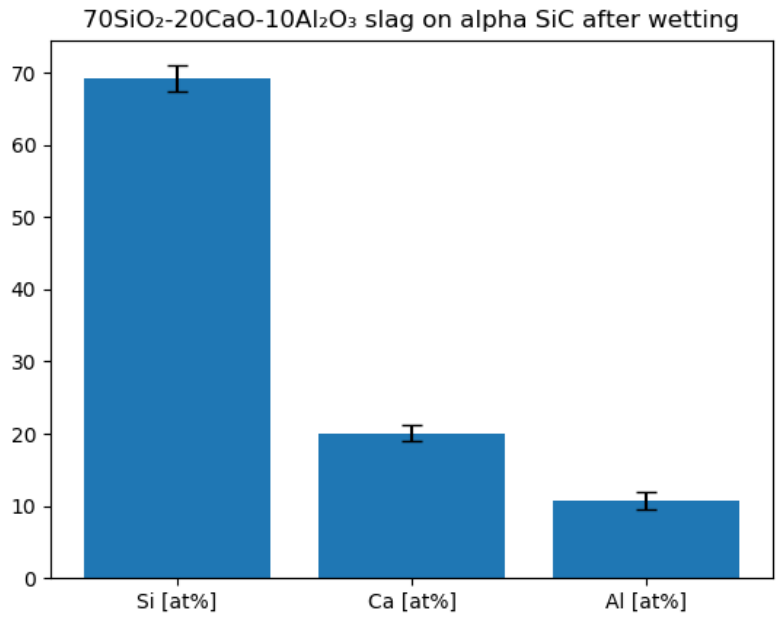

Figure 81: Si, Ca, and Al composition of the slag from EDS, with standard deviation

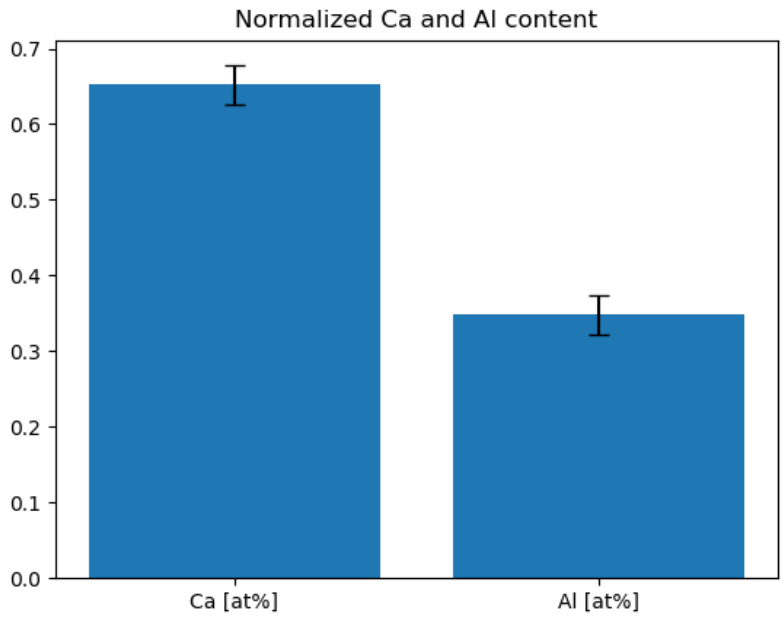

Figure 82: Normalized Ca and Al content in the slag after wetting, with standard deviation.

4.3.11 Before and after wetting

Figure 17 shows the compositions of the slags before and after the wetting experiments.

Table 17: Composition of the slags before and after wetting

	Before wetting			After wetting		
Slag no.	SiO_2 [at%]	CaO [at%]	Al_2O_3 [at%]	SiO_2 [at%]	CaO [at%]	Al_2O_3 [at%]
1	58.89	24.16	16.96	47.56	29.19	23.25
2	57.44	32.46	10.11	46.48	42.99	10.52
3	52.93	44.00	3.06	48.00	48.55	3.44
4	62.85	23.94	13.21	64.06	24.32	11.61
5	61.29	32.17	6.54	55.60	37.95	6.46
6	70.21	23.34	6.45	70.67	23.43	5.90
7	58.89	24.16	16.96	73.15	16.25	10.60
8	70.21	23.34	6.45	84.88	5.01	10.12
9	58.89	24.16	16.96	63.60	23.18	13.22
10	70.21	23.34	6.45	73.16	21.18	5.66

5 Discussion

5.1 Porosity

5.1.1 Sinterted SiC

The porosity of the sintered SiC were measured to be from 4% to 15% (14). Little indication of open porosity can be seen from the SEM pictures (A), but surface roughness in terms of small bumps in the surface and some particles are shown. This implies that the actual porosity of the sintered SiC is lower than what the analysis suggests. There were little visual difference between the pieces which suggest that the porosity percentages should be quite similar between all the pieces. The pore size distributions (15) show that the detected pores are small in size, and that there were no major holes or crevices.

5.1.2 Transformed Coal

The measured porosity of the transformed coal ranged from under 10% to around 50% (17). From the SEM pictures (A) one can see that there is a large variation in pore size, pore density, and pore amount between the different pieces. This is further supported by the pore size distribution (18) which shows a large spread of pore sizes with some being much larger than others. From the SEM picture at 1000x magnification (20) it is apparent that in addition to the larger pores in the structure, there is a high degree of porosity in the bulk material as well.

5.1.3 Alpha SiC

The measured porosity of the alpha SiC ranged from around 17% to 60% (21). From the SEM picture (A) it shows that the pieces have areas of darker material which can register as pores. They also show that there are mainly larger pores and crevices. The SEM picture at 1000x magnification supports that the main porosity comes from the larger pores in the structure because it shows that the bulk material has little apparent porosity. This is further supported by the pore size distribution (22) which shows that a lot of the detected pores have sizes of several thousands of pixels.

5.1.4 Porosity errors

There are several factors that causes errors in the porosity analysis. The threshold chosen to separate the pores and the bulk material could not be chosen to only detect pores as the surface roughness and the different tones of the material were detected before all pores were. This could have been mitigated better by setting a higher cutoff for analyse particle size as this would have removed more of the smallest detected pores which were in majority not pores. The pieces could have been polished to minimize the effect of surface roughness, but it was decided that polishing them were not the best decision because the pieces were going to be used further and polished substrates would act less like materials found in furnaces.

The high standard deviation in the average porosity for test on transformed coal and alpha SiC comes from the fact that there are a large variation both between the pieces and also between different areas on the pieces. It is clear that the porosity is on average high, but it is not possible

to get a quantitative results from this porosity analysis.

5.2 Wetting

5.2.1 Wetting on sintered SiC

The $55SiO_2 - 20CaO - 25Al_2O_3$ slag (#1)(26) showed differing signs of reaction during the wetting. There were clear signs of reactions for sample 1, but sample 2 and 3 showed very few signs of reaction and the signs showed were very subdued. This might be because the real temperature differed between sample 1 and sample 2 and 3. It was observed after the experiments that sample 1 reached its liquidus point at a lower temperature, detected by the thermocouple, than sample 2 and 3. This suggests that the temperature during the experiment were higher which causes an increase in reaction rate as supported by Hou et al.[44]. The contact angles for sample 1 were found to vary between 30°and 110°. The bubbling reactions were observed throughout the test, but they were most pronounced when the slag had high contact angles. The contact angle for sample 2 and 3 were in the 80°-90°range. This can have been the slag wetting an oxide layer on the substrate as these angles are similar to the angles found by Seo et al. for $55SiO_2 - 30CaO - 15Al_2O_3$ slag on SiO_2 at 1350°C, but they also found that the angle rapidly decreased with rising temperature. If the wetting is between the slag and the oxide layer then it would mean that the real holding temperature was so low that the oxide layer could keep stable regardless of the lack of an oxygen rich atmosphere, which I find unlikely. When compared to wetting of SiC by $60\%SiO_2 - 40\%CaO$ slag[32] one can see that the contact angle are much lower for the $60\%SiO_2 - 40\%CaO$ slag, but this slag had a higher CaO fraction. The experiments by Mailliart et al.[33] had slag with closer CaO fraction ($62SiO_2 - 23CaO - 15Al_2O_3$). They found a contact angle close to 50°at 1590°C. The gap in contact angle from this might imply that the SiO_2/Al_2O_3 fraction have a significant impact on the wetting.

The $55SiO_2 - 30CaO - 15Al_2O_3$ slag (#2)(28) showed signs of reaction throughout all the experiments, but there were very few signs of reaction towards the end when the slag reach a steady contact angle. The contact angles varied mainly between 45°and 80°. The reactions were much more pronounced when the slag had high contact angles. Sample 1 reached an apparent steady contact angle of under 20°, while sample 2 and 3 reached apparent steady contact angles at around

45°. The steady contact angles for sample 2 and 3 are close to what where found by Mailiart et al.[33] (50°), with their lower CaO content explaining their slightly higher angle. It is uncertain why sample 1 reach a significantly lower steady contact angle.

The $55SiO_2 - 40CaO - 05Al_2O_3$ slag (#3)(30) showed signs of reaction throughout all the experiments. The contact angle varied between 45°and 90°for sample 2 and 3, and between 50°and 100°for sample 1. The contact angles for the samples showed signs of becoming steady towards the end with angles of 100°for sample 1, 55°for sample 2, and 80°for sample 3. The varying contact angles makes it hard to compare, but the angle from sample 3 are close to angles of $60\%SiO_2 - 40\%CaO$ slag on SiC[32].

The $60SiO_2 - 20CaO - 20Al_2O_3$ slag (#4)(32) showed signs of reaction throughout all the experiments with no signs of slowing. It was not clear if the reactions were more intense at high or low angles. Each sample acted the same as the others for this slag. The contact angle fluctuated between 50°and 120°. The constant reactions makes it hard to find any good comparisons.

The $60SiO_2 - 30CaO - 10Al_2O_3$ slag (#5)(34) showed signs of reaction throughout all the experiments. The reactions seemed to be more intense at higher angles. The reactions seem to become slightly less intense towards the end of the tests. The angles varied between 40°and 125°for the first 40 minutes, and varied between 25°and 80°for the rest of the test. The constant reactions makes it hard to find any good comparisons.

The $70SiO_2 - 20CaO - 10Al_2O_3$ slag (#6)(36) showed signs of reaction throughout all the experiments. It was not clear if the reactions were more intense at high or low angles. There were no signs of the reactions becoming less intense over time. Each sample acted the same as the others for this slag. The contact angles varied between 40°and 100°. The constant reactions makes it hard to find any good comparisons.

When comparing the average contact angle with basicity (47), little to no clear trend can be seen. If slag #5 is an outlier then there could be a trend of decreasing contact angle with increasing basicity up to 0.5 basicity, but there is no way of knowing if it is an outlier. Of the slags at around 0.3 basicity, slag#6 has a lower average contact angle than the others. Slag #6 has higher SiO_2 content and lower Al_2O_3 content than slag #1 and #4. Of the slags with basicity of around 0.47,

slag #2 have the lowest average contact angle. Slag #2 have lower SiO_2 and higher Al_2O_3 content than slag #5. The contact angle does not seem to be dependent on the SiO_2/Al_2O_3 fraction at constant CaO based on the results for slags #1, #2, #4, #5, and #6. These results are quite uncertain as all the average contact angles are not steady state angles and they have a very high standard deviation from the reactions happening. There is also only one slag with basicity of 0.8 which makes any trend at this basicity uncertain.

Every slag showed signs of reaction in the form of bubbling and movement. The reactions are likely equation (1.7) or (2.5) as suggested by Mailliart et al.[33] They believed that the most likely culprit for the bubble formation were dissolved oxygen in the slag caused by the oxygen rich atmosphere. I find this to be unlikely in this experiment as it is done in an argon atmosphere. The argon atmosphere promotes the reactions, because of the lack of SiO and CO gas, in accordance with le Chatelieer's principle. It is unlikely that any reaction between the SiC and the CaO took place because of the low activity of CaO[43]. Both of the suggested reactions are thermodynamically possible.

$$2SiO_{2(l)} + SiC_{(s)} = 3SiO_{(g)} + CO_{(g)} \tag{1.7}$$

$$SiC_{(s)} + Al_2O_{3(l)} = Al_2O_g + SiO_g + CO_g \tag{2.5}$$

5.2.2 Wetting on transformed coal

The $55SiO_2 - 20CaO - 25Al_2O_3$ slag (#7)(38) bubbled while they penetrated into the substrate, but not during the initial rapid spreading. After the initial spreading, the contact angle kept quite constant ant under 20°while the slag penetrated into the substrate. The rapid penetration into the substrate mad it so the hold time were very short.

The $70SiO_2 - 20CaO - 10Al_2O_3$ slag (#8) have only one sample because the sample kept rolling off the substrate before the holding temperature was reached. Bubbles were observed while the slag penetrated into the substrate, but not during the initial rapid spreading. After the initial spreading, the contact angle dropped slowly down to 15°before it stabilized and kept this angle until it had fully penetrated the substrate.

The bubbling from the slag on transformed coal were only observed while the slag penetrated into the substrate. This can be signs of reaction, but it can also be gas being purged from the porous substrate. The low contact angles before they penetrated into the substrate (¡20°) fits with the wetting of powder SiC substrate by Safarian and Tangstad [32], with exception that their slag penetrated fully in a matter of second compared to several minutes.
Comparisons of the average wetting angle and the basicity(48) are too uncertain to get any good results from. Slag #7 have a large standard deviation, and slag #8 have only one sample and most of the angle measurements are manual which have little to no impact on the average.

5.2.3 Wetting on alpha SiC

The $55SiO_2-20CaO-25Al_2O_3$ slag (#9)(42) showed signs of reaction throughout the experiment. The large crevices allowed the slag to rapidly flow through the substrate. The contact angle went initially from 40°to 90°before it dropped gradually towards 20°, all while they flowed through the substrate. The fast flow rate through the substrate made it so that the hold time was very short.
The $70SiO_2-20CaO-10Al_2O_3$ slag (#10)(44) showed signs of reaction throughout the experiment. The contact angle rose to between 60°and 80°after the initial spreading sample 1 held a relatively constant angle until it flowed through the substrate. Sample 2 dropped and fluctuated between 25°and 40°until it flowed completely through the substrate.
There seem to be a positive correlation between the basicity and the wetting angle 49. The uncertainty of this correlation is however large, because there are only two different slags tested on alpha SiC, the hold time is short because of the high porosity, and that a lot of the angle measurements are manual which have little to no impact on the average. The rapid flow through the crevices in the substrate fits with what were described by Cazabat and Stuart [27]. The reactions spotted are likely the same reactions that are observed on wetting on sintered SiC 5.2.1.

5.2.4 Comparison

The wettability of the slags were found to be neutral to good, with some of the slags acting non wetting at points during their reactions. Several of the slags moved around the substrates

during the wetting tests. This is likely caused by the heterogeneity of the substrate surface. The heterogeneity can be caused by the unevenness and removal of the oxide layer which causes different contact angles and different reaction and reaction intensities. It can also be caused by differing surface roughness and pore location or by chemical variations in the substrate.

5.2.5 Error sources

There are several error sources in the wetting tests. Firstly, the sample holder is not perfectly plane. A slight tilt have been observed that can cause the angle on one side of the slag drop to be different than the other side. The tilt can also cause the slag to move more easily, or cause the substrate edge to slightly cover the slag. Secondly the program collecting the contact angles can at times have problems picking up the angles. This can be caused by the slag being obscured by the protective graphite curtain or the substrate edge, additional droplets or particles, too low drop volume, or to low contact angle. The transformed coal is not chemically homogeneous. It has SiC, carbon, and silicon phases unevenly distributed around the pieces. There is also a high degree of porosity that is not evenly distributed. The biggest error source for the alpha SiC are the large pores and crevices that are unevenly distributed in the material. Error sources for the sintered SiC are the surface roughness which would affect the slags differently depending on their wettability [24]. The substrate thickness of the sintered SiC substrates were thicker than the substrates used for calibration, which can have caused a lower real temperature than intended at the slag. There might also be some residue from the cutting of the substrates that remained on the substrate after cleaning.

5.3 EDS

5.3.1 Sintered SiC

The average composition of the $55SiO_2 - 20CaO - 25Al_2O_3$ slag on sintered SiC (#1) were found to be composed of around 38% Si, 23% Ca, and 37% Al after wetting(51). The standard deviation for the average composition were quite high. The Ca/Al fraction from before and after wetting were close to unchanged (7), which implies that no reaction between SiC and Al_2O_3 have occurred. When comparing the compositions from before and after wetting (17) then one can see that the

SiO_2 content have gone down. This implies that a reaction between SiO_2 and SiC has occurred.
The average composition of the $55SiO_2 - 30CaO - 15Al_2O_3$ slag on sintered SiC (#2) were found to be composed of around 42% Si, 39% Ca, and 28% Al after wetting(54). The standard deviation for the average composition were small. The Ca/Al fraction from before and after wetting had increased by 25% (8), which can imply that a reaction between SiC and Al_2O_3 have occurred. When comparing the compositions from before and after wetting (17) then one can see that the SiO_2 content have gone down and the CaO content have gone up. This implies that a reaction between SiO_2 and SiC has occurred. Composition in the interface area between the slag and the substrate were measured. When it were compared to the slag droplet then it shows a slightly higher Si content. This can come from the SiC in the area.
The average composition of the $55SiO_2 - 40CaO - 05Al_2O_3$ slag on sintered SiC (#3) were found to be composed of around 46% Si, 47% Ca, and 7% Al after wetting(58). The standard deviation for the average composition were small. The Ca/Al fraction from before and after wetting were close to unchanged (9), which can imply that no reaction between SiC and Al_2O_3 have occurred. When comparing the compositions from before and after wetting (17) then one can see that the SiO_2 content have gone down. This implies that a reaction between SiO_2 and SiC has occurred. Composition in the interface area between the slag and the substrate were measured. When it were compared to the slag droplet then it shows a slightly higher Al content and slightly lower Ca content. The Ca content is probably unchanged as the result is within the standard deviation and because a CaO-SiC reaction is unlikely because of the very low activity of CaO [43].
The average composition of the $60SiO_2 - 20CaO - 20Al_2O_3$ slag on sintered SiC (#4) were found to be composed of around 57% Si, 22% Ca, and 21% Al after wetting(62). The standard deviation for the average composition were small. The Ca/Al fraction from before and after wetting increased by around 15% (10), which can imply that a reaction between SiC and Al_2O_3 have occurred. When comparing the compositions from before and after wetting (17) then one can see that the SiO_2 content are close to unchanged. This can imply that no reactions between SiO_2 and SiC has occurred.
The average composition of the $60SiO_2 - 30CaO - 10Al_2O_3$ slag on sintered SiC (#5) were found to be composed of around 53% Si, 30% Ca, and 12% Al after wetting(65). The standard deviation for

the average composition were small. The Ca/Al fraction from before and after wetting increased by around 20% (11), which can imply that a reaction between SiC and Al_2O_3 have occurred. When comparing the compositions from before and after wetting (17) then one can see that the SiO_2 content have gone down. This implies that a reaction between SiO_2 and SiC has occurred. Composition in the interface area between the slag and the substrate were measured. When it were compared to the slag droplet then it shows a higher Si and Ca content, which can imply that a reaction between SiC and Al_2O_3 have occurred. The uncertainty for this is high because the standard deviations for the interface area are high.

The average composition of the $70SiO_2-20CaO-10Al_2O_3$ slag on sintered SiC (#6) were found to be composed of around 67% Si, 22% Ca, and 11% Al after wetting(69). The standard deviation for the average composition were small. The Ca/Al fraction from before and after wetting increased by around 7% (12), which can imply that a reaction between SiC and Al_2O_3 have occurred. When comparing the compositions from before and after wetting (17) then one can see that the SiO_2 content are close to unchanged. This can imply that no reactions between SiO_2 and SiC have occurred.

5.3.2 Transformed coal

The average composition of the $55SiO_2 - 20CaO - 25Al_2O_3$ slag on transformed coal (#7) were found to be composed of around 71% Si, 11% Ca, and 18% Al after wetting(65). The standard deviation for the average composition were large. The Ca/Al fraction from before and after wetting decreased by around 17% (11). When comparing the compositions from before and after wetting (17) then one can see that the SiO_2 content have increased.

The average composition of the $78SiO_2 - 4CaO - 18Al_2O_3$ slag on transformed coal (#8) were found to be composed of around 71% Si, 11% Ca, and 18% Al after wetting(65). The standard deviation for the average composition were large. The Ca/Al fraction from before and after wetting decreased by around 17% (11). When comparing the compositions from before and after wetting (17) then one can see that the SiO_2 content have increased.

The lower Ca/Al fraction of the slags on transformed coal can be explained by aluminium pollutants in the substrate. The higher Si content can be explained by the fact that the slag infiltrated

the substrate and it has surrounded the substrate particles, which the EDS picks up.

5.3.3 Alpha SiC

The average composition of the $55SiO_2 - 20CaO - 25Al_2O_3$ slag on alpha SiC (#9) were found to be composed of around 56% Si, 20% Ca, and 24% Al after wetting(81. The standard deviation for the average composition were small. The Ca/Al fraction from before and after wetting increased by around 23% (16), which can imply that a reaction between SiC and Al_2O_3 have occurred. When comparing the compositions from before and after wetting (17) then one can see that the SiO_2 content have increased. This can imply that the EDS are picking up the SiC content of the substrate.

The average composition of the $70SiO_2 - 20CaO - 10Al_2O_3$ slag on alpha SiC (#10) were found to be composed of around 69% Si, 20% Ca, and 11% Al after wetting(81. The standard deviation for the average composition were small. The Ca/Al fraction from before and after wetting were close to the same (16), which can imply that no reaction between SiC and Al_2O_3 have occurred. When comparing the compositions from before and after wetting (17) then one can see that the SiO_2 content have slightly increased. This can imply that the EDS are picking up the SiC content of the substrate.

5.3.4 Comparison

The EDS results can give some indication to what reactions are happening. Slag 1 showed only indications of reactions with SiO_2, but the standard deviation was very high. Slag 2, 5, and 9 show indications of reactions with both SiO_2 and Al_2O_3. Slag 4 and 6 showed only indications for reactions with Al_2O_3. Slag 3 and 10 showed no indications of reaction. The EDS results for slag 7 and 8 showed clear signs of metallic pollutants from the substrate which causes the results to be to uncertain. The results for slag 9 and 10 are also uncertain because the hold time were quite short during the wetting. It is odd that slag 3 and 10 shows no signs of reaction from the EDS when there were clear signs of reactions during the wetting tests.

5.3.5 Error sources

There were several sources of error. Firstly the EDS picked up Si content from the substrate for the tests with transformed coal and alpha SiC. This is because the slag penetrated and surrounded the substrate particles. Secondly metallic pollutants existed in the transformed coal substrates. Thirdly inattentive handling of the samples before the SEM caused some of the samples to have traces of Na and Cl on them. Finally the prepared SEM samples could have an angle to them.

6 Conclusion

Wetting characteristics of different $SiO_2 - CaO - Al_2O_3$ slags were tested on three different substrate made from SiC materials. Porosity analysis showed that the sintered SiC substrates were quite dense with porosity under 10%, the transformed coal were quite porous with porosity over 25%, and the alpha SiC presented large holes and crevices an had a porosity of over 35%. The wetting test found that reactions between the slag and the substrate happened in all cases. The reactions were determined to most likely be between SiC and SiO_2 or between SiC and Al_2O_3. The contact angle did not reach a steady state for most of the slags, which coupled with the intensity of the reactions, made it hard to determine proper contact angles and hard to make a comparison with other experiments. The slags were found to wet the substrates in most cases, but some slags appeared non wetting at times during the test. EDS was used to characterize the slags after wetting. The differences in composition between before and after wetting were used to help determine the possible reactions. The EDS results did indicate that for most of the slags, the reactions were between SiC and SiO_2 or between SiC and Al_2O_3 or both, but no clear trend between composition or basicity and what reaction the EDS indicates were found.

6.1 Further work

Further work should in my opinion focus on getting clear results by limiting the reactions. Using an atmosphere that of the products of the proposed reactions, such as CO, would limit the reactions in accordance with le Chatelier's principle. Using CO would be a closer approximation to a real

furnace as CO is an existing gas specie int silicon furnaces. Reactions could also be limited by doing the wetting on highly polished dense materials to limit the surface interactions. Investigations into the reactions of the slag SiC system should be done in a separate controlled environment. Lastly further composition analysis should be done with a more precice system than SEM EDS such as EPMA WDS.

References

1. Merete Tangstad and Nils E. Kamfjord. Silicon and ferrosilicon. In Merete Tangstad, editor, *Metal production in Norway*, pages 97–120. Akademika, Trondheim, 2013.

2. Guðrún Sævarsdottir. Electrical control of the si production process, hsm. Lecture in TMT4306 Metal production- Ferroalloys, Iron and Steel, September 2021.

3. Merete Tangstad. Ferrosilicon and silicon technology. In M. Gasik, editor, *Handbook of Ferroalloys, 1. ed.*, pages 179–220. Butterworth-Heinemann, Trondheim, 2013.

4. Anders Schei, Johan Kr. Tuset, and Halvard Tveit. Production of high silicon alloys. 1998.

5. Daniel H. Filsinger and Daniel B. Bourrie. Silica to silicon: Key carbothermic reactions and kinetics. *J. Am. Ceram. Soc.*, 73(6):1726–1732, 1990.

6. Marit B. Folstad and Merete Tangstad. Sio2-cao-al2o3 slags inside si/fesi furnaces. 2021.

7. Alexander S. Mukasyan. Silicon carbide. In Inna P. Borovinskaya, Alexander A. Gromov, Evgeny A. Levashov, and d Alexander S. Rogachev Yuri M. Maksimova, d Alexander S. Mukasyana, editors, *Concise Encyclopedia of Self-Propagating High-Temperature Synthesis*, pages 336–338. Elsevier, Düsseldorf, 2017.

8. Nicholas G. Wright and Alton B. Horsfall. Silicon carbide: The return of an old friend. In *Material Matters Volume 4 No. 2*, pages 43–45. Aldrich Chemical Co., Inc., Milwaukee, 2009.

9. Houyem Abderrazak and Emna Selmane Bel Hadj Hmida. Silicon carbide: Synthesis and properties. In Rosario Gerhardt, editor, *Properties and Applications of Silicon Carbide*, pages 361–389. IntechOpen, Rijekaf, 2011.

10. Henry N. jr. Baumann. The relationship of alpha and beta silicon carbide. 1952.

11. Sethulakshmy Jayakumari and Merete Tangstad. Transformation of beta-sic from charcoal, coal, and petroleum coke to alpha-sic at higher temperatures. *Metallurgical and Materials Transactions B*, 51:2673–2688, 2020.

12. S.C. Singhal. Thermodynamic analysis of the high-temperature stability of silicon nitride and silicon carbide. *Ceramurgia International*, 2(3):123–130, 1976. ISSN 0390-5519. doi: https://doi.org/10.1016/0390-5519(76)90022-3. URL https://www.sciencedirect.com/science/article/pii/0390551976900223.

13. Siwei Li, Zude Feng, Yongsheng Liu, Wenbin Yang, Weihua Zhang, Laifei Cheng, and Litong Zhang. Microstructural evolution of coating-modified 3d c/sic composites after annealing in wet oxygen at different temperatures. *Corrosion Science*, 52(9):2837–2845, 2010. ISSN 0010-938X. doi: https://doi.org/10.1016/j.corsci.2010.04.032. URL https://www.sciencedirect.com/science/article/pii/S0010938X10002192.

14. T. Narushima, T. Goto, T. Hirai, and Y. Iguchi. High-temperature oxidation of silicon carbide and silicon nitride. *Materials Transactions, JIM*, 38(10):821–835, 1997. doi: 10.2320/matertrans1989.38.821.

15. Dong Jun Park, Yang Il Jung, Hyun Gil Kim, Jeong Yong Park, and Yang Hyun Koo. Oxidation behavior of silicon carbide at 1200°c in both air and water–vapor-rich environments. *Corrosion Science*, 88:416–422, 2014. ISSN 0010-938X. doi: https://doi.org/10.1016/j.corsci.2014.07.052. URL https://www.sciencedirect.com/science/article/pii/S0010938X14003795.

16. Fabrice Amy, Y. Hwu, Christian Brylinski, and P. Soukiassian. Room temperature initial oxidation of 6h- and 4h-sic(0001) 3x3. *Materials Science Forum - MATER SCI FORUM*, 353-356:215–218, 01 2001. doi: 10.4028/www.scientific.net/MSF.353-356.215.

17. K.C. Mills. Structure of liquid slags. In Verein Deutscher Eisenhüttenleute, editor, *Slag Atlas 2nd ed.*, pages 2–6. Verlag Stahleisen, Düsseldorf, 1995.

18. P. Herasymenko. Electrochemical theory of slag-metal equilibria. part i.—reactions of manganese and silicon in acid open-heart furnace. *Trans. Faraday Soc.*, pages 1245–1254, 1938.

19. P. Herasymenko. Electrochemical theory of slag-metal equilibria. part ii.—the reactions of chromium in the acid open-hearth furnace. *Trans. Faraday Soc.*, pages 1254–1257, 1938.

20. K.C. Mills. Viscosities of molten slags. In Verein Deutscher Eisenhüttenleute, editor, *Slag Atlas 2nd ed.*, page 349. Verlag Stahleisen, Düsseldorf, 1995.

21. B. J. Keene. Surface tension of slag systems. In Verein Deutscher Eisenhüttenleute, editor, *Slag Atlas 2nd ed.*, pages 403–462. Verlag Stahleisen, Düsseldorf, 1995.

22. Thomas Young. Iii. an essay on the cohesion of fluids. *Phil. Trans. R. Soc.*, 95:65–87, 1805.

23. B. J. Keene. Contact angle and work of adhesion between ferrous melts and non-metallic solids. In Verein Deutscher Eisenhüttenleute, editor, *Slag Atlas 2nd ed.*, pages 513–539. Verlag Stahleisen, Düsseldorf, 1995.

24. R. N. Wenzel. *Ind. Eng. Chem*, 28:988, 1936.

25. G. V. Samsonov, A. D. Panasyuk, and G. K. Kozina. Wetting of refractory carbides with liquid metals. *Soviet Powder Metallurgy and Metal Ceramics*, pages 874–878, November 1968.

26. Longquan Chen and Elmar Bonaccurso. Effects of surface wettability and liquid viscosity on the dynamic wetting of individual drops. *Physical Review E 90*, 2014.

27. A. M. Cazabat and M. A. Cohen Stuart. Dynamics of wetting: effects of surface roughness. *The Journal of Physical Chemistry*, 90(22):5845–5849, 1986. doi: 10.1021/j100280a075. URL https://doi.org/10.1021/j100280a075.

28. Ilhan A. Aksay, Carl E. Hoge, and Joseph A. Pask. Wetting under chemical equilibrium and nonequilibrium conditions. *The Journal of Physical Chemistry*, 78(12):1178–1183, 1974.

29. K. Landry and N. Eustathopoulos. Dynamics of wetting in reactive metal/ceramic systems: linear spreading. *Acta Materialia*, 44(10):3923–3932, 1996. ISSN 1359-6454. doi: https://doi.org/10.1016/S1359-6454(96)00052-3. URL https://www.sciencedirect.com/science/article/pii/S1359645496000523.

30. Ingvild Brynjulfsen, Astrid Bakken, Merete Tangstad, and Lars Arnberg. Influence of oxidation on the wetting behavior of liquid silicon on si3n4-coated substrates. *Journal of Crystal Growth*, 312(16):2404–2410, 2010. ISSN 0022-0248. doi: https://doi.org/10.1016/j.jcrysgro.2010.05.006. URL https://www.sciencedirect.com/science/article/pii/S0022024810003209.

31. Yaqiong Li, Lifeng Zhang, and Zineb Benouahmane. *Effect of Oxidation on Wetting Behavior between Silicon and Silicon Carbide*, pages 237–242. Springer International Publishing, Cham, 2016. ISBN 978-3-319-48093-0. doi: 10.1007/978-3-319-48093-0_30. URL https://doi.org/10.1007/978-3-319-48093-0_30.

32. Jafar Safarian and Merete Tangstad. Wettability of silicon carbide by cao-sio2 slags. *Metallurgical and Materials Transactions B*, 40:920–928, 2009.

33. O. Mailliart, V. Chaumat, and Fiqiri Hodaj. Wetting and interfacial interactions in the cao–al2o3–sio2/silicon carbide system. *Journal of Materials Science - J MATER SCI*, 45: 2126–2132, 2010.

34. Sung-Mo Seo, Dong-Sik Kim, and Young Hyun Paik. Wetting characteristics of cao- sio2- al2o3 ternary slag on refractory oxides, al2o3, sio2 and tio2. *Metals and Materials International*, 7 (5):479–483, 2001.

35. Chaeyeon Yoo, Jaewoo Myung, and Yongsug Chung. Wetting and spreading kinetics between liquid cao–sio2 slags and a solid sio2. *ISIJ International*, 61(12):2923–2928, 2021.

36. M. Kowalski, P.J. Spencer, and D. Neuschiltz. Phase diagrams. In Verein Deutscher Eisenhüttenleute, editor, *Slag Atlas 2nd ed.*, page 105. Verlag Stahleisen, Düsseldorf, 1995.

37. M. B. Folstad, M. Ksiazek C, and M. Tangstad. Slag in the tapping area in a si furnace. *Silicon for the Chemical and Solar Industry XV*, pages 119–127, 2020.

38. K.F Jusnes, R. Hjelmseth, M.B. Folstad, N.S. Ditlefsen, and M. Tangstad. Investigation of slag compositions and possible relation to furnace operation of a fesi75 furnace. 2020.

39. J Nell and C Joubert. Phase chemistry of digout samples from a ferrosilicon furnace. In *The 13th International Ferroalloys Congress*, pages 265–271, 2013.

40. Shokouh Haghdani, Merete Tangstad, and Kristian Etienne Einarsrud. An investigation on the relationship between structure and viscosity of silicate slags. *Available at SSRN 3922156*, 2021.

41. Jeff Kline, Merete Tangstad, and Gabriella Tranell. Effects of calcium oxide on the silicate structure during slag refining of silicon: a raman spectroscopic study. pages 1510–1512, 2010.

42. Shokouh Haghdani, Merete Tangstad, and Kristian Etienne Einarsrud. A raman-structure model for the viscosity of sio2-cao-al2o3 system. *Metallurgical and Materials Transactions B*, 53(3):1733–1746, 2022.

43. M. Allibert, R. Parra, C. Sain-Jours, and M Tmar. Thermodynamic activity data for slag systems. In Verein Deutscher Eisenhüttenleute, editor, *Slag Atlas 2nd ed.*, pages 225–255. Verlag Stahleisen, Düsseldorf, 1995.

44. Yong Hou, Guo-Hua Zhang, and Kuo-Chih Chou. Reaction behavior of sic with cao–sio¡sub¿2¡/sub¿–al¡sub¿2¡/sub¿o¡sub¿3¡/sub¿ slag. *ISIJ International*, 61(3):745–752, 2021. doi: 10.2355/isijinternational.ISIJINT-2020-605.

45. Sh. Haghdani, M. Tangstad, and K. E. Einarsrud. A raman-structure model for the viscosity of sio2–cao–al2o3 system, manuscript. 2021.

46. H. Hoover, G. Sævarsdottir, and M. Tangstad. Electrical resistivity of partially transformed silicon carbide made from coal. 2021.

A Porosity

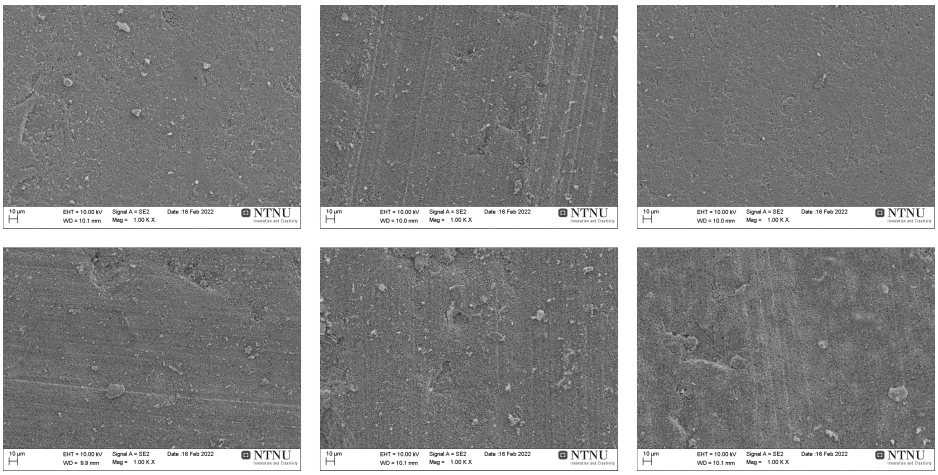

Figure 83: SEM pictures of all the sintered SiC pieces for porosity analysis. #1: top left, #2: top center, #3: top right, #4: bottom left, #5: bottom center, #6: bottom right.

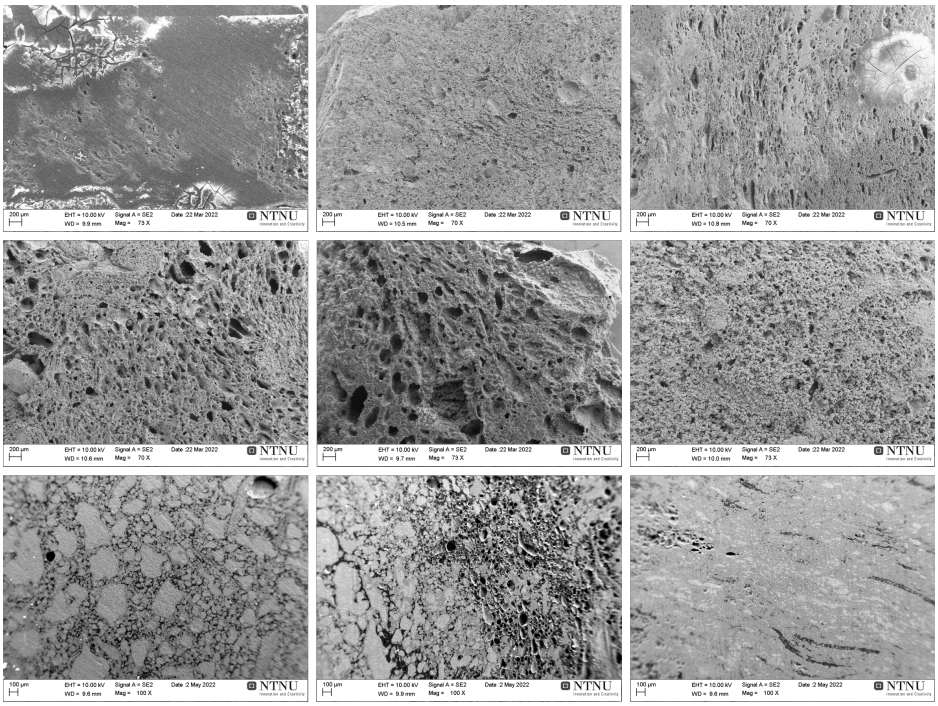

Figure 84: SEM pictures of all the transformed coal pieces for porosity analysis. #1: top left, #2: top center, #3: top right, #4: middle left, #5: middle center, #6: middle right #7: bottom left, #8: bottom center, #9: bottom right.

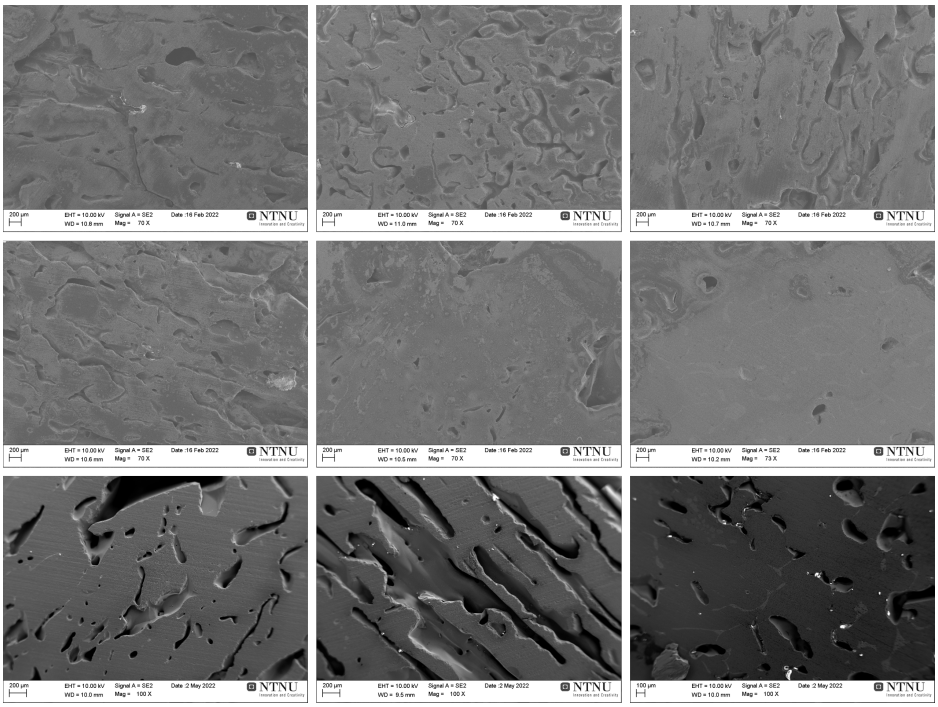

Figure 85: SEM pictures of all the alpha SiC pieces for porosity analysis. #1: top left, #2: top center, #3: top right, #4: middle left, #5: middle center, #6: middle right #7: bottom left, #8: bottom center, #9: bottom right.

Baumann, Jesper Ludvig Saxlund

Wetting properties SiO2-CaO-Al2O3 slag and SiC

NTNU
Norwegian University of
Science and Technology